Electrical Properties of Doped and Undoped PZT Thin Films Prepared by a Sol-Gel Method

By

Jimmy Xing

Thesis Submitted to the Faculty of the
Virginia Polytechnic Institute and State University
in partial fulfillment of the requirement for the degree of
Master of Science
in
Materials Science and Engineering

Approved:

S. B. Desu, Chairman

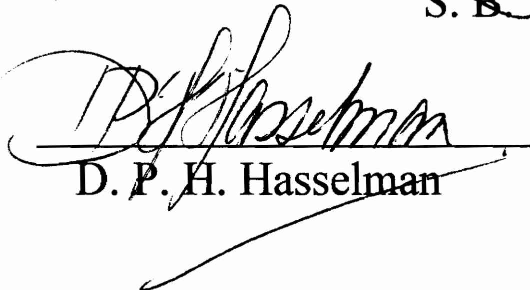

D. P. H. Hasselman

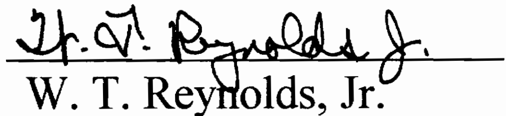

W. T. Reynolds, Jr.

February, 1994

Blacksburg, Virginia

.2

5655
V855
1994
X564
c.2

Electrical Properties of Doped and Undoped PZT Thin Films Prepared by a Sol-Gel Method

By

Jimmy Xing

Committee Chairman: Seshu B. Desu

Materials Science and Engineering

(Abstract)

Fatigue and electrical degradation including low voltage breakdown of ferroelectric lead zirconate titanate $Pb(Zr_xTi_{1-x})O_3$ (i.e. PZT) thin films are the major limitations for commercial memory applications of these films. It is noted that the presence of oxygen vacancies and their entrapment at the electrode-ferroelectric interfaces are the sources of the degradation phenomena. Attempts were made in this study to solve these problems: 1) by minimizing oxygen vacancy entrapment at the interfaces by employing RuO_2 electrodes; 2) by lowering the oxygen vacancy concentration in PZT films using donor doping (e.g. La^{3+} at Pb^{2+} site and Nb^{5+} at Ti/Zr^{4+} site).

For this study, PZT thin films were prepared by a sol-gel method and deposited on both $Pt/Ti/SiO_2/Si$ and $RuO_2/SiO_2/Si$ substrates. The microstructure and electrical properties, such as hysteresis properties, fatigue, leakage current, time dependent dielectric breakdown (TDDB) and retention, were studied with regard to the Zr/Ti ratio, the excess lead, the annealing temperature, the electrode material and the doping amount. Furthermore, the pyrochlore to perovskite phase transformation of PZT on RuO_2 electrodes was also investigated.

It was shown that PZT films (Zr/Ti=50/50) with 10 at.% excess lead annealed at 650°C for 30 min possessed the best electrical properties for ferroelectric memory application. In confirmation with earlier theoretical and experimental results, no polarization loss was observed up to 10^{11} switching cycles for the PZT films deposited on RuO_2 electrodes. However, the low Schottky barrier at the interfaces between RuO_2 and PZT films resulted in a higher leakage current at a high electric fields. Donor doping of PZT films decreased carrier concentrations in PZT films, and thus, decreased the leakage current to acceptable limits. In addition, it was also noted that the pyrochlore to perovskite phase transformation of PZT on RuO_2 was similar to that of PZT on Pt electrodes.

It can be concluded that the combination of RuO_2 electrodes and donor doping produced PZT films with high fatigue endurance and low leakage currents which are suitable for memory applications.

Acknowledgements

I would like to express my sincere appreciation to my advisor, Dr. S. B. Desu, for his guidance and support, and in particular, his endless enthusiasm. I also wish to thank the other members of my advisory committee, Dr. D. P. H. Hasselman and Dr. W. T. Reynolds, Jr., for their comments, suggestions and encouragement.

I am also very grateful to all members of the thin film group, and in particular to Dr. Chien-Hsiung Peng, Warrent. C. Hendricks, Dilip P. Vijay, Dr. Ting-Kai. Li, Mayukh Bhattacharya, Cai-Liang Thio and Justin Gaynor, for their cooperation and friendship.

Table of Contents

Chapter 1:. Introduction 1

1.1 Ferroelectric Memory 2

1.2 Electrical Property Requirements 7

1.3 PZT Ferroelectric Materials 11

1.4 Research Objectives 15

Chapter 2: Electrical Properties of Sol-Gel Derived PZT Thin Films on RuO_2 Substrates 16

2.1 Introduction 16

2.2 Experimental Procedure 17

2.3 Results and Discussions 20

2.4 Summary 49

Chapter 3: Electrical Properties of Doped PZT Thin Films Made by a Sol-Gel Method 53

3.1 Introduction 53

3.2 Sample Preparation 57

3.3 Results and Discussion 58

3.4 Summary 86

Chapter 4: Summary 88

Appendix A 90

Appendix B 91

References 92

Vita 96

List of Figures

Fig. 1.1	Ferroelectric Hysteresis Loop	3
Fig. 1.2	Structure of a Proposed Ferroelectric Memory Cell	5
Fig. 1.3	Ferroelectric Perovskite Crystal Type ABO3	13
Fig. 1.4	Lead Zirconate-Lead Titanate Phase Diagram	14
Fig. 2.1	Modified PZT Sol-Gel Process	19
Fig. 2.2	PZT XRD Patterns (1)	21
Fig. 2.3	Pyrochlore Stability Region	23
Fig. 2.4(A)	PZT XRD Patterns (2)	25
Fig. 2.4(B)	PZT XRD Patterns (3)	26
Fig. 2.5	Microstructure of PZT (1)	28
Fig. 2.6	Microstructure of PZT (2)	29
Fig. 2.7	Microstructure of PZT (3)	30
Fig. 2.8	Microstructure of PZT (4)	31
Fig. 2.9	Microstructure of PZT (5)	33
Fig. 2.10	Microstructure of PZT (6)	34
Fig. 2.11	Remanent Polarization as a Function of Zr/Ti Ratio (I)	37
Fig. 2.12	Remanent Polarization as a Function of Zr/Ti Ratio (2)	38
Fig. 2.13	Remanent Polarization as a Function of T & Excell Lead	39
Fig. 2.14	PZT Hysteresis Loop (1)	40
Fig. 2.15	PZT Hysteresis Loop (2)	41
Fig. 2.16	Fatigue Endurance of PZT	43
Fig. 2.17	Leakage Current as a Function of Annealing Temperature	45

Fig. 2.18 Leakage Current as a Function of Excess Lead 47

Fig. 2.19 Leakage Current as a Function of Zr/Ti Ratio 48

Fig. 2.20 PZT I-V Curves on RuO2 and Pt Electrodes 50

Fig. 3.1 Cross-sectional SEM of PZT on Pt Electrodes 59

Fig. 3.2 Microstructure of PZT on (a)Pt and (b)RuO_2 61

Fig. 3.3 Microstructure of PLZT (6%) on (a)Pt and (b)RuO_2 62

Fig. 3.4 Microstructure of PLZT on Pt 63

Fig. 3.5 Microstructure of PNZT on Pt 65

Fig. 3.6 Microstructure of PNZT on RuO_2 66

Fig. 3.7 Polarization as a Function of Nb Doping Amount 67

Fig. 3.8 Remanent Polarization as a Function of Doping Amount 69

Fig. 3.9 Coercive Field as a Function of Doping Amount 70

Fig. 3.10 Fatigue Endurance of PLZT on RuO_2 72

Fig. 3.11 Fatigue Endurance of PNZT on Pt 73

Fig. 3.12 Fatigue Endurance of PLZT on Pt 76

Fig. 3.13 TDDB of PZT on Pt & RuO_2 77

Fig. 3.14 TDDB of PNZT on Pt 78

Fig. 3.15 TDDB of PLZT on Pt 79

Fig. 3.16 Leakage Current as a Function of Doping Amount 81

Fig. 3.17(A) I-V Curves of PZT & PLZT 82

Fig. 3.17(B) I-V Curves of PZT & PNZT 83

Fig. 3.18 Retention of PNZT (6%) on RuO_2 84

Fig. 3.19 Retention of PLZT (4%) on Pt 85

Chapter 1. Introduction

The read/write memory devices that dominate fast-access data storage in computer systems are the semiconductor memories in the form of dynamic and static random access memories. Silicon dioxide capacitors were typically used in dynamic RAM memory cells to store charge and hence data. These memory devices are volatile; they lose all their information whenever power is lost. For systems that require nonvolatility, silicon-based programmable ROM (PROM), erasable programmable ROM (EPROM), and electrically erasable programmable ROM (EEPROM) were developed. However, their read/write speed and endurance are inferior to those of dynamic RAM's.

It is well known that a ferroelectric crystal with tetragonal perovskite structure has at least two polarization states. The two zero-field values of remanent polarization $\pm P_r$ are equally stable. Thus, no applied field or voltage is required to maintain the memory. This bistable operation may be contrasted with the operation of memories such as nematic and liquid-crystal display devices, which relax back to a single favored state if the applied voltage is interrupted, or with Si DRAMs, which require a "refresh" voltage many times per second to maintain their stored information. The idea of using ferroelectric thin film in a capacitor as a nonvolatile storage element was therefore introduced. Since ferroelectric materials have a very high dielectric constant, they are also considered to be a good substitute of silicon dioxide for fabricating higher density DRAM chip (256 M and 1 GBites). This thesis is focused on the study of the electrical properties of the lead zirconate titanate (PZT) ferroelectric thin films for memory applications. Chapter 1 gives the introduction to the composition, processing and characterization of the PZT ferroelectric materials as well as their property requirements for memory applications.

Chapter 2 studies the PZT compositional effect on the electrical properties, especially the degradation properties fatigue and leakage current, by employing the conductive oxide electrode material RuO_2. Chapter 3 studies the improvement of PZT reliability properties by La and Nb donor doping.

1.1 Ferroelectric Memory

The ferroelectricity of a ferroelectric material is characterized by the spontaneous polarization P_s of the ferroelectric phase. This spontaneous polarization can be reoriented by an external field. The region with uniform alignment of electric dipoles (uniform spontaneous polarization) in a ferroelectric crystal is called a ferroelectric domain. These domains are randomly arrayed preceding the application of an external field and the overall polarization is zero. Once an external field is applied, the domains are aligned along the external field and show high macroscopic polarization. When the external field is high enough to switch all the domains in the crystal, the saturated hysteresis loop which is shown in Fig.1.1 can be achieved. The polarization under the saturated applied field is called saturated polarization. A remanent polarization P_r remains even though the external field is withdrawn.

The hysteresis loop is a typical phenomenon of a ferroelectric material. It has two stable states at a zero field: positive P_r and negative P_r. The "0" and "1" states required for the Boolean algebra of binary computer memories can be encoded in the ±Pr states of the ferroelectric materials (say $+P_r$="0" and $-P_r$="1"). The readings of these two states are destructive. Two positive pulses are applied to the ferroelectric memory capacitor; the first one switches the ferroelectric from whatever state to $+P_s$ while the second

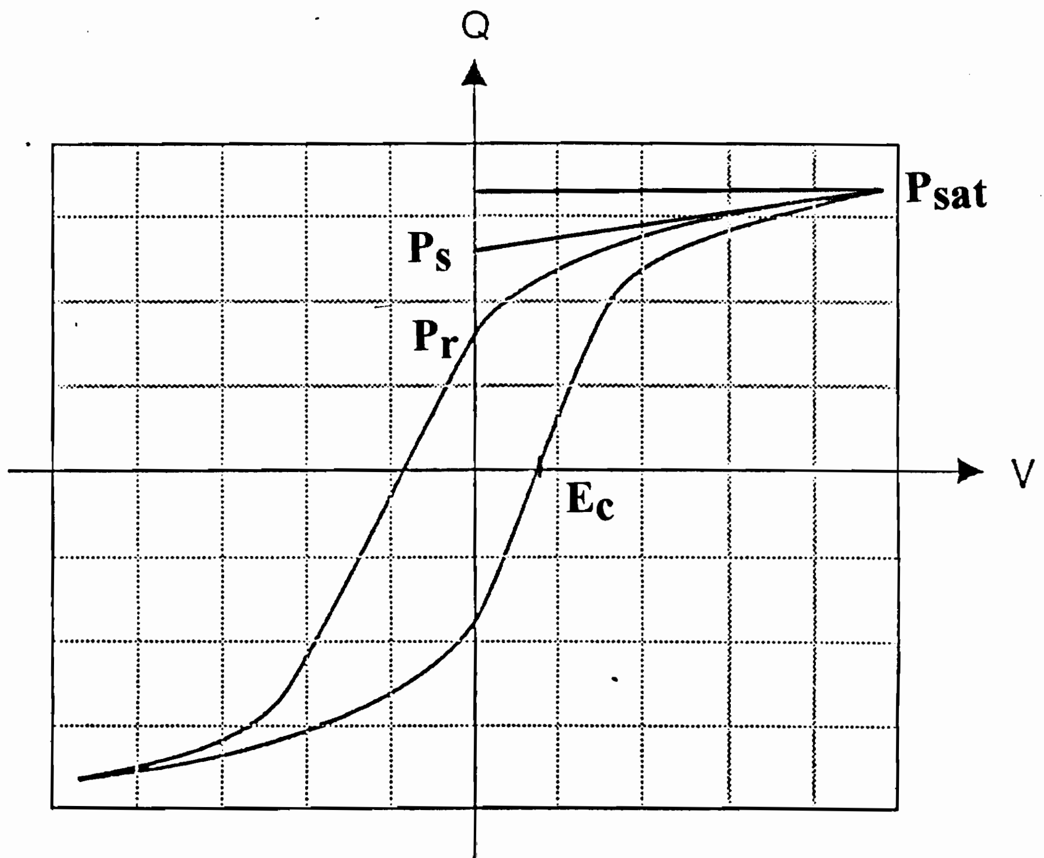

Fig. 1.1 Ferroelectric Hysteresis Loop

one is used as the reference pulse. The current difference between these two pulses after the switching is sensed. If the stored data were a zero ($+P_r$), a small current which is proportional to (P_s-P_r) after the application of the positive pulse is observed; if a one was stored ($-P_r$), the positive pulse will switch the memory from $-P_r$ to $+P_s$, and a high current which is proportional to (P_s+P_r) occurred. The "0" or "1" state can be determined as long as the sense amplifier can distinguish the dP(1) and the dP(0) current. All data are in the zero state after the reading (destructive reading), so two negative pulses are required to reset the ferroelectric memory to a original "1" state. This is the basic principle of a ferroelectric thin film capacitor as a nonvolatile memory device. Fig.1.2 shows the structure of a ferroelectric memory on CMOS.

The high dielectric constant of the ferroelectric materials can be used in the design of high density DRAMs. Currently a silicon nitride-silicon oxide sandwich layer is used in the DRAM system. The density of a DRAM chip can not go higher than 64 Mbit even though a trench design was introduced to compensate for the low dielectric constant of SiO_2. However, if a high-dielectric constant ferroelectric material is used as a thin film capacitor, with the same capacitance, the capacitor area will be much smaller than that of the Si_3N_4-SiO_2 trench capacitor (trench geometry provides greater capacitive area of the capacitor). 64 Mbit and 256 Mbit DRAM can be fabricated by employing the high dielectric constant ferroelectric materials [37].

The current memory market consists of 14 generically different kinds of digital memories in use [13] which can be divided into three major groups: semiconductor memories, magnetic memories and optical memories. The semiconductor memories have a variety of applications and dominate the fast-access memories market. Static random access memories (SRAMs) are optimized for the high-speed applications such as cache; dynamic random access memories (DRAMs) have a slightly lower speed compared to the

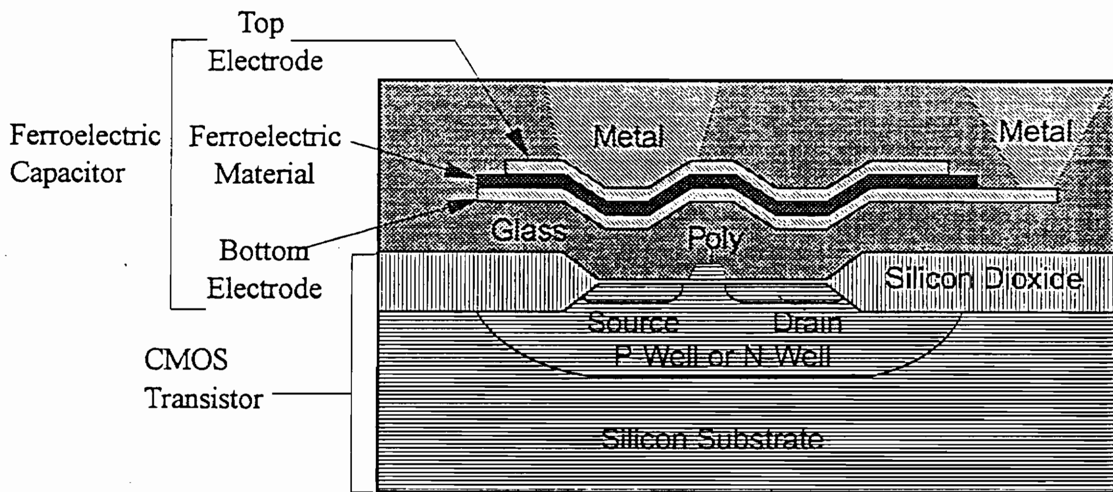

Fig. 1.2 Structure of a Proposed Ferroelectric Memory Cell

SRAMs and require continued circulation of data; nonvolatile memories are mostly silicon-based read-only memories, such as PROM, EPROM, and EEPROM, which can be read either destructively (DRO) or nondestructively (NDRO) with a much lower speed than the RAMs.

The second major memory segment are the magnetic memories. The most well-known magnetic memories are the magnetic disk and tape. They are the slowest and most inexpensive memory devices used for permanent data storage. Magnetic core and plated wire, on the contrary, are the most expensive memory devices and can be used as random access memories. Their speed is about one order lower than that of DRAMs. Higher density memories can be fabricated in the form of magnetic bubbles and permalloy thin films with an access speed two orders of magnitude higher than that of the magnetic tape and disk. The optical memories form the third group of memories. They are characterized by high density and write once read many operation (WORM), and used only for archival storage [4].

Two kinds of memory can be produced using ferroelectric materials: high density DRAM and nonvolatile ferroelectric RAM. The ferroelectric RAM (FRAM) has a good radiation resistance due to the storage of data by polarization instead of electric charge. Their compatibility with the silicon RAMs processing technology results in low cost per bit particularly when compared to magnetic storage elements. In summary, ferroelectric thin film memories offer nonvolatility, high density, high stability, high access speed and low cost. Their applications will greatly simplify the existing collections of computer memories, which will still include tape and disk systems for archival storage, inexpensive high-density DRAMs and ultrafast SRAMs, while most of the other memory devices now in use may be rendered obsolete.

1.2 Property Requirements

Ferroelectric lead zirconate titanate (PZT) system was investigated to be the possible materials used in ferroelectric memories in this study. Several properties need to be optimised for a successful implementation in ferroelectric memories in addition to good hysteresis properties. These properties are mostly the reliability properties, including fatigue, aging, imprint, time dependent dielectric breakdown (TDDB), and electrical degradation (leakage current). The following section will give a summary of the electrical properties required for both FRAM and DRAM applications.

Ferroelectric Properties. The hysteresis loop of a ferroelectric material describes the amount of charge a ferroelectric capacitor stores as a function of the applied voltage. For FRAM application, it is desirable for the two coercive voltage points to be symmetrical and less than 2.5 V to integrate the ferroelectric thin film memory capacitor into standard Si CMOS integrated circuits (ICs), for which the standard logic levels are 5.0 V (±10%). The other consideration is to maximize the switchable polarization (nonlinear polarization) and minimize the unswitchable polarization (linear polarization). The overall electric displacement D is the sum of these two polarizations:

$$D = \varepsilon_0 \varepsilon E_A + P_S \qquad (1.1)$$

Only the nonlinear polarization can be used to store data since the electric field is zero after writing in FRAM. The difference between the positive and negative remanent polarizations $2P_r$ is used to distinguish between the "0" and "1" states, so it should be large enough to be sensed. For the sense amplifier design used in the GaAs memory, the

minimum polarization for a capacitor of 20 μm^2 is 1 $\mu C/cm^2$. The nonlinear term can be decreased by decreasing the dielectric constant and thus the squareness of the hysteresis loop is increased . However, the opposite should be done for the DRAM application, in which a constant electric field is added on the ferroelectric capacitor, therefore a high dielectric constant is desired.

In summary, the material requirements for the nonvolatile FRAM are different from those of DRAM. In nonvolatile memory, a square hysteresis loop is required with high switchable polarization (both saturated polarization P_s and remanent polarization P_r) and low coercive field. A low dielectric constant is desired for the squareness of the loop. In DRAM, a high dielectric constant is desired since the nonswitchable polarization instead of the switchable polarization is used to store the data, and the hysteresis loop is not desired.

Endurance. In a ferroelectric memory cell, both the writing and the reading can switch the ferroelectric memory, therefore the endurance of a ferroelectric memory to the switching cycles must be considered. In PZT materials, it is observed that the polarization degrades with switching cycles, or the materials become fatigued after many cycles of switching. To achieve the goal of applying the PZT ferroelectric memory IC to wherever standard DRAM are used now, an endurance of greater than 10^{12} read/write cycles is required.

It is noted that the fatigue behavior of a ferroelectric material is the consequence of moving and trapping of mobile ions, mainly oxygen vacancies. They are moving back and forth under alternating pulses. When they hit sites with lower chemical potential, such as grain boundaries and the ferroelectric-electrode interfaces, they can be trapped at these sites. Thus an internal electric field has been built up and will pin the domains. The more domains being pinned, the less domains can be switched, so that the switchable

polarization will decrease. For ferroelectric materials, the polarization typically degrades to 50% of its original value after 10^6 read/erase/rewrite cycles on Pt electrodes [13].

Either decreasing the trap sites of the mobile ions or lowering the chemical potential difference between these sites and the bulk can increase the endurance of the ferroelectric materials. It is possible to release the trapped ions in the grain boundaries by giving them energy to overcome the chemical potential barrier. In PZT, trapped domain walls can be "depinned" by applying a voltage higher than 5 V but less than the breakdown voltage, and the original polarization can be partly recovered. In the interfaces, the high chemical potential difference comes from the lattice mismatch between the film and the electrode, and thus the electrode selection is very important in obtaining good endurance properties. Some ceramic electrodes, such as RuO_2, have a much smaller lattice mismatch with the PZT film than that of the metal electrodes like Pt, so they can improve the PZT endurance significantly.

Retention (Aging). When the ferroelectric is applied in nonvolatile memory, the length of time a ferroelectric can maintain its polarization state must be determined. In general, charge does not leak off PZT ferroelectric cells, which are simply very small capacitors. However, under some circumstances, such as high temperature and radiation, this degradation will become severe. The expected retention time for ferroelectric memories is at least 10 years.

One of the causes of aging is space charge buildup which gives rise to internal bias. It can be expressed by an experimental equation as:

$$K = K_0(1-\alpha T)\ln t/t_0 \tag{1.2}$$

where K is the dielectric constant at time t, α is the probability constant of domain motion, and T is temperature. The space charges such as oxygen vacancies migrate under an internal field which is formed by remanent polarization and build up at the interfaces and the grain boundaries. The space charges will balance the remanent polarization and cause the aging problem.

Leakage Current. Under a constant electric field, there is a small amount of current that goes through a ferroelectric thin film capacitor. This leakage current will cause loss of charge in the storage capacitor over a period of time, especially in a 1-Transistor DRAM cell, and the capacitor has to be refreshed periodically to keep its contents.

The leakage current is always non-ohmic. It is controlled by several types of conduction mechanisms, such as simple oxygen diffusion, grain boundary potential barrier height, space charge limited current, Poole-Frenkel emission, Schottky emission etc.. Poole-Frenkel emission occurs in the bulk of the material due to different trap levels. Schottky emission occurs at the interfaces between the ferroelectric and the electrode where a Schottky barrier is formed. The Schottky emission is more important since its contribution to the leakage current is significant. It can be expressed as:

$$J = A^{**}T^2\exp[(-\phi_B + c\sqrt{E})/kT], \quad E = V/d \tag{1.3}$$

where J is the current density, A** is the effective Richardson constant, ϕ_B is the effective Schottky barrier height and c is a constant.

Time Dependent Dielectric Breakdown (TDDB). The readout of a nonvolatile ferroelectric memory is destructive and will cause fatigue problem. However, a nondestructive electrical readout is possible for a DRAM structure, which is subjected to a

constant voltage rather than open circuit conditions. Leakage current is the first parameter considered in this structure which tells how well they can hold the charge; the other parameter to be considered is the TDDB, which describes how long they can stay in these conditions without breaking down, or getting shorted.

The phenomenon of TDDB is poorly understood, but once again, it is thought to be caused by mobile defects in the material. A ferroelectric RAM using a nondestructive readout with cells maintained continuously at 5.0 V can be fabricated if the TDDB could be completely eliminated. One idea is to make ultrapure ferroelectric memories with virtually no mobile ions by molecular beam epitaxy (MBE) technique.

In summary, the electrical degradations that prevent the PZT ferroelectric from being used in memory are mainly fatigue, leakage current, retention and TDDB. The property requirements for non-volatile memory applications for a capacitor with capacitor size 1 μm × 1 μm and thickness 0.1 μm are:

1. Dielectric Constant: 300
2. Coercive Field ≤ 75 kV/cm ($V_c = 0.75$ V)
3. Remanent Polarization ≥ 10 $\mu C/cm^2$
4. Fatigue Life ≥ 10^{12} cycles
5. Leakage Current ≤ 2×10^{-7} A/cm^2
6. Breakdown Field ≥ 1 MV/cm

1.3 PZT Ferroelectric Materials

The PZT materials has highly desirable physical and electrical properties. Among them are high resistance due to their tight crystal lattice, thermal and chemical stability,

high Curie point exceeding 350°C, typical ceramic hardness, high spontaneous polarization and easy integration with the CMOS transistors. The word PZT refers to lead zirconate titanate, a wide range of compositions from pure lead titanate to lead zirconate. Fig.1.3 and Fig.1.4 show the crystal structure and the phase diagram of the PZT system. As Zr replaces Ti in $PbTiO_3$, the amount of tetragonal distortion (c/a ratio) decreases. At about 53 mol% $PbZrO_3$, an abrupt change in the crystal structure of the solid solution is observed and the composition at this morphotropic phase boundary (MPB) achieves maximum dielectric constant and ferroelectric effects and thus it has attracted most interest. Solid solutions higher in $PbZrO_3$ content than 53 mol% have rhombohedral crystal structure while at lower content have tetragonal structure. At $PbZrO_3$ content higher than 90 mol%, the crystal structure is orthorhombic. The tetragonal and rhombohedral phases are ferroelectric, while the orthorhombic phase is antiferroelectric.

There are several considerations in picking a right technique to deposit the PZT films. First of all, the desirable phase and electrical properties should be achieved, with as low a processing temperature as possible. Secondly, the cost should be low while the throughput for volume production should be high. For PZT materials, the amorphous phase transforms to the pyrochlore phase first, then to the perovskite phase at an elevated temperature. Only the perovskite phase has its remarkable ferroelectric properties. A successful deposition technique for PZT should achieve the complete perovskite phase at a temperature as low as possible.

Solution deposition uses material's soluble or liquid compounds as precursors. A solution is made with a desired composition and deposited on a substrate directly by spin coating. Later heat treatment is employed to remove the volatile impurities and achieve the desired phase of the material. The advantages of this technique are obvious: the composition of the solution can be accurately controlled, the deposited film is very

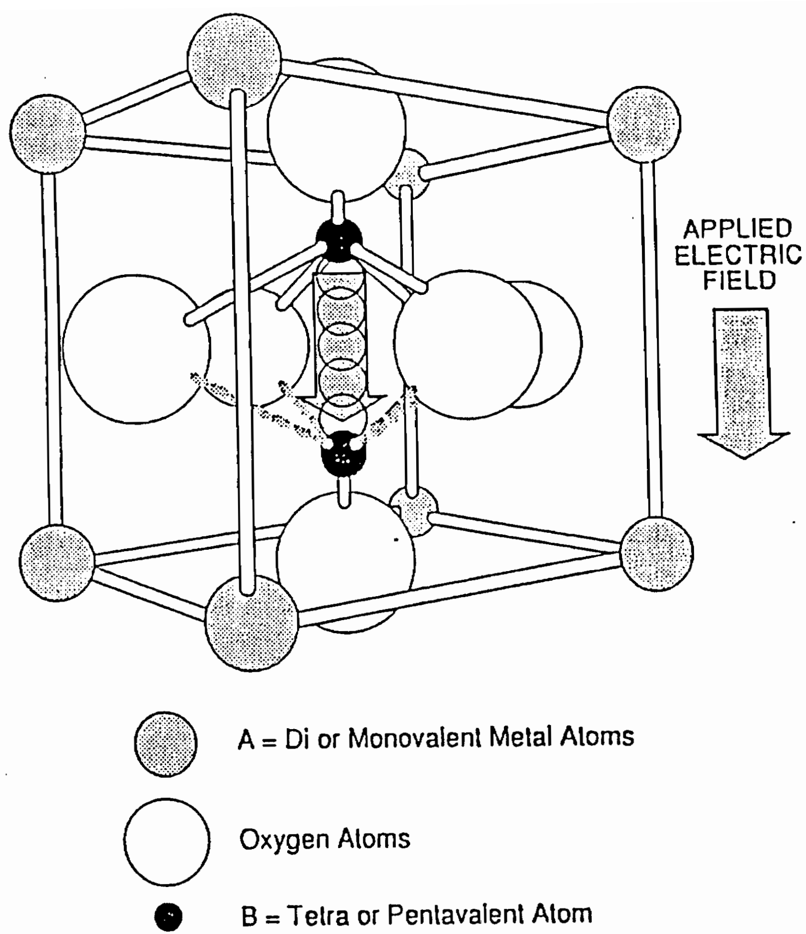

Fig. 1.3 Ferroelectric Perovskite Crystal Type ABO_3

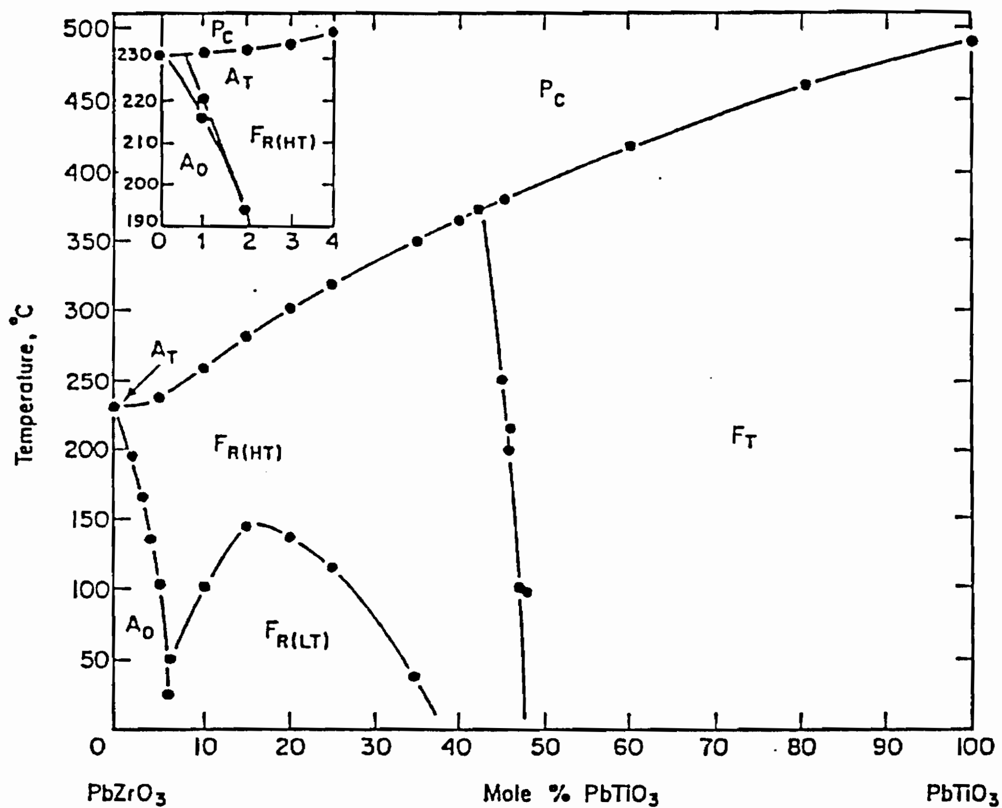

Fig. 1.4 Lead Zirconate-Lead Titanate Phase Diagram

homogeneous, the cost of the processing is low and dopants can be introduced very easily. The commonly used solution deposition techniques are metal organic decomposition (MOD) and sol-gel. The differences between these two are not only the different precursors they use, but also the hydrolysis and gelation in the sol-gel technique which is not seen in the MOD. Hydrolysis will decrease the number of C-H bonds in the sol-gel solution, therefore the film contraction during the annealing will be smaller than the film prepared by the MOD method. The sol-gel technique is used in this study to prepare varied composition of PZT films.

1.4 Research Objectives

PZT ferroelectric materials have some major drawbacks that keep them from being used in memory systems, most of which are memory reliability problems. For DRAM applications, the reading is nondestructive so that a constant voltage is adding on the capacitor cell all the time. Leakage current and TDDB will occur under these circumstances and cause material failure. In the nonvolatile memory FRAM application, the reading is destructive and the charge is stored in an open circuit; fatigue and retention are the major concerns.

The objective of this study is to decrease the PZT electrical degradation for DRAM and FRAM applications. Two ways were employed to achieve this goal: by using RuO_2 electrode materials and by introducing donor La and Nb into PZT structure. Five parameters were studied in this research: Zr/Ti ratio, excess lead amount, electrode materials (Pt or RuO_2), annealing temperature, and La and Nb doping amount. An attempt was made to achieve the best electrical properties of PZT by optimizing these composition and processing conditions.

Chapter 2. Electrical Properties of Sol-Gel Derived PZT Thin Films on RuO_2 Electrodes

Abstract

Ferroelectric lead zirconate titanate ($Pb(Zr_xTi_{1-x})O_3$) thin films were prepared by a sol-gel method and deposited on RuO_2 electrodes using spin-coating. The phase transformation behavior and electrical properties were studied with regard to the Zr/Ti ratio, excess lead, and annealing temperature. The results indicated that the phase transformation of PZT on RuO_2 was similar to that on Pt electrodes. The fatigue endurance of PZT films on RuO_2 increased significantly compared to those on Pt electrodes. However, the leakage current of RuO_2/PZT/RuO_2 capacitors is slightly higher than that of Pt/PZT/Pt capacitors.

2.1. Introduction

Ferroelectric materials are useful for nonvolatile FRAM and high density DRAM because of their hysteresis properties and high dielectric constant, respectively. However, PZT materials show early fatigue on Pt electrodes which comes from the movement and entrapment of the defects (mainly oxygen vacancies) resulting from the processing of PZT thin films. The PZT thin film forms a Schottky barrier with Pt electrode due to large work function differences, and the resulting space charge of the Schottky barrier can trap oxygen vacancies. This results in the deterioration of the ferroelectric properties.

Desu et al. used RuO_2 electrodes in place of Pt electrodes and achieved very good fatigue endurance of the PZT thin films [17]. RuO_2 can form nonstoichiometric compound

RuO_{2-x} without considerable change on their conductivities, therefore the oxygen vacancies will be accommodated in the RuO_2 structure without forming an insulting layer at the PZT-electrode interfaces. The fatigue endurance of the PZT films thus improves significantly. In this study, an attempt was made to completely characterize PZT films on RuO_2 electrodes. The PZT pyrochlore to perovskite phase transformation temperature, hysteresis properties, fatigue endurance and leakage current were investigated with regard to the Zr/Ti ratio, excess lead and annealing temperature of the PZT films.

2.2. Experimental Procedure

The Zr/Ti ratios studied here were: 0/100, 20/80, 30/70, 40/60, 50/50, 60/40, 80/20, 100/0. Three different excess lead proportions of 2, 5, and 10 at.% were added to the solution to compensate the lead loss during the heat treatment of PZT. Five different annealing temperature of 500°C, 550°C, 600°C, 650°C, and 700°C with a fixed time of 30 minutes were also studied to identify the complete pyrochlore to perovskite phase transformation temperature.

The RuO_2 films were deposited on oxidized silicon wafers. A 100 to 120 nm SiO_2 buffer layer was formed by wet-oxygen oxidation silicon wafer in the furnace at 950°C for 1 hour. The bottom electrode of RuO_2 was reactively sputtered onto the oxidized silicon substrate in an oxygen atmosphere using a pure Ru target. The ratio of the argon and the oxygen flowing rate was 4/1, and the pressure of the sputtering chamber was kept at 2×10^{-4} Torr while the substrate temperature was maintained at 200°C during the sputtering. The sputtering current was 200 mA and the RuO_2 film thickness thus obtained was about 500 nm at a deposition rate of 50 nm/min [17]. The films were annealed at 650°C for 30 min to release the internal stress and achieve the stoichiometric RuO_2 after the sputtering.

The PZT solutions were made by a sol-gel method and later deposited on the RuO_2 electrodes by spin coating. The films were annealed at different temperatures to achieve the ferroelectric perovskite phase. Circular RuO_x top electrodes (dia=0.006 in.) were deposited on the annealed PZT films using a stainless steel shadow mask for electrical property measurements.

The sol-gel method used to prepare the PZT films was first suggested by Yi, Wu and Sayer [18], and then modified by Kwok et al. [21] to achieve more uniform film microstructure, longer solution shelf life and better electrical properties. Fig.2.1 shows the flow chart of this modified sol-gel method for PZT film preparation that was used in this study. The precursors used to make the sols were Zr n-propoxide and Ti i-propoxide. Lead was added in the form of lead acetate hydrate. Gels arised from the hydrolysis and condensification of these alkoxides under the catalysis of an acid or a base [19].

The solution was filtered through a 0.45 μm filter and then deposited on the RuO_2 electrodes by spin coating at a speed of 2000 rpm for 30 seconds. The coated film was baked on a hot plate at 150°C for 5 minutes to remove the organic solvent. A 0.4 M solution was made. The spin-coating and baking cycles were repeated four times to obtain a thickness of about 450 nm film.

The hysteresis properties and fatigue endurance of the RuO_x/PZT/RuO_2 capacitors were characterized using the standardized RT66A system. The bottom electrode was exposed by scratching out the PZT films using a diamond pen. The hysteresis properties measured in this experiments were under the applied voltage of 5 V, which is less than the saturating voltage. The electric field thus applied is about 111 kV/cm, which is close to the electric field actually used in the reading and writing of the semiconductor memories (0.75 V for a 100 nm film, or 75 kV/cm). In the fatigue properties measurement, a 5 V square wave with a frequency of 10^6 Hz was employed.

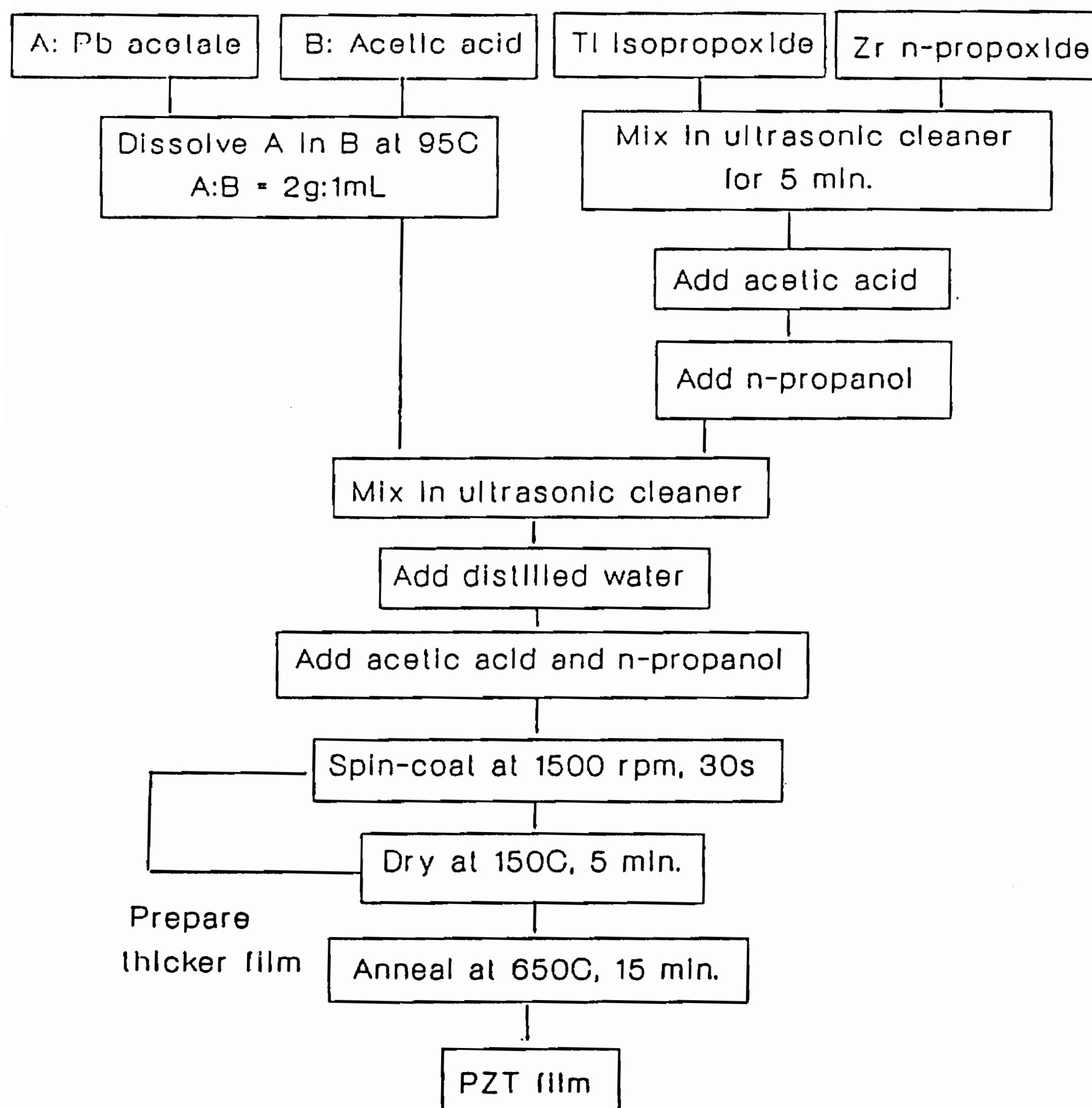

Fig. 2.1 Modified PZT Sol-Gel Process

The total number of switching cycles could be up to 10^{11} for 10^5 seconds. The leakage current was characterized using a computer-controlled electrometer at which only the stabilized current was recorded at a given electric field.

X-ray diffraction patterns were taken for all samples after annealing from a 2θ value of 20° to 60°. The pyrochlore phase shows its (222) peaks at a 2θ of 29.5°. The complete phase transformation of a given PZT composition is evidenced by the complete disappearance of this peak. A Philip STEM system was used to examine the microstructure of the PZT films after annealing. Secondary electron signal was used to investigate the topography of the PZT films while the backscattered electron signal was used to investigate the grain structure. The operating voltage was 20 kV.

2.3. Results and Discussions

A. Composition and Microstructure Characterization

Fig.2.2 shows the XRD patterns of two samples annealed at different temperatures, one has the composition of Zr/Ti=80/20 with 2 at.% excess lead, the other has the composition of Zr/Ti=50/50 with 10 at.% excess lead. It shows that the temperature T_c^{Per} at which perovskite phase is completely formed for the 50/50 sample is 600°C, while for the 80/20 sample T_c^{Per} is 650°C. In other words, samples with different composition and excess lead require different heat treatments to complete the same phase transformation.

The PZT pseudo phase diagrams with different excess lead content are shown in Fig.2.3. The curves plot the T_c^{Per} as a function of Zr/Ti ratio and excess lead. The phases present below the curves are mixtures of the pyrochlore and perovskite phases, while

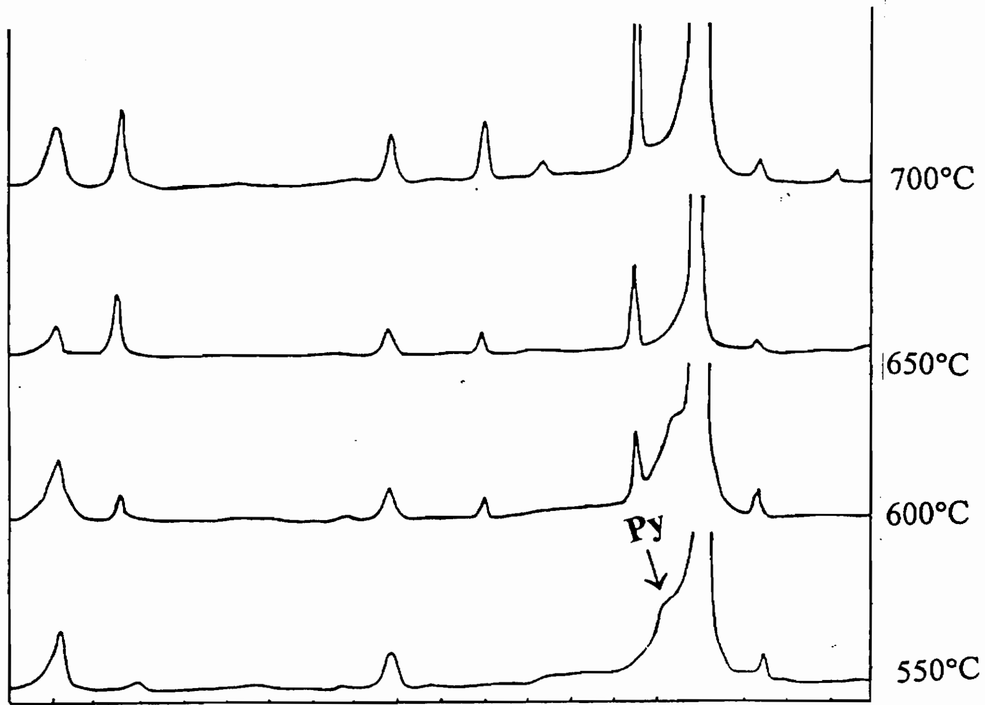

PZT: 80/20 (2% excess lead)

PZT: 80/20 (2% excess lead)

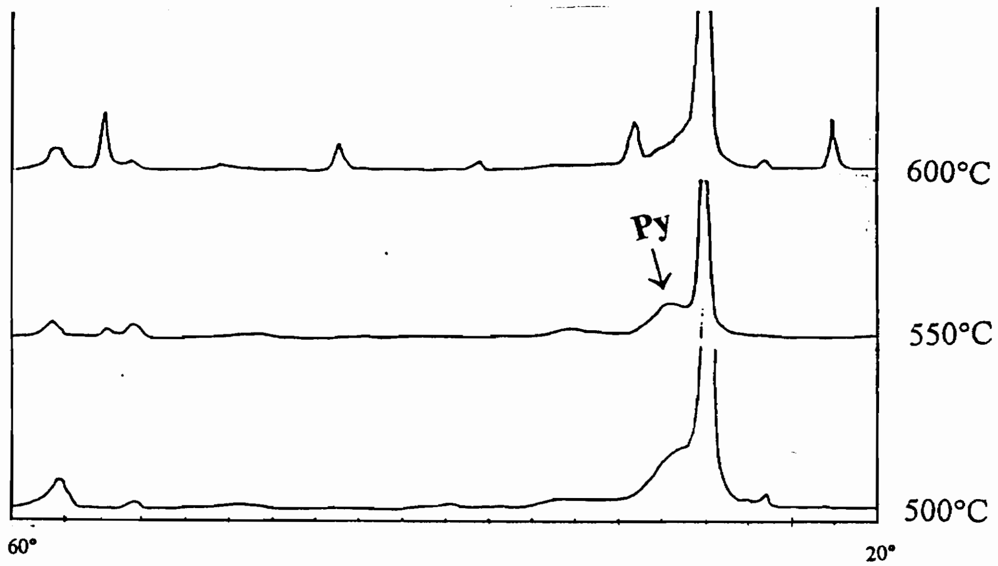

PZT: 50/50 (10% excess lead)

Fig. 2.2 PZT XRD Patterns (1)

above the curves pure perovskite was formed.

Kwok et al. have published the curves for the T_c^{Per} as a function of Zr/Ti ratios on Pt electrodes [20]. It shows the same trend for PZT thin films on RuO_2 electrodes. T_c^{Per} increases as the Zr/Ti ratio increases. For pure lead titanate, 500°C or even lower for 30 min is enough for the formation of the perovskite phase, while for the pure lead zirconate, T_c^{Per} has to go up to 650°C. The 10 at.% excess lead pseudo phase diagram shows a 600°C flat step at compositions around the MPB, i.e., from a Zr/Ti ratio of 30/70 to 60/40.

The ferroelectric phase transformation is a two-step process involving the nucleation and growth of the perovskite phase. In the first step, the formation of nuclei requires the formation of an interface between the perovskite phase and the pyrochlore matrix, so the interface energy is the barrier to nucleation. When the particle has reached the critical size where the overall interface energy is equal to the overall volume energy decrease, the free energy of the system begin to favor larger nuclei and grain growth begins. This is the second step. The nucleation rate of the pure lead titanate perovskite phase is very high due to the low pyrochlore-perovskite interface energy γ. As the Zr/Ti ratio increases, this interface energy γ increases. In other words, the nucleation barrier will increase with the Zr/Ti ratio. Less nuclei will form for higher Zr/Ti ratios, and thus the grain size will become larger. The perovskite phase transformation will be completed much faster if the nucleation rate is high. A higher temperature will have to be employed for samples with a high nucleation barrier, therefore the complete perovskite phase transformation temperature will increase with the Zr/Ti ratio.

The different amounts of excess lead also play an important role on the phase transformation. The pseudo phase diagrams for different amount of excess lead do not show any differences for Zr/Ti ratios lower than 40/60 or higher than 80/20. At the

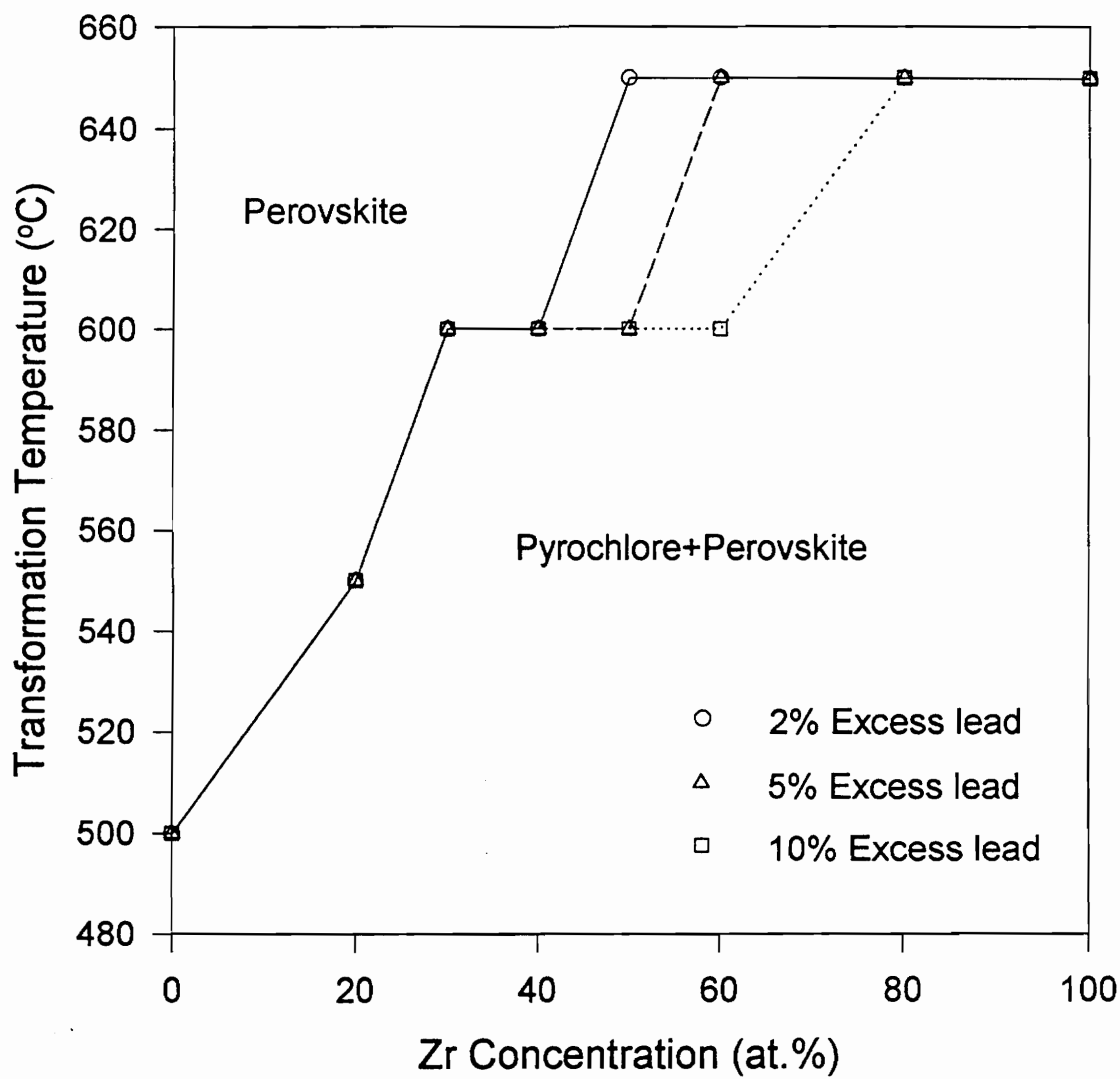

Fig. 2.3 Pyrochlore Stability Region

composition of 50/50, 2 at.% excess lead PZT requires a T_c^{Per} of 650°C while 5 at.% and 10 at.% excess lead samples require a T_c^{Per} of 600°C. At the composition of 60/40, 5 at.% and 10 at.% excess lead curves separate out with the 5 at.% excess lead samples requiring a T_c^{Per} of 650°C while the 10 at.% excess lead samples require a T_c^{Per} of 600° C. It can be concluded that the excess lead only functions in the composition around the MPB, and the higher the content of the excess lead, the lower the T_c^{Per}.

Fig.2.4A shows the XRD diagram of 50/50 composition with 2 at.% and 5 at.% excess lead, and Fig.2.4B shows that of the 60/40 composition with 5 at.% and 10 at.% excess lead. The difference in the T_c^{Per} can easily be seen.

It is possible that excess lead accelerates the perovskite phase transformation by the formation of a low melting point compound with the PZT. From the PbO-TiO_2 phase diagram derived from powder processing, a eutectic compound with a melting point of 830°C can be found at a composition of about 90 at.% PbO and 10 at.% TiO_2. This temperature will be much lower for the sol-gel derived samples. Small amounts of liquid could form at the grain boundaries of the sol-gel derived PZT at temperatures as low as 600°C. For Ti-rich PZT, the nucleation rate is high and the grain growth rate is not as important for the completion of the phase transformation. For Zr-rich PZT, however, the PbO-TiO_2 eutectic liquid is hard to form. Therefore, no significant excess lead effect on T_c^{Per} was observed for samples in these two regions. When the composition falls in the region around the MPB, however, the grain growth rate will determine the rate of the perovskite phase transformation, and the excess lead effect shows up.

Fig.2.5 shows the SEM micrographs of lead titanate and the 30/70 composition, both with 10 at.% excess lead and 650°C annealing temperature. The secondary electron mode and a 50,000 magnification were used in these two samples. For the case of lead titanate, the grains are well developed with small pin holes seen in the grain boundary

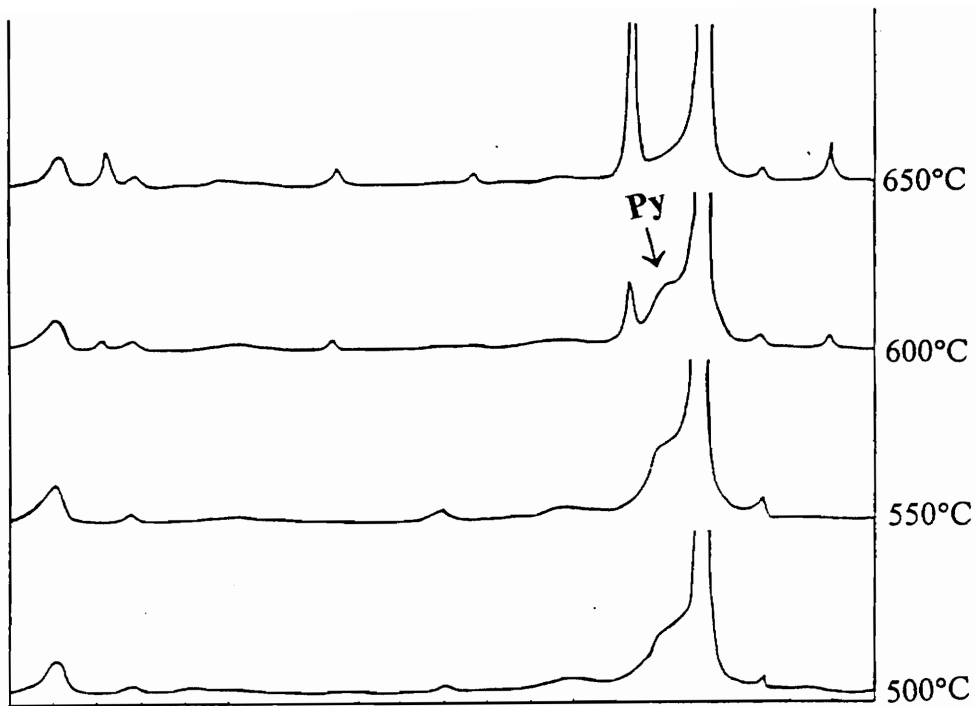

PZT: 50/50 (2% excess lead)

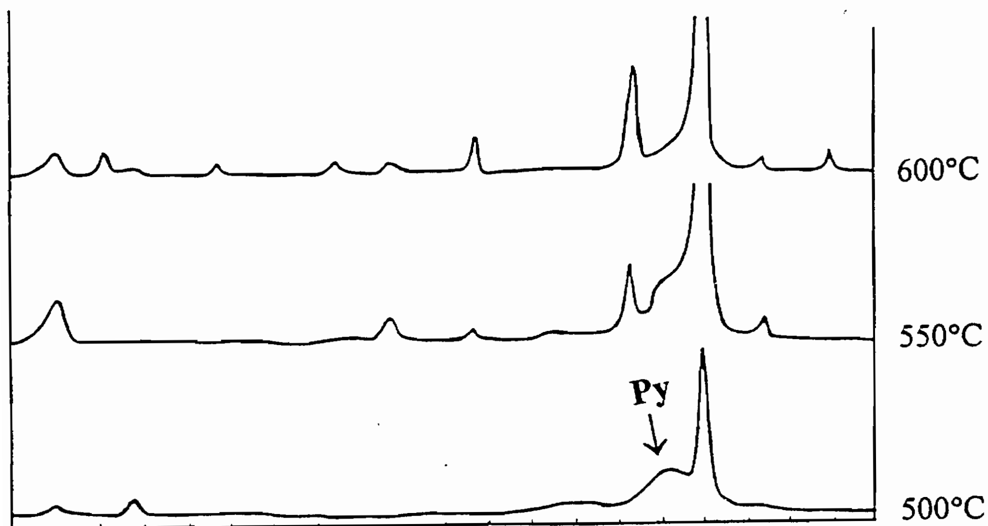

PZT: 50/50 (5% excess lead)

Fig. 2.4A PZT XRD Patterns (2)

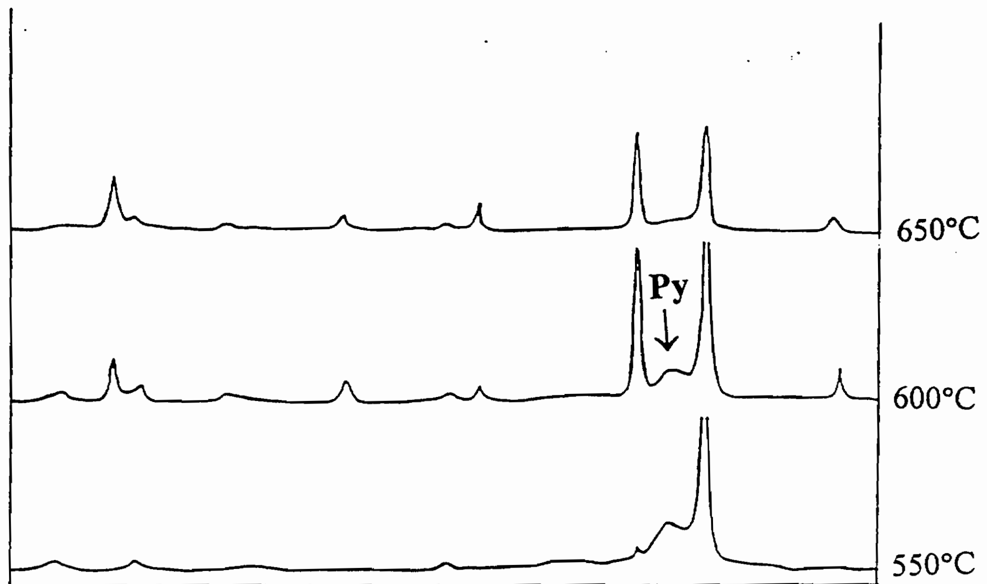

PZT: 60/40 (5% excess lead)

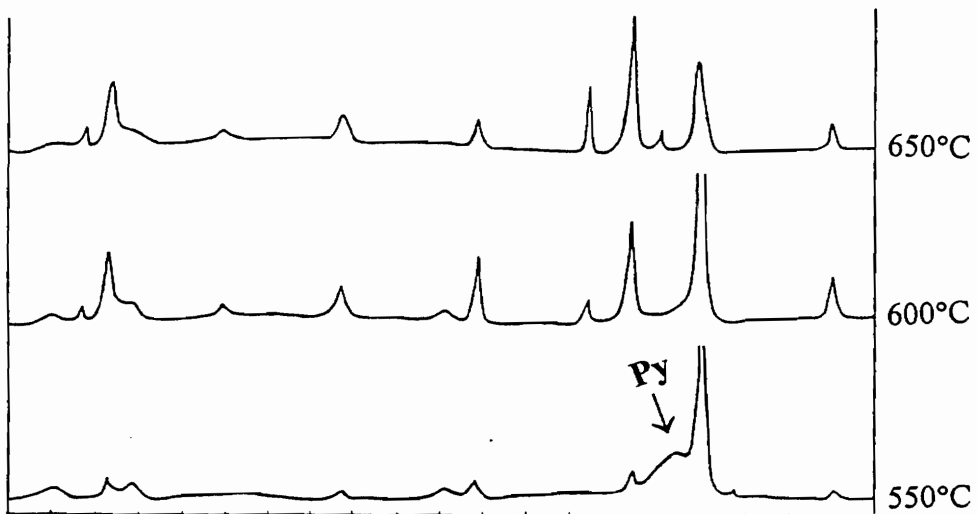

PZT: 60/40 (10% excess lead)

Fig. 2.4B PZT XRD Patterns (3)

region. For the 30/70 PZT sample, the surface is very smooth and the grain size is much larger than that of the lead titanate sample. In Fig.2.6, the 50,000 magnification SEM micrographs of a 40/60 composition with 5 at.% excess lead annealed at 700°C and a 60/40 composition with 10 at.% lead annealed at 650°C have been compared. The 40/60 composition micrograph is in secondary electron mode with a 45° tilt, while the 60/40 composition is in backscattered electron mode. Both of them show a well developed grain structure, but the grain size of the 60/40 sample is larger than that of the 40/60 sample. Fig.2.7 shows another comparison of 30/70 and 80/20 with 10 at.% excess lead annealed at 650°C. Once again the 80/20 sample has a larger grain size than that of the 30/70.

The grain size of the PZT thin films on RuO_2 electrode will increase with the Zr/Ti ratio of the PZT composition. This is also true for films on RuO_2 electrodes. The high nucleation rate will make the phase transformation faster and hence PZT with lower Zr/Ti ratio can complete the phase transformation at lower temperatures.

Fig.2.8 shows the microstructure of the 50/50 sample with 10 at.% excess lead annealed at different temperatures. All micrographs were taken in backscattered electron mode. The 500°C annealed sample shows no perovskite grains at all. Some sparsely distributed grains can be seen in the 550°C annealed sample. In the 600°C annealed sample, the perovskite grains are well developed, and they grow much larger under the 650°C annealing condition. This result is consistent with the XRD studies that the complete transformation temperature of the PZT 50/50 composition with 10 at.% excess lead is 600°C.

Fig.2.9 is the micrograph of the 50/50 composition with 10 at.% excess lead annealed at 650°C. It was taken in the secondary electron mode with a magnification of 100,000. It shows a thick grain boundary on the surface of the sample. A comparison of the secondaryelectron mode micrograph and the backscattered electron mode micrograph

(a)

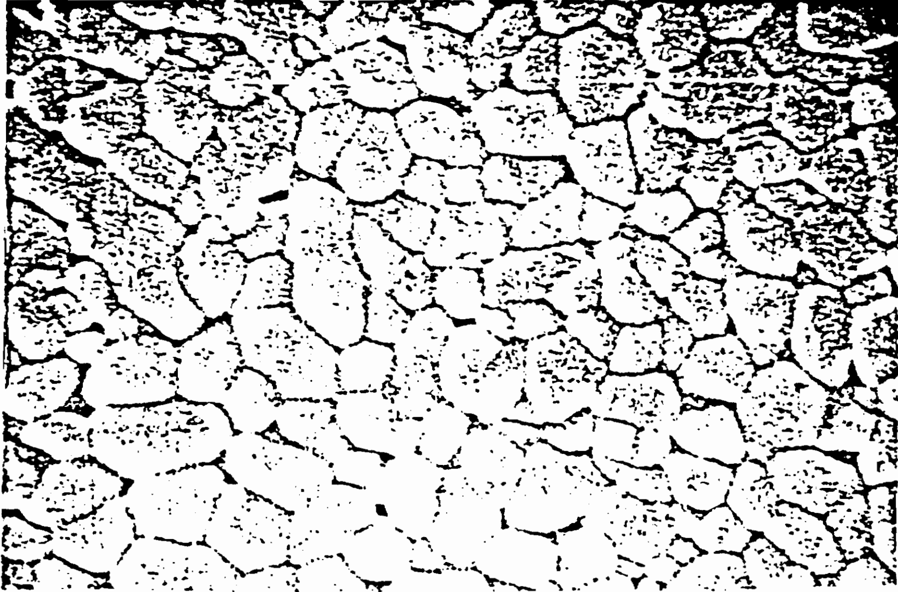

(b)

Fig. 2.5 Microstructure of (a)lead titanate and (b)PZT 30/70, with 10% excess lead annealed at 650°C. mag. ×50,000, SEM SEC mode.

(a)

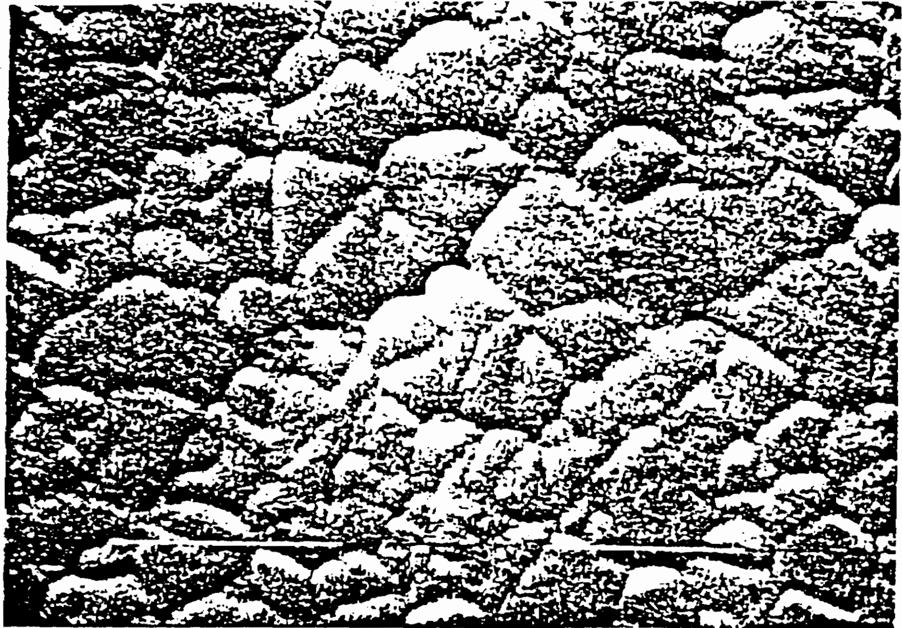

(b)

Fig. 2.6 Microstructure of (a)PZT 40/60 with 5% excess lead annealed at 700°C and (b)PZT 60/40 with 10% excess lead annealed at 650°C. BSC mode.

(a)

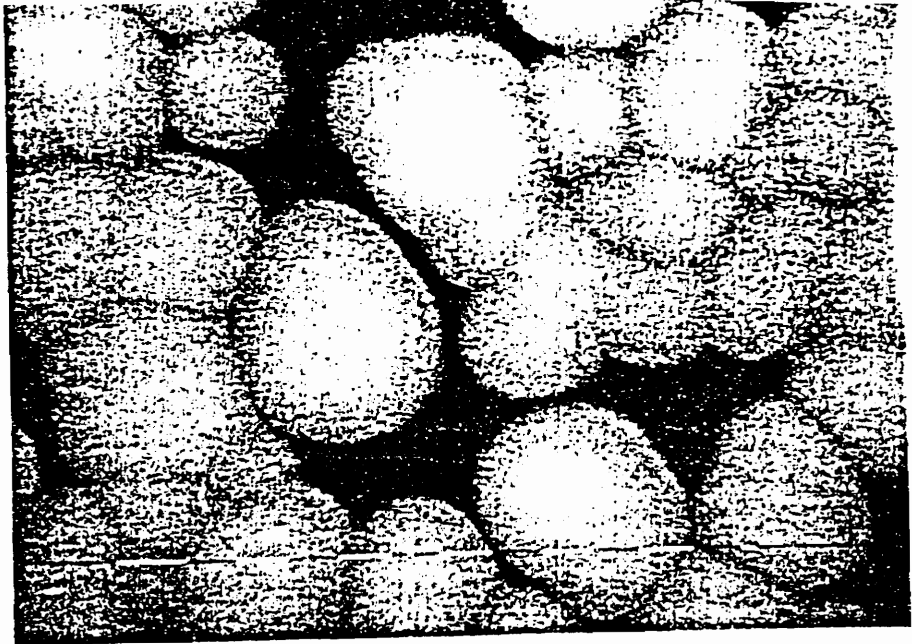

(b)

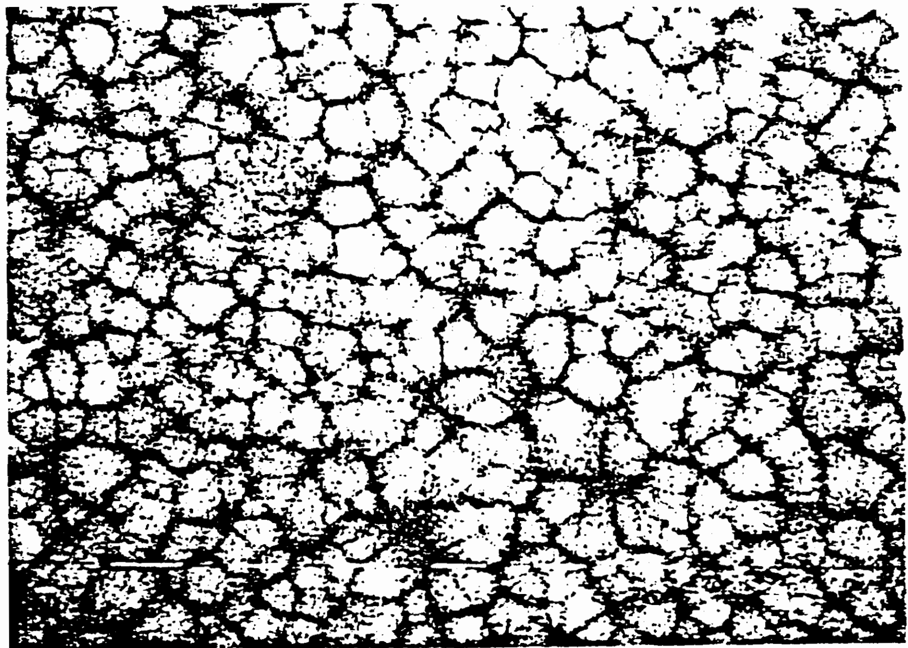

Fig. 2.7 Microstructure of (a)PZT 80/20 and (b)PZT 30/70, with 10% excess lead annealed at 650°C mag. ×50,000, SEM BSC mode

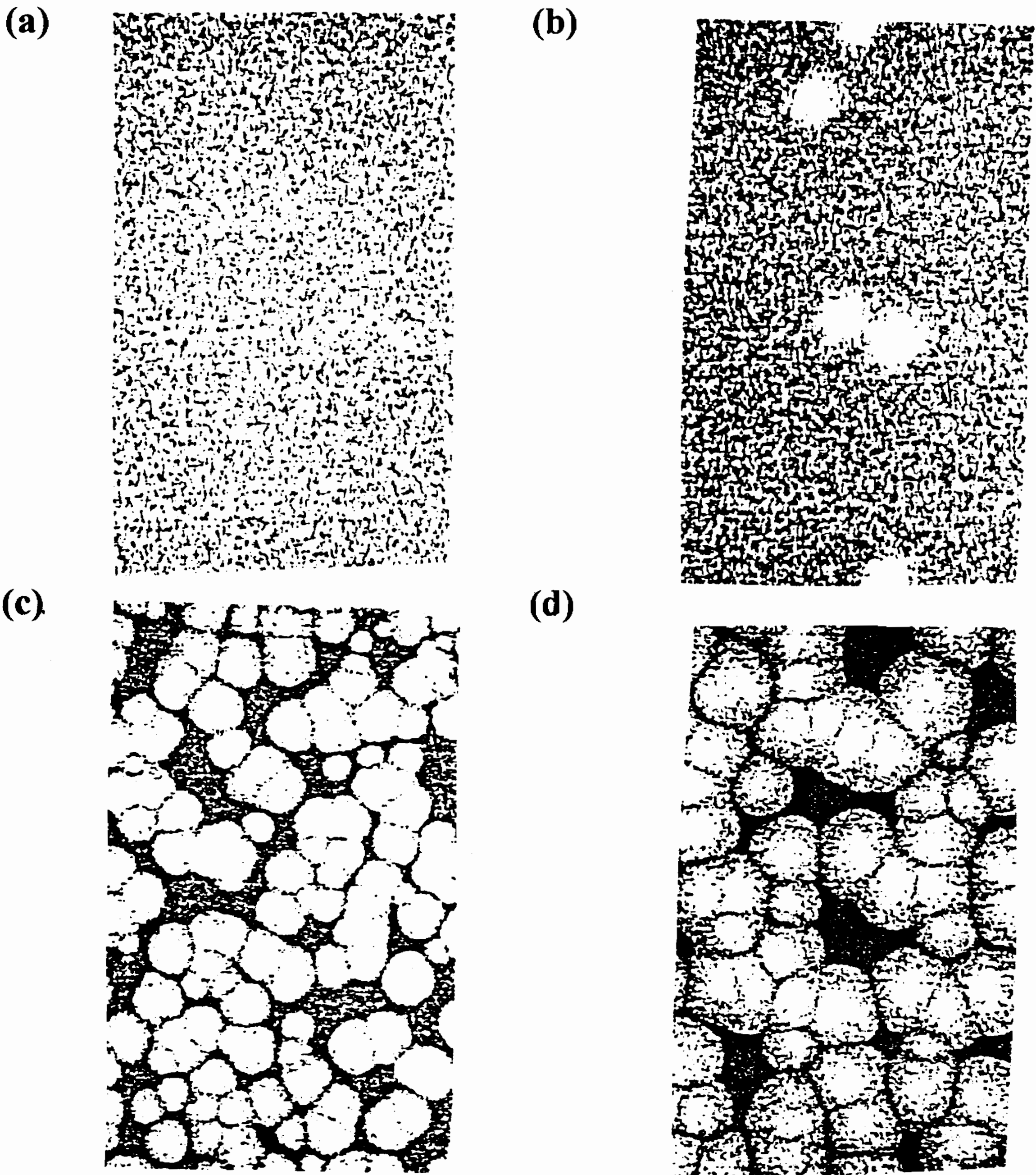

Fig. 2.8 Microstructure of PZT 50/50 with 10% excess lead annealed at (a)500°C, (b)550°C, (c)600°C and (d)650°C. mag. ×12,500, SEM BSC mode

is also shown in Fig.2.9 at a magnification of 50,000. The grain boundary area shows up dark while the grain interior shows up bright in the backscattered image. That means the grain boundary is lead deficient since the lead has the highest Z in PZT and should have a high backscattering coefficient. Fig.2.10 gives two different magnification micrographs for a 60/40 sample with 10 at.% excess lead annealed at 650°C. It can be observed under low magnification that the Pb-deficient grain boundary region is small compared to the grain interior region.

In a TEM study done by Chang it was shown that the grain boundary region for sol-gel derived PZT films is the pyrochlore phase while the grain interior is the perovskite phase [25]. A small amount of pyrochlore phase that could not be detected by XRD still existed after the sample was annealed above the perovskite transformation completion temperature. This is probably due to excess lead residing in the grain boundaries after annealing. On the surface of the PZT sample, the lead in the pyrochlore phase is easier to volatilize than that in the perovskite phase and hence the grain boundary region is lead deficient.

In summary, the XRD analysis of the PZT system shows that the T_c^{Per} increases as the Zr/Ti ratio increases. The excess lead lowers the T_c^{Per} of the PZT in the compositional region around the MPB.

The SEM study of the samples with different Zr/Ti ratio shows that the grain size is a strong function of the Zr/Ti ratio. Pure lead titanate has a very small grain microstructure, and the grain size increases as the Zr/Ti ratio increases.

No significant difference was observed between the pseudo phase diagrams of PZT films on the Pt electrodes and those on the RuO_2 electrodes. The nucleation of the perovskite phase is therefore not very substrate dependent, and can be considered to be homogeneous.

(a)

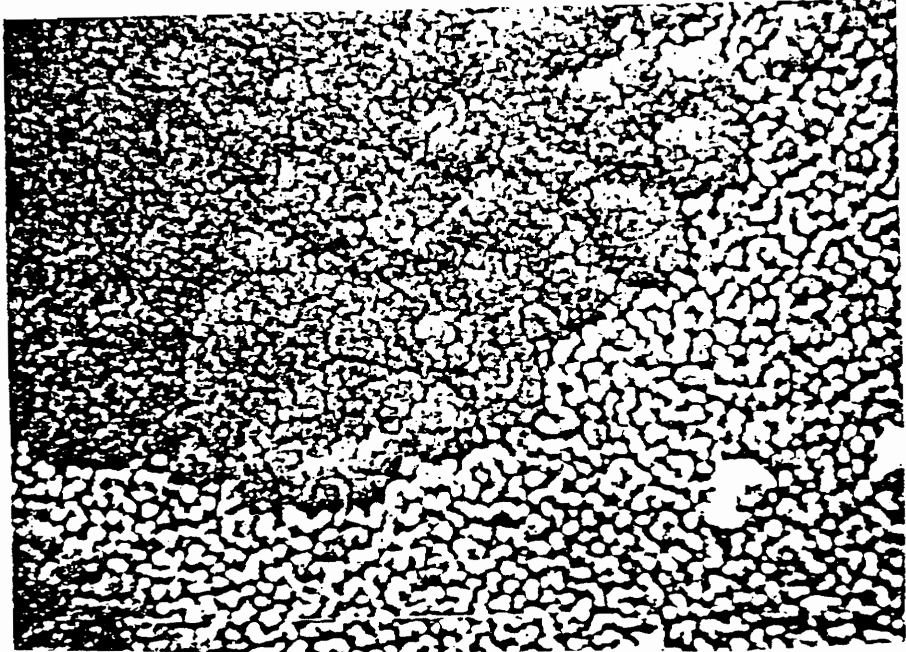

(b)

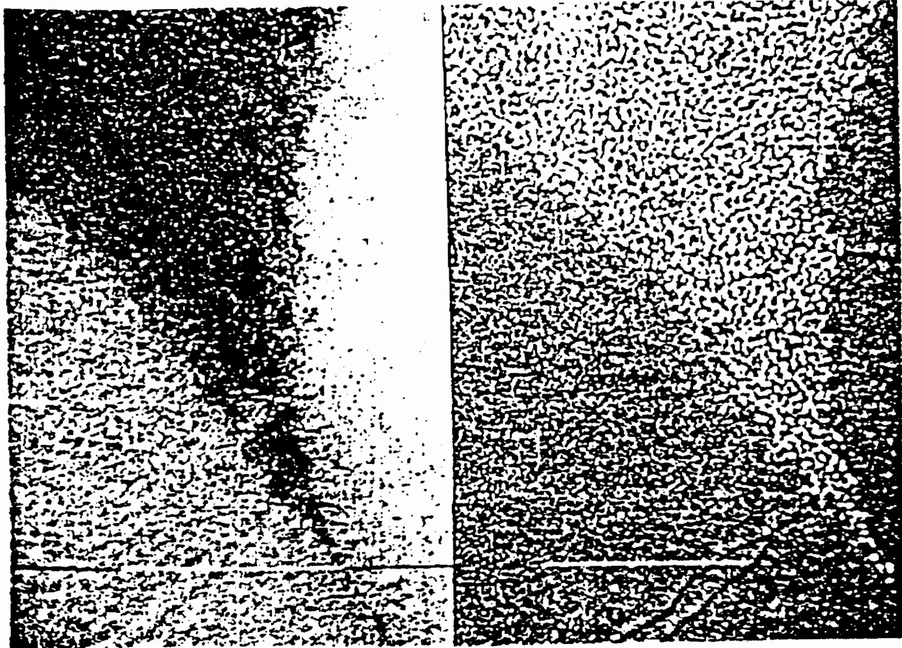

Fig. 2.9 Microstructure of PZT 50/50 with 10% excess lead annealed at 650°C. (a)×10,000 SEC mode, and (b)×50,000, left BSC mode, right SEC mode

(a)

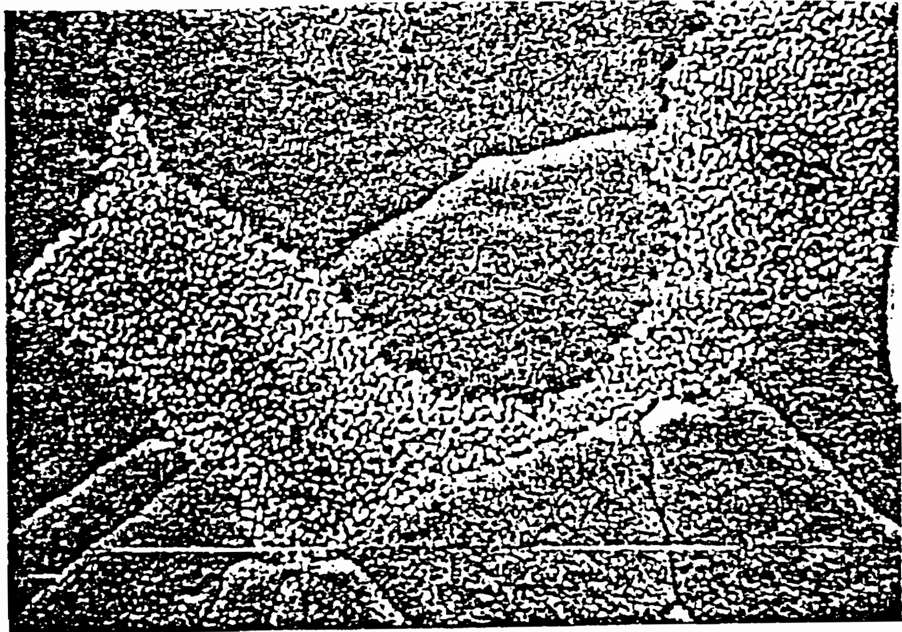

(b)

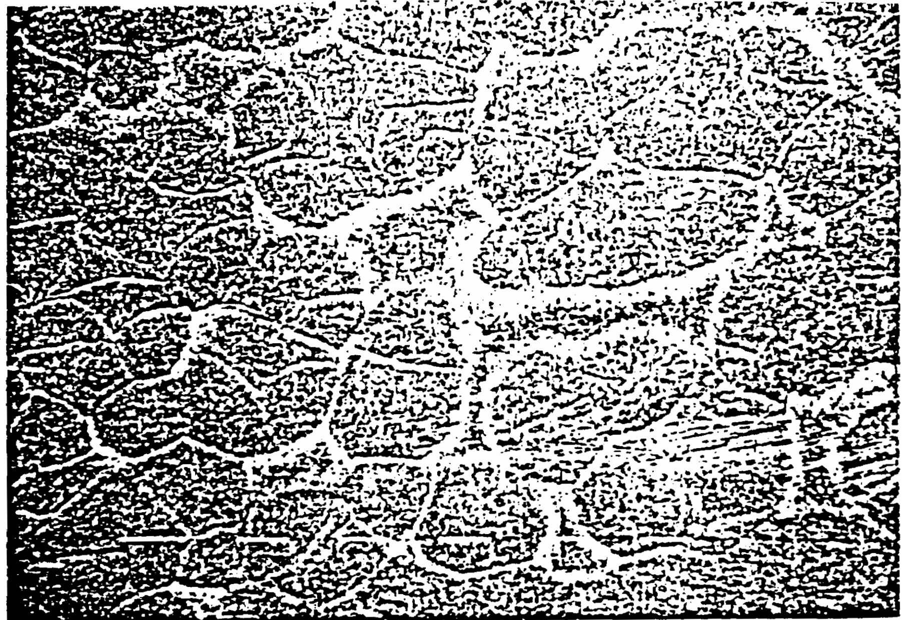

Fig. 2.10 Microstructure of PZT 60/40 with 10% excess lead annealed at 650°C, SEC mode, 20° tilt (a)×50,000 and (b)×12,500

B. Electrical Properties

Hysteresis Properties. The remanent polarization P_r depends largely on the composition of the PZT films. The P_r value increases as the Zr/Ti ratio increases before reaching the morphotropic phase boundary (Zr/Ti=53/47) where it achieves its maximum value, and drops down drastically thereafter. Fig.2.11 and Fig.2.12 show the relationship between P_r and the Zr/Ti ratio under different processing conditions and compositions. For samples annealed at 650°C for 30 min with 2 at.% excess lead, Pr increases from less than 10 $\mu C/cm^2$ at a composition of Zr/Ti=20/80 to about 34 $\mu C/cm^2$ at the composition of Zr/Ti=50/50, then drops down to 22 $\mu C/cm^2$ at Zr/Ti=60/40. Fig.2.12 shows the P_r curve as a function of the composition for samples annealed at 700°C with 5 at.% excess lead, which has the same trend as that in Fig.2.11. Pr achieves its maximum value of 20 $\mu C/cm^2$ at three compositions around the MPB.

Although a series of solutions with different compositions were made, no electrical properties could be obtained from two extreme cases of pure lead titanate and lead zirconate. Lead zirconate is not a ferroelectric but rather an antiferroelectric and thus no hysteresis properties was observed. Lead titanate is ferroelectric. However, the lead titanate samples had very low resistance. The RT66A system is limited to measuring samples with a resistance above 60 kΩ.

Fig.2.13 shows the variation in Pr with annealing temperature for different amounts of excess lead at the composition of Zr/Ti=50/50. The P_r is relatively insensitive to the annealing temperature above 620°C. The highest Pr achieved was 37 $\mu C/cm^2$ for a 620°C annealing temperature with 10 at.% excess lead. Two typical hysteresis loops were shown in Fig.2.14 and 15 for the 50/50 composition with 10 at.% excess lead annealed at 600°C and 700°C, respectively.

The effect of the excess lead on the hysteresis properties is not very clear. No significant difference was observed in the Pr values for 2, 5, and 10 at.% excess lead samples annealed above 620°C. For 50/50 PZT, the 5 and 10 at.% excess lead samples have a T_C^{Per} of 600°C, while the T_C^{Per} for 2 at.% excess lead sample is between 600°C and 650°C. From Fig.2.13 it can be concluded that all samples have completely transformed, since the remanent polarization becomes insensitive to both the annealing temperature and the amount of excess lead.

The curve relating remanent polarization and composition obtained in this study is comparable to that on the Pt electrodes. The remanent polarization achieves its maximum value at the morphotropic phase boundary (MPB), which is the boundary between the tetragonal phase and the rhombohedral phase. The tetragonal phase has six polarization directions and the rhombohedral phase has eight. The MPB composition contains both the rhombohedral phase and the tetragonal phase, therefore has all fourteen polarizations. The domains can switch easier with more polarization directions, resulting in a higher remanent polarization [21].

In summary, the Zr/Ti ratio, the amount of excess lead, and the annealing temperature have different effects on the remanent polarization. The annealing temperature and the amount of excess lead determine the perovskite phase transformation, but by themselves do not have any effect on the remanent polarization. When the phase transformation is complete, the remanent polarization is insensitive to the annealing temperature and the excess lead. An annealing temperature around 620°C or higher is required to achieve the pure ferroelectric phase, and the composition around the MPB (Zr/Ti=53/47) has the best hysteresis properties.

Fatigue Properties. The fatigue properties of the PZT materials are very important for their applications to nonvolatile memories since both the reading and writing

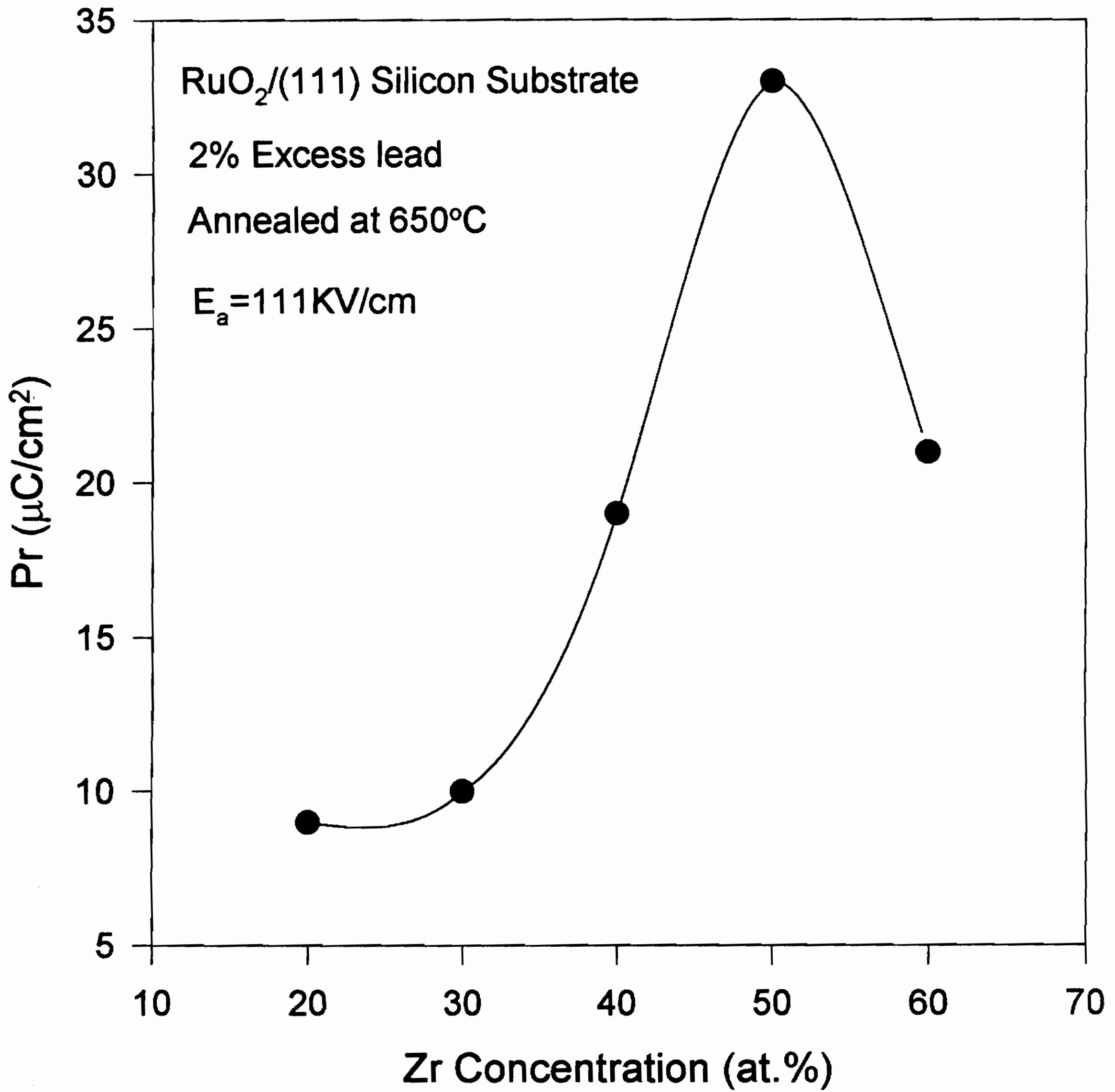

Fig. 2.11 Remanent Polarization as a Function of Zr/Ti Ratio (1)

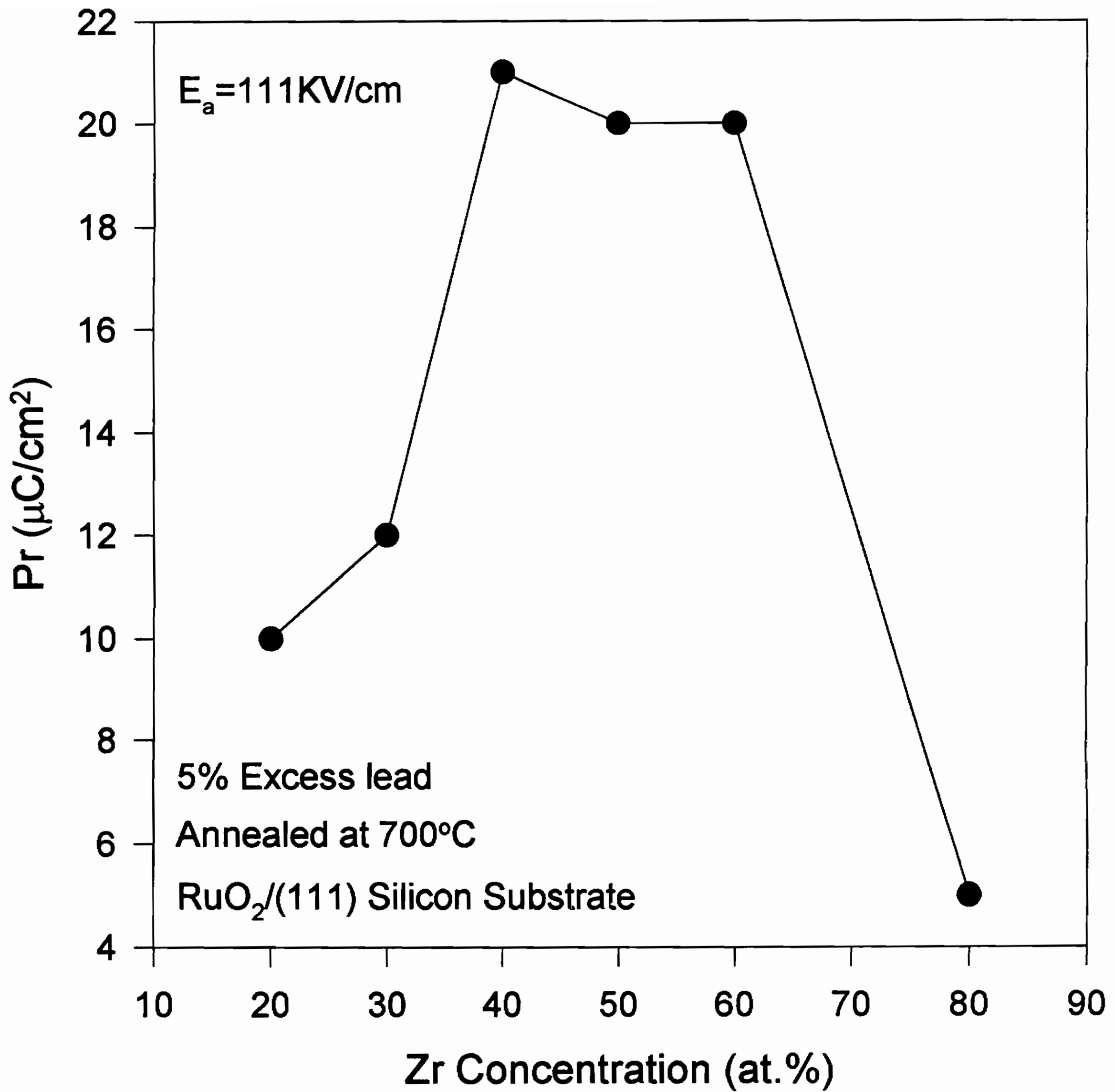

Fig. 2.12 Remanent Polarization as a Function of Zr/Ti Ratio (2)

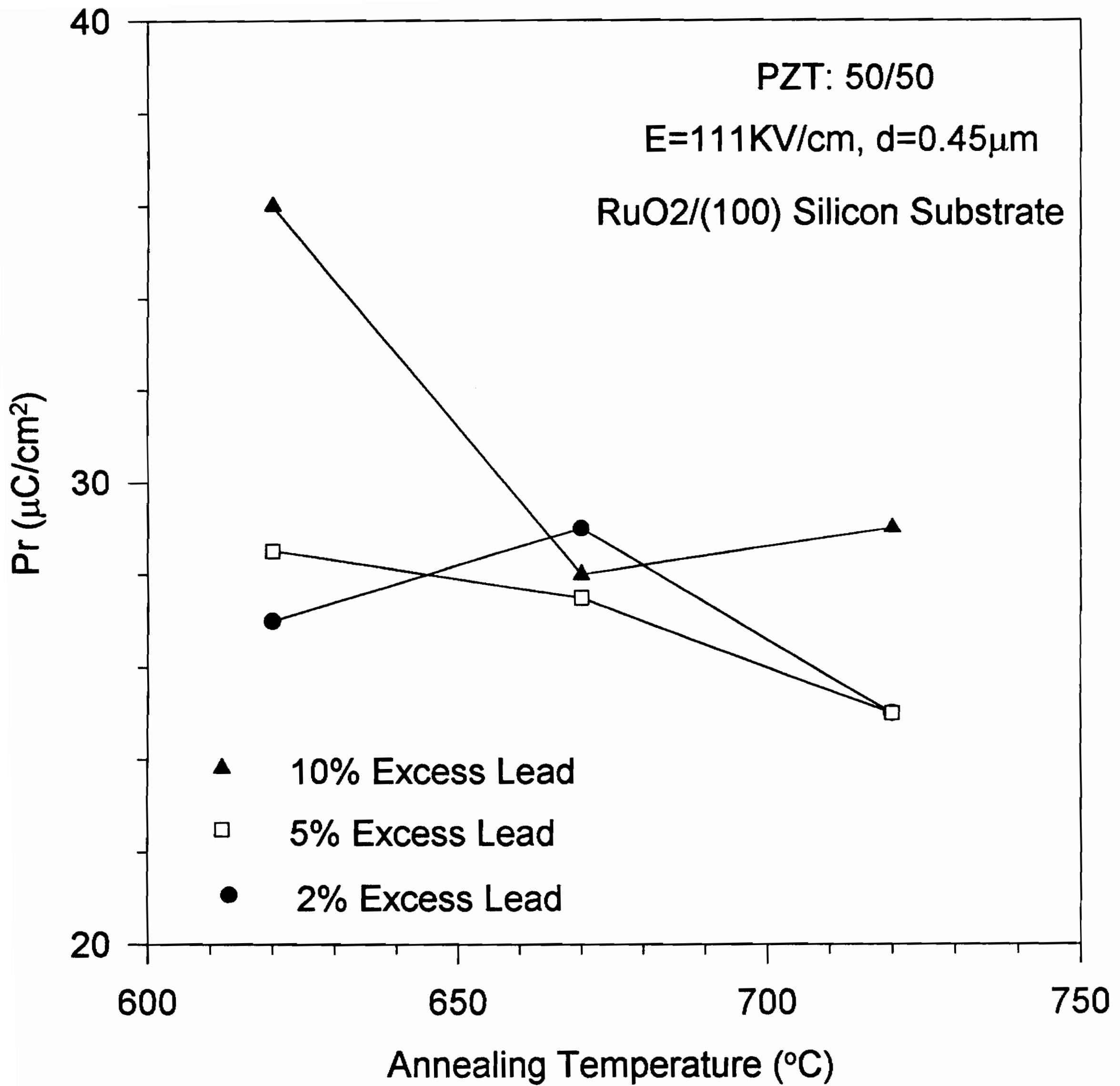

Fig. 2.13 Remanent Polarization as a Function of Annealing Temperature & Excess Lead

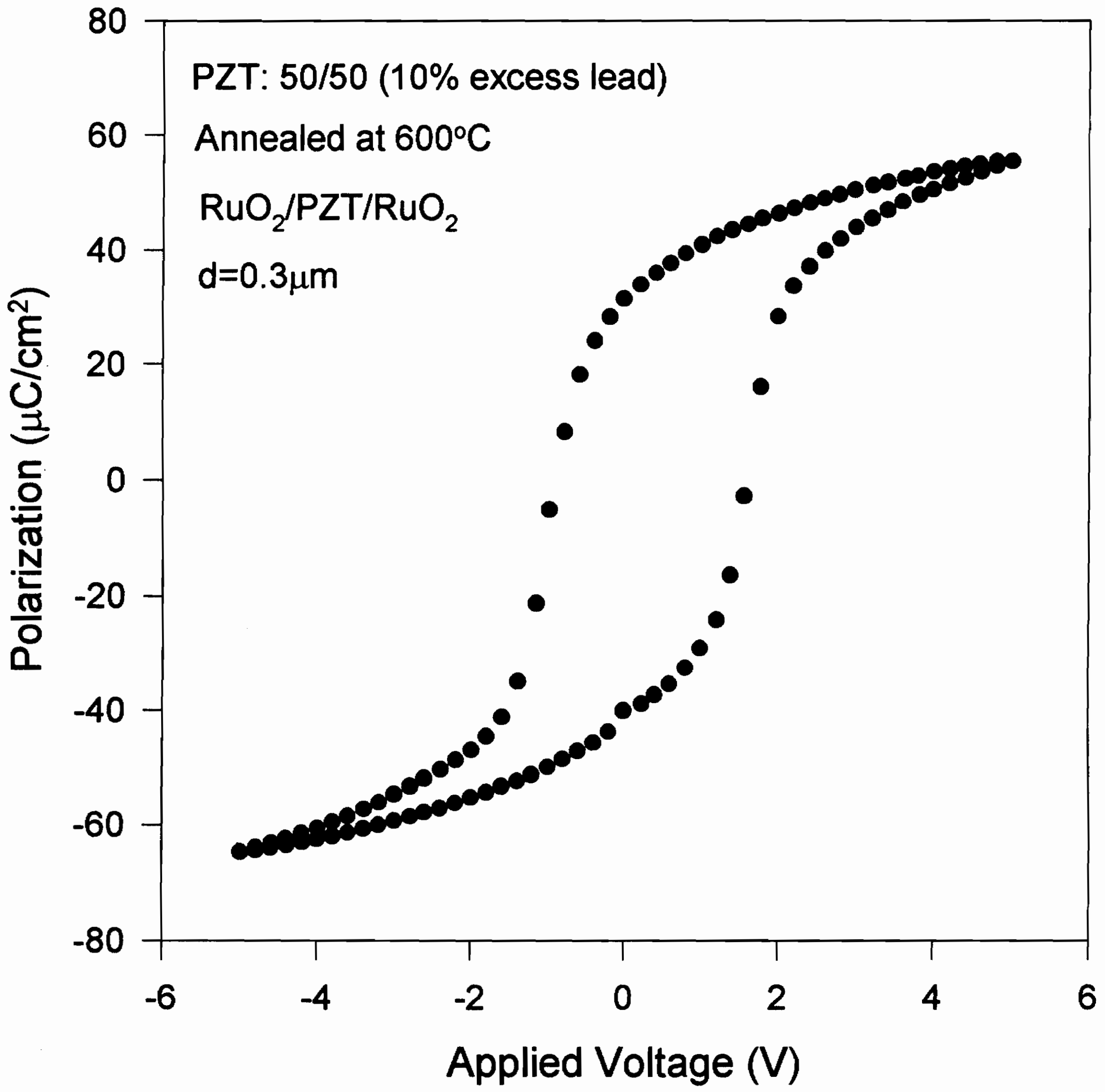

Fig. 2.14 PZT Hysteresis Loop (1)

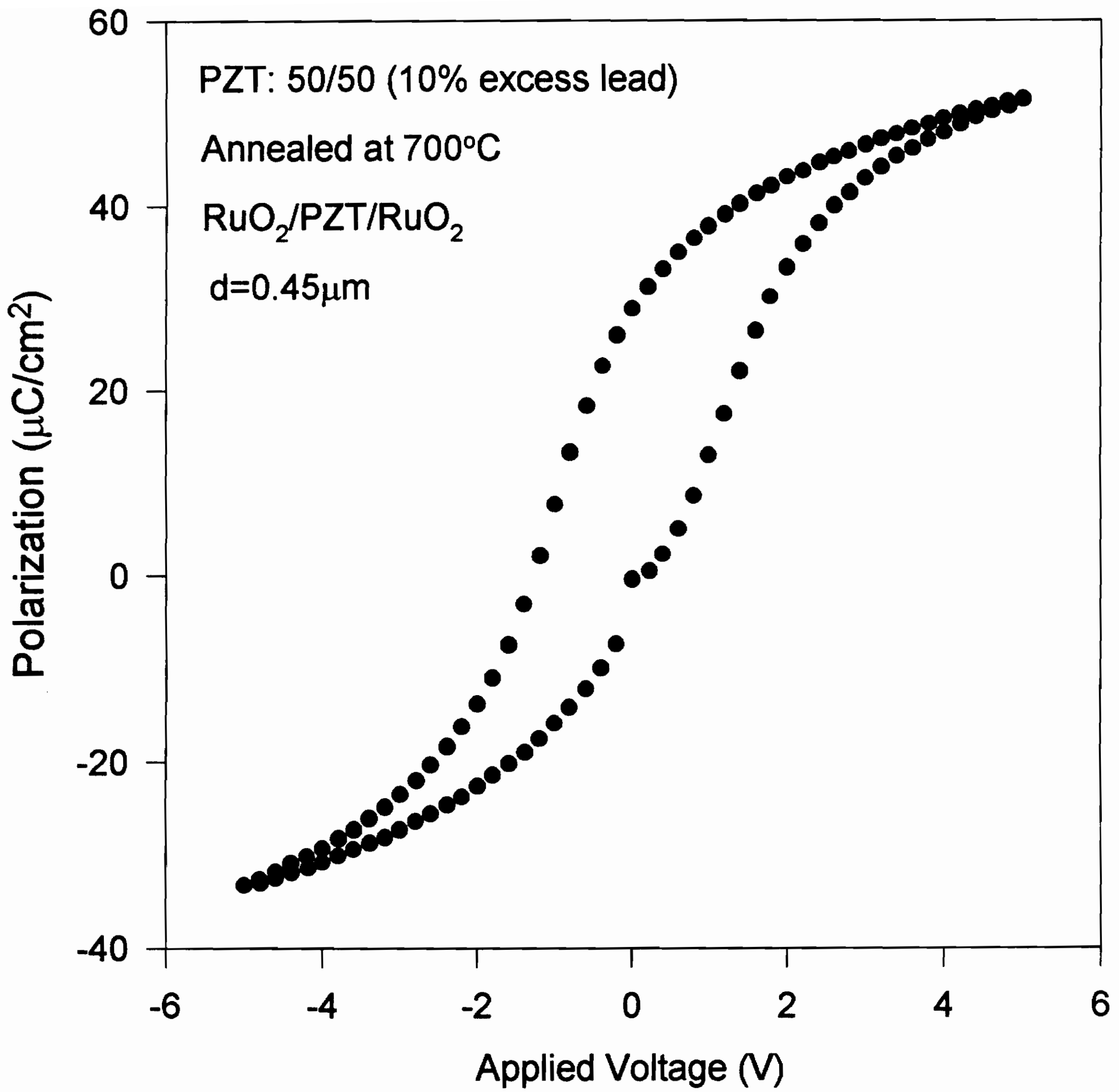

Fig. 2.15 PZT Hysteresis Loop (2)

of a ferroelectric memory may require the memory state to be switched. The life of the memory element is directly related to the number of switching cycles it can withstand. A 10^{12} cycles fatigue endurance for the ferroelectric memories is suggested.

Fig.2.16 shows the fatigue measurement of PZT 50/50 composition with 10 at.% excess lead annealed at 700°C for 30 min. The hysteresis loop obtained is shown in Fig.2.15. No polarization loss was observed for switching cycles up to 10^{11}. The same behavior was observed for other samples in this study up to 10^9 switching cycles. It can be concluded that employing RuO_2 electrodes can improve the PZT endurance up to 10^{11} switching cycles.

Oxygen vacancy movement and their entrapment at the electrode/ferroelectric interfaces are the primary reasons for the fatigue. RuO_2 electrode materials can consume the oxygen vacancies by increasing their oxygen non-stoichiometry and thus, prevent the space charge development at the interface. Therefore, the fatigue endurance of PZT on RuO_2 electrodes has been greatly improved.

Leakage Current. Fig.2.17 shows the effect of annealing temperature on the leakage current. The leakage current has the lowest value of 40 nA/cm^2 for the samples annealed at a temperature of 550°C. The leakage current increases by about one order of magnitude for samples annealed at 600°C and 650°C. The 600°C and 650°C annealed samples show similar leakage current values. When the annealing temperature increases to 700°C, the leakage current increases abruptly to 0.8 mA/cm^2, which is about 3 orders of magnitude higher than the value obtained for the 600°C and 650°C annealed samples. In other words, the leakage current increases as the annealing temperature increases.

For the PZT 50/50 samples, the complete perovskite phase ransformation occurs around 600°C, and the leakage current shows a very stable value in this range up to 650° C. The typical leakage current value is about 0.2-0.3 μA/cm^2. When the annealing

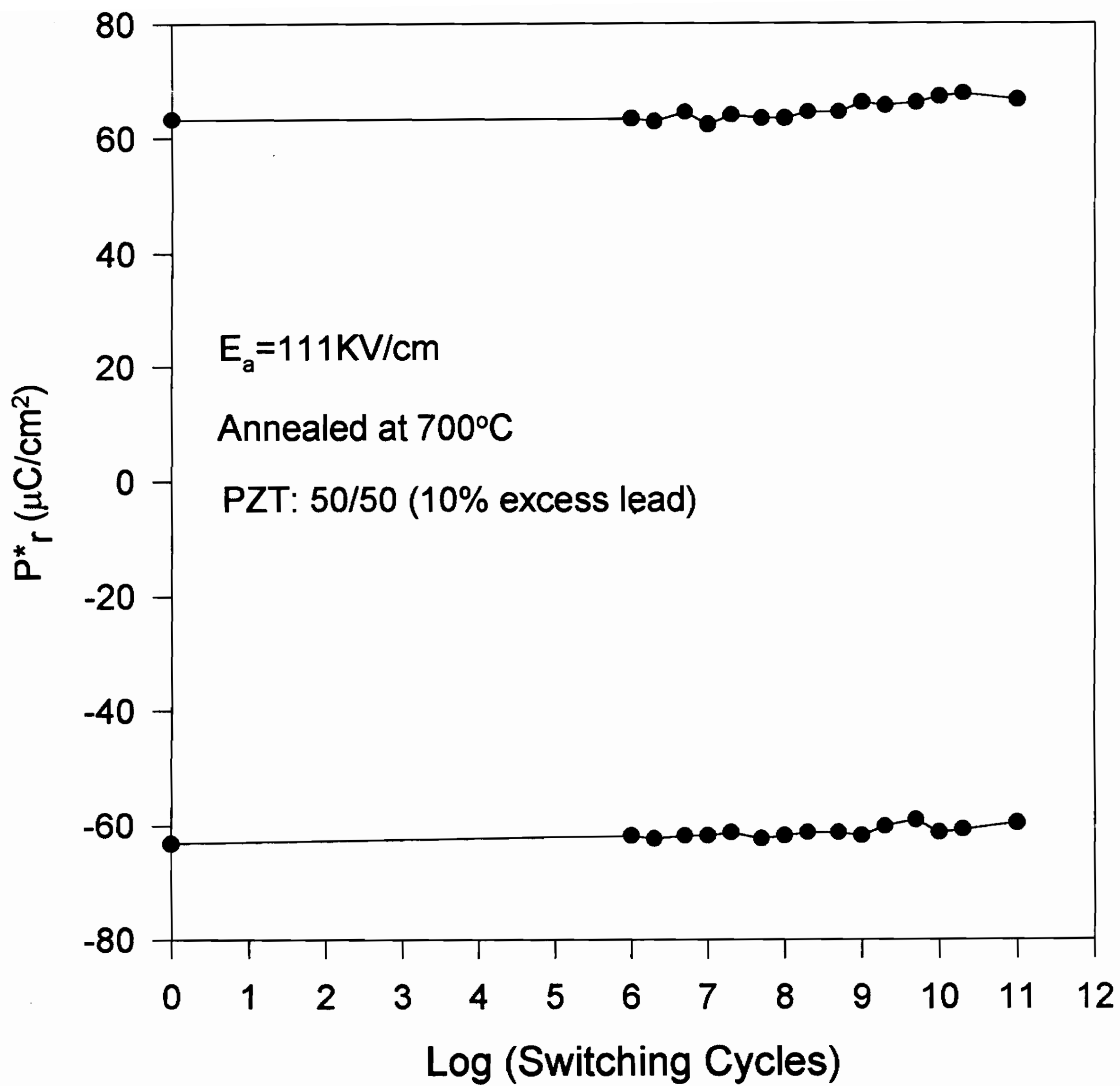

Fig. 2.16 Fatigue Endurance of PZT

temperature increases to 700°C, the leakage current increases by about three orders of magnitude to 0.8 mA/cm^2. This dramatic change of leakage current can be correlated to the high rate of evaporation of the PbO at high annealing temperatures. The greater loss of PbO will induce higher lead vacancy and oxygen vacancy concentration, which will serve to increase the leakage current. For the samples annealed at 550°C the perovskite phase transformation is incomplete and a leakage current as low as 40 nA/cm^2 has been observed. The SEM micrograph shows that the perovskite grains are all well separated with very thick grain boundaries. In the grain boundary electrical degradation model, the grain boundary is considered to be the conduction barrier, or the conductivity in the grain is higher than that in the grain boundaries. Consequently, the leakage current will be lower in the samples with thicker grain boundaries.

The effect of different amount of excess lead on the leakage current is shown in Fig.2.18. The maximum values for both the 650°C and 700°C annealed samples were obtained for the 5 at.% excess lead samples.

The maximum leakage current occurs at 5 at.% excess lead, and decreases as the excess lead decreases. It is reported that the optimal amount of excess lead falls in the range of 5 to 10 at.% [8]. Excess lead amounts of less than 5 at.% will reduce the perovskite transformation rate and second phase pyrochlore will remain in the film. The XRD analysis of the 2 at.% excess lead sample annealed at 650°C show no second phase peak, but the much lower hysteresis values compared to that of the 5, 7, and 10 at.% excess lead samples suggests that small amounts of nonferroelectric phases could exist in the film and deteriorate the ferroelectric properties. These phases could be either pyrochlore or ZrO_2, both of which have higher resistivities than the perovskite phase and thus can lower the leakage current value. For excess lead above 5 at.%, the leakage current decreases with larger amounts of excess lead up to 10 at.%. It can be explained

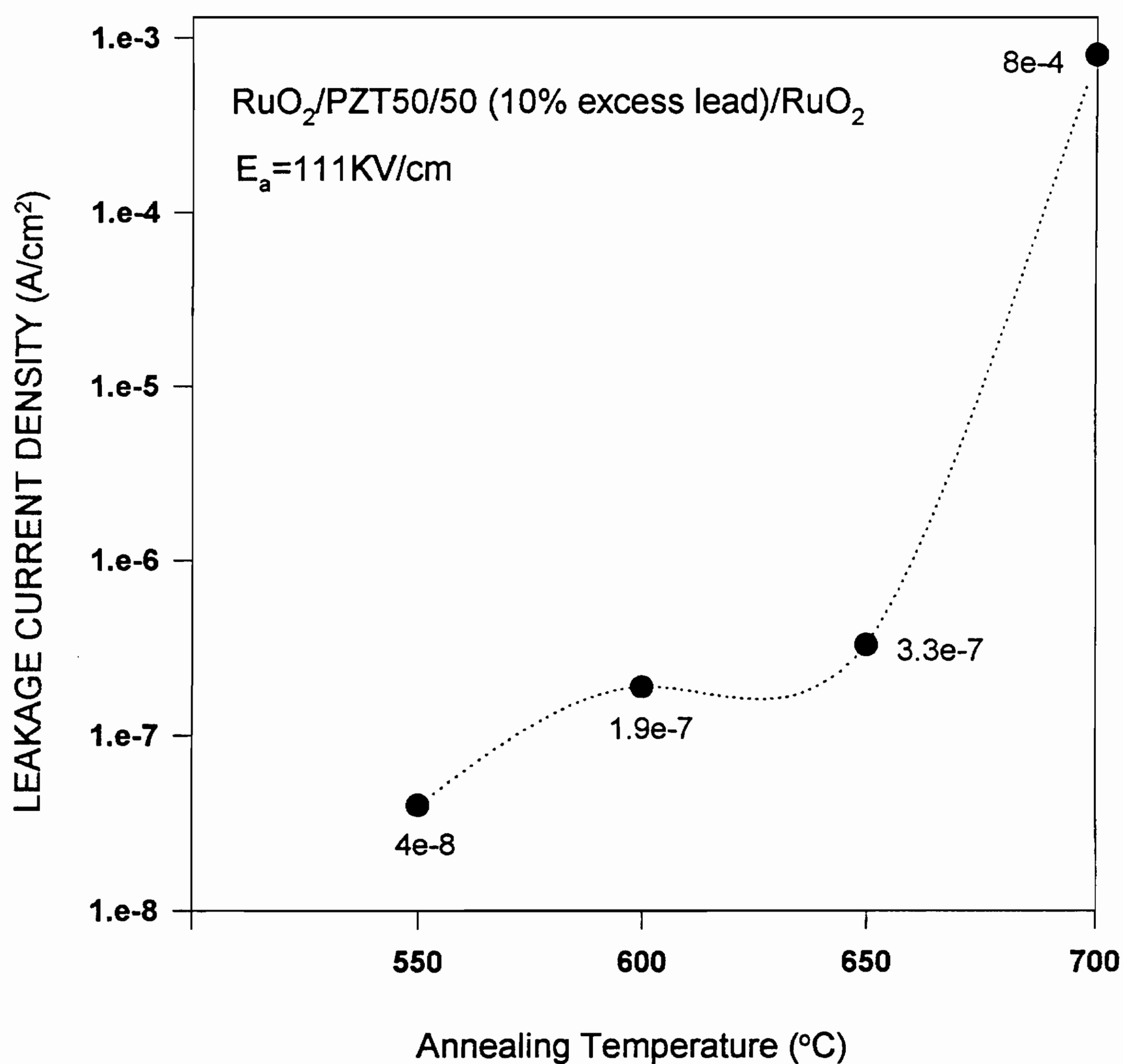

Fig. 2.17 Leakage Current as a Function of Annealing Temperature

that the excess lead can compensate the lead lost during the annealing process and thus lower the space charge density in the film. The SEM micrographs for the 10 at.% excess lead also shows that the excess lead can result in the high resistivity grain boundary regions between the perovskite grains. It is the low vacancy concentration and the thick grain boundary regions that keep the leakage current down.

Fig.2.19 shows the compositional effect on the leakage current. Pure lead titanate was found to have an extremely high leakage current value of 12.8 A/cm^2. It falls by about four orders of magnitude in the range of Zr/Ti varying from 20/80 to 40/60. A minimum value of 0.33 $\mu A/cm^2$ has been observed at the composition with Zr/Ti=50/50. The leakage current increases to several mA/cm^2 when the Zr/Ti ratio increases to 80/20.

The leakage current was found to be relatively insensitive to composition except for the pure lead titanate which is very leaky and the 50/50 composition which has very high resistivity. In general, compositions in both the tetragonal and rhombohedral phase area show almost the same leakage current value of a few mA/cm^2.

The high leakage current obtained for the pure lead titanate is abnormal since it is reported that pure lead titanate has a dc conductivity of 2 to 5×10^{-11} $\Omega^{-1}cm^{-1}$ [34], and pure lead titanate single crystal has excellent hysteresis properties, giving a remanent polarization of 75 $\mu C/cm^2$ [22]. The reason for the high leakage current in the lead titanate films in this study can be attributed to the stress caused by the processing conditions. Lead titanate has a Curie point of 490°C and undergoes a large contraction during the cubic-to-tetragonal transformation [33]. The processing temperature of the lead titanate samples is above 500°C. A large stress results when the samples are cooled to room temperature due to the transformation of high temperature cubic phase to low temperature tetragonal phase. From the SEM micrographs of the lead titanate, a well developed grain structure and some pin holes can be observed. The thin grain boundary

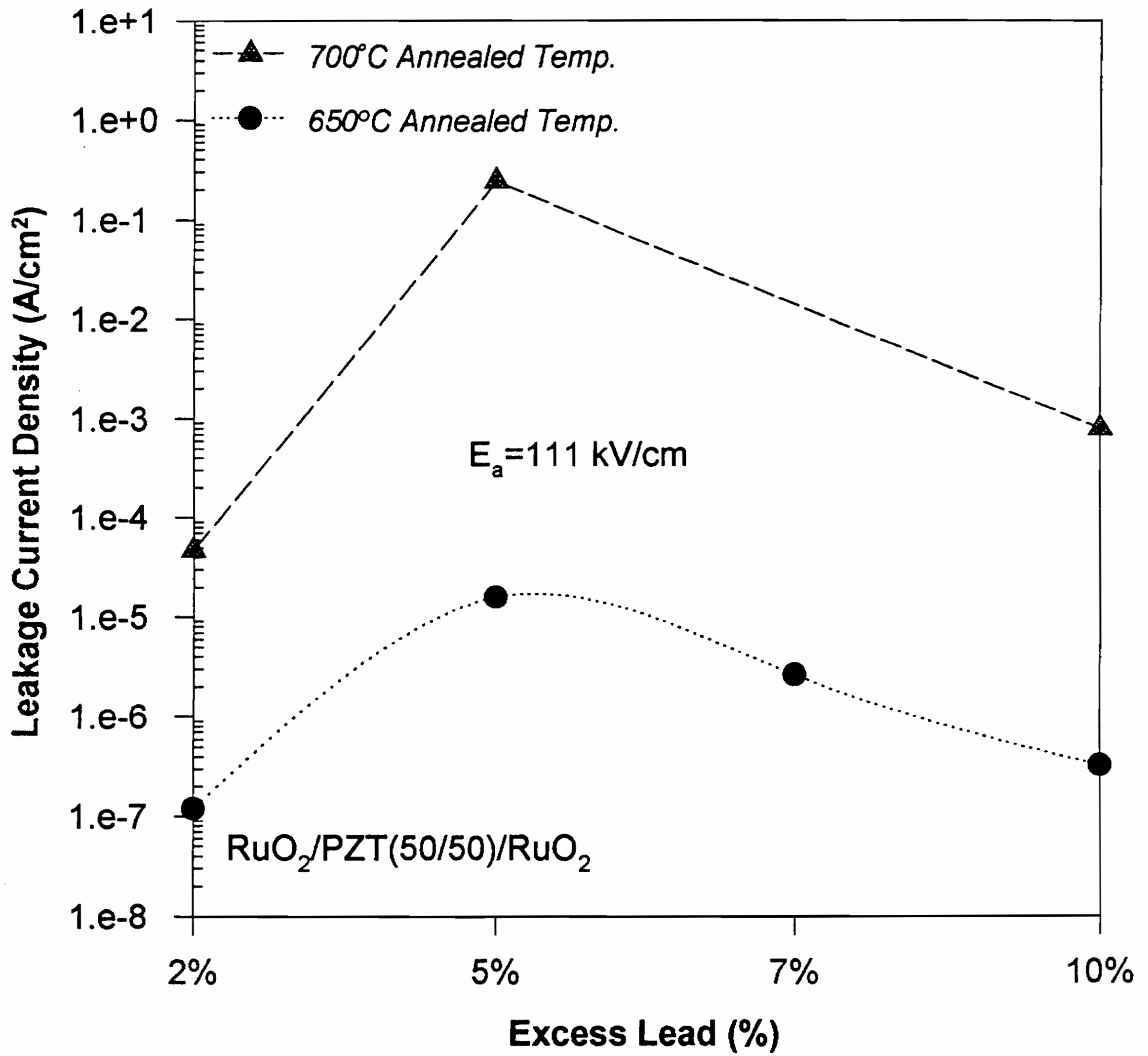

Fig. 2.18 Leakage Current as a Function of Excess Lead

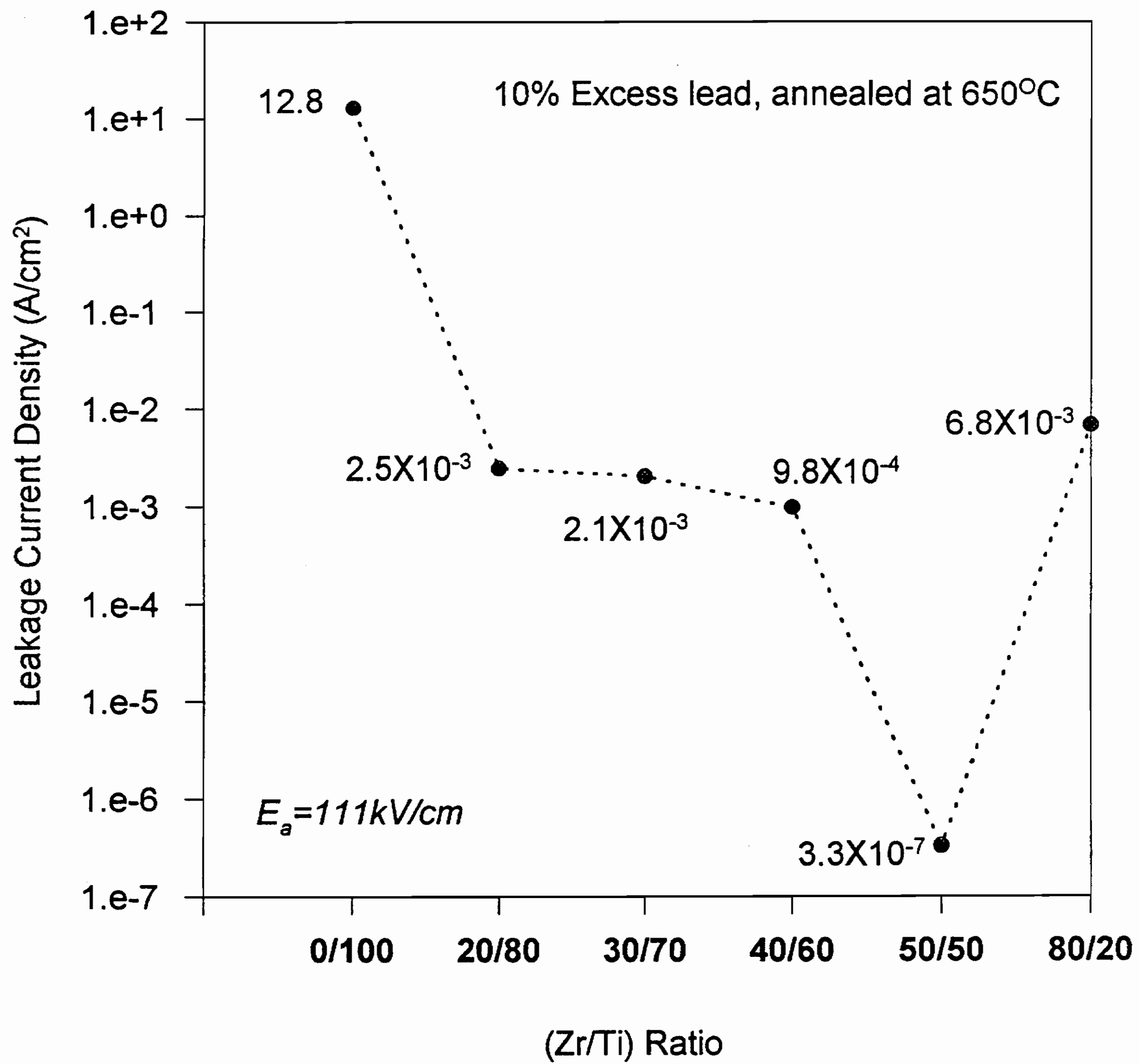

Fig. 2.19 Leakage Current as a Function of Zr/Ti Ratio

region and the pin holes in the film may also contribute to the high leakage current value.

Both the tetragonal and the rhombohedral phases exist at the MPB composition. The low leakage current value can be explained by the higher activation energy for space charges moving from one phase to the other, while the activation energy in either pure tetragonal or pure rhombohedral phase samples are lower and more uniform. Consequently, the leakage current has almost the same value for samples whose Zr/Ti ranges from 20/80 to 80/20 while it decreases markedly at the composition of 50/50. The SEM micrographs show very thick grain boundary regions on the film surface, which will also increase the resistivity of the film.

Fig.2.20 shows the comparation of the I-V curves of PZT 50/50 with 7 at.% excess lead annealed at 650°C for 30 min on Pt and RuO_2 electrodes, respectively. Although the RuO_2 electrode can increase the fatigue endurance of the PZT films, it increases theleakage current as well.

2.4. Summary

No fatigue has been observed for films on the RuO_2 electrodes up to 10^{11} cycles as expected in this study, but the leakage current is too high to be accepted for the memory applications. The processing parameters have been used to control the structure and morphology of the films and thus their electrical properties. The optimal conditions for the processing of PZT thin films in this study were found to be a composition Zr/Ti=50/50, 10% excess lead, and a 650°C for 30 min annealing. The typical values of the electrical properties under these conditions were $2P_r$=45 $\mu C/cm^2$ and the leakage current=0.33 $\mu A/cm^2$.

It is required a $P_r \geq 10$ $\mu C/cm^2$, a leakage current$\leq 1 \times 10^{-8}$ A/cm^2 and a fatigue life

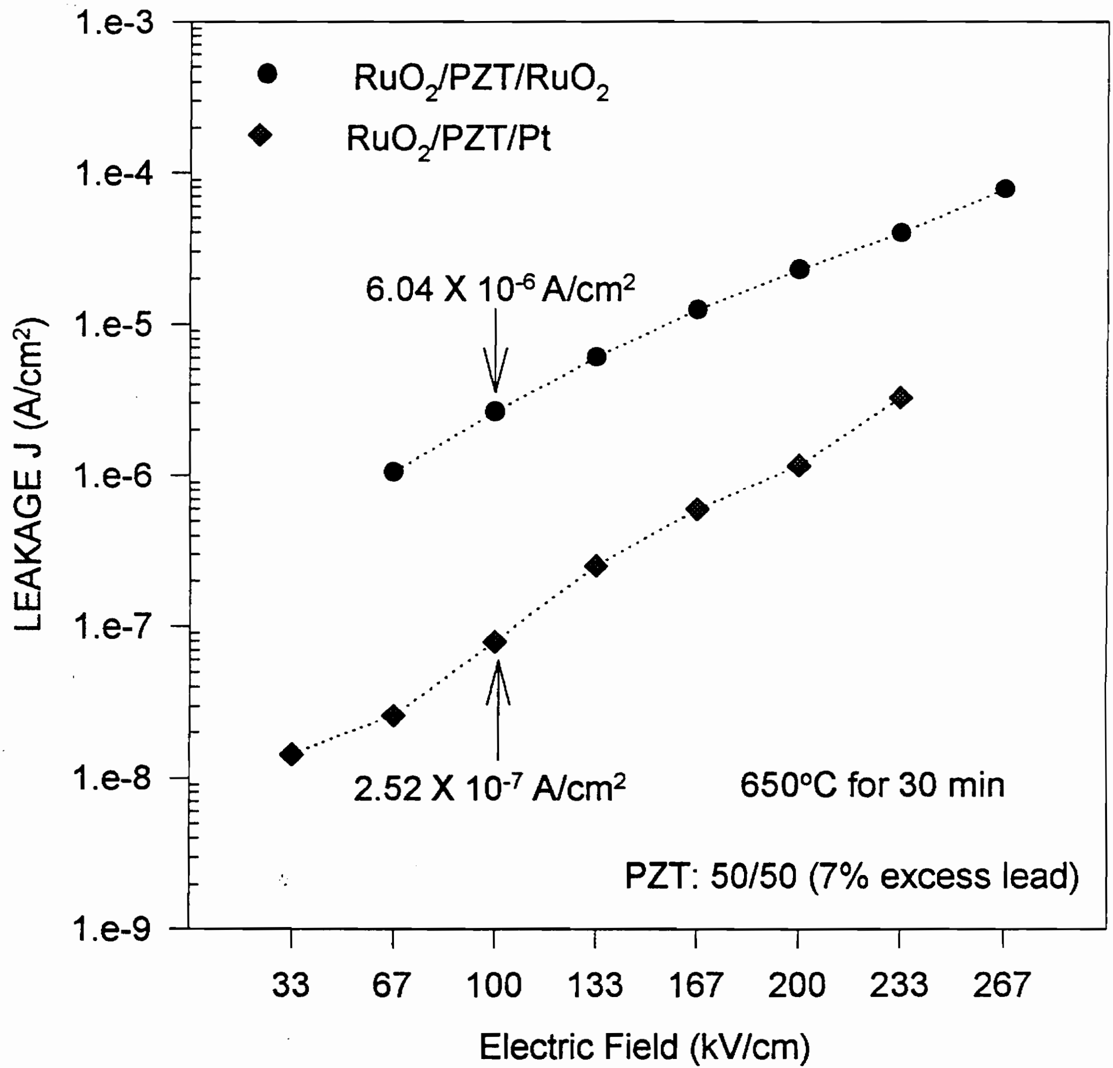

Fig. 2.20 PZT I-V Curves on RuO_2 & Pt Substrates

larger than 10^{12} cycles for the NVDRAM applications. The PZT samples meet the requirements of fatigue life and remanent polarization for large scale applications, but the leakage current is still too high.

Based on the study of the composition, microstructure and electrical properties of the PZT thin films on RuO_2, the following conclusions can be drawn:

(1) The PZT thin film phase transformation behavior on RuO_2 electrodes is similar to that on Pt electrodes: the T_c^{Per} increases with the Zr/Ti ratio.

(2) The grain size increases with the Zr/Ti ratio, while the rate of the perovskite transformation decreases with the Zr/Ti ratio.

(3) The excess lead can assist the perovskite phase transformation in the compositional region around the MPB.

(4) PZT films show the highest remanent polarization values at the composition that is close to the MPB.

(5) The different excess lead amounts do not show any observable effect on the remanent polarization for samples which are completely transformed to perovskite phase.

(6) The fatigue endurance for all PZT samples on RuO_2 was extremely good, no polarization loss was observed up to 10^{11} switching cycles.

(7) The leakage current increases with the annealing temperature.

(8) The leakage current values in the tetragonal and rhombohedral phases are almost the same (a few mA/cm^2), while the 50/50 composition has the lowest leakage current value of 0.33 $\mu A/cm^2$ and the pure lead titanate has the highest leakage current value of 12.8 A/cm^2.

(9) The fatigue endurance and the remanent polarization properties meet the requirements for memory applications, while the leakage current value needs to be lowered by an order of magnitude.

Chapter 3. Microstructure and Electrical Properties of Doped PZT Thin Films Made by a Sol-Gel Method

Abstract

La and Nb doped $Pb(Zr_xTi_{1-x})O_3$ (i.e. PZT) ferroelectric thin films on both Pt and RuO_2 electrodes were prepared by the sol-gel method and spin-coating. The effect of doping on the microstructure, hysteresis properties, fatigue, leakage current, retention and time dependent dielectric breakdown were studied. The results indicate that the addition of La and Nb tends to improve all the reliability properties of PZT thin films by lowering the oxygen vacancy concentration. The combination of RuO_2 electrodes and donor doping produced PZT films with high fatigue endurance and low leakage currents which are suitable for memory applications.

3.1. Introduction

Ferroelectric materials have attracted much interest in recent years since their applications may cause a revolution in the current semiconductor memory industry. The ferroelectric material lead zirconate titanate ($Pb(Zr_xTi_{1-x})O_3$ or PZT) is considered to be one of the best candidates to be used as memory materials since it is a well-studied system with outstanding ferroelectric properties. However, the reliability of PZT is still under question and has been the major concern of the current studies. The most important

reliability issues include fatigue, leakage current, retention and time dependent dielectric breakdown (TDDB).

The degradation of ferroelectric properties in PZT is considered to be caused by the movement and entrapment of the defects in the ferroelectric films under an applied electric field. When a ferroelectric is initially poled, an internal field is built in. Defects will move to the domain walls and the electrodes under the internal field and neutralize the remanent polarization charges leading to their reduction [26]. A reduction model of Schottky barrier height by such a neutralization mechanism has been suggested by Bernacki [27]. The ceramic metal interface plays a very important role in the entrapment of the vacancies. These vacancies are mainly oxygen vacancies since they have high mobility in the PZT films [25]. The entrapment is due to the much lower free energy level in the interface compared to the bulk, and the vacancies will be easily trapped by the interface once they move close to the interface under the applied electric field.

The entrapment of the vacancies can be decreased considerably using conductive oxide electrode such as RuO_2 [17]. RuO_2 can react with oxygen vacancies and form nonstoichiometric compound RuO_{2-x} without observable change on their conductivities, and therefore the fatigue endurance can be improved significantly. However, an interlayer will form between the electrode and the ferroelectric during the high temperature processing. This interlayer can act as a linear capacitor which will reduce the spontaneous polarization and increase the initial polarization decay leading to a larger gap in the hysteresis loop measured by the standardized RT66A system [26]. The low Schottky barrier in the interface will also increase the leakage current, which is the major drawback in the applications of the RuO_2 electrodes.

In this study, an attempt was made to solve the degradation problems by lowering the defect concentration in the PZT thin films. Donor doping is considered to be the most

suitable way to achieve this goal. The donors used in this study are lanthanum and niobium which substitute the A site and the B site in the PZT films, respectively.

The p-type conduction in PZT thin films is due to a small amount of acceptor impurities. The presence of acceptors can result in oxygen vacancies being created in the film. Trivalent acceptors substitute the B sites in PZT films as shown below:

$$A_2O_3 \xrightarrow{2TiO_2} 2A' + 3O_O + V_O^{\cdot\cdot} \quad (3.1)$$

where A represents the acceptor, and monovalent acceptors substitute for A sites in PZT:

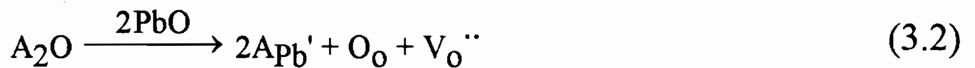

$$A_2O \xrightarrow{2PbO} 2A_{Pb}' + O_O + V_O^{\cdot\cdot} \quad (3.2)$$

The other source of oxygen vacancies is the PbO loss at elevated temperatures:

$$Pb_{Pb} + O_O \longrightarrow PbO\uparrow + V_{Pb}'' + V_O^{\cdot\cdot} \quad (3.3)$$

When the donors La and Nb are introduced into the PZT structure, a certain amount of oxygen vacancies will be compensated:

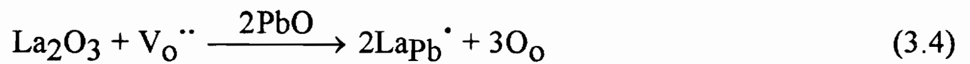

$$La_2O_3 + V_O^{\cdot\cdot} \xrightarrow{2PbO} 2La_{Pb}^{\cdot} + 3O_O \quad (3.4)$$

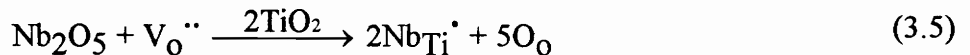

$$Nb_2O_5 + V_O^{\cdot\cdot} \xrightarrow{2TiO_2} 2Nb_{Ti}^{\cdot} + 5O_O \quad (3.5)$$

In addition, the effect of the acceptor is also compensated:

$$La_2O_3 + A_2O_3 \longrightarrow 2La_{Pb}^{\bullet} + 2A_{Ti}' + 6O_O \qquad (3.6)$$

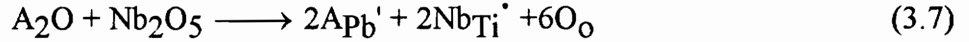

$$A_2O + Nb_2O_5 \longrightarrow 2A_{Pb}' + 2Nb_{Ti}^{\bullet} + 6O_O \qquad (3.7)$$

Since the donor doping can reduce the oxygen vacancies and compensate the acceptor impurities, the oxygen vacancy concentration after doping will be much lower than that before doping.

In this study, donors were introduced in the PZT films in different amounts up to 6 at.%, using both Pt and RuO_2 electrodes. Their hysteresis, fatigue, leakage current and retention properties were measured and compared to show the effect of the doping elements and the doping amounts.

Chang and Desu [25] have performed considerable work on La and Nd doped-PZT prepared by the metal organic decomposition (MOD) method, focusing on the microstructure. Their results show that Nb doping in PZT decreases the leakage current of the films. In this study, a more effective sol-gel method was used to prepared La and Nb doped PZT films on both Pt and RuO_2 electrodes, and detailed electrical characteristics were investigated. The sol-gel method includes a hydrolysis step which can break most of the C-H bonds in the solution; so the C content in the films before annealing is much less than that of the film made by MOD. Less shrinkage during annealing and higher density films result after the annealing [8]. This study will complement the study conducted by Chang et al. in terms of more complete characterization of the electrical properties of doped PZT films.

PNZT will be used to represent the Nb doped PZT films, and PLZT will represent the La doped films. The effect of the doping amount, the bottom electrode type and the donor type were the main factors studied in this experiment.

3.2. Experimental Procedure

The precursors used in this study for the dopants were lanthanum acetate hydrate $La(Ac)_3 \cdot 1.5H_2O$ obtained from Alfa, and niobium V ethoxide $C_{10}H_{25}O_5Nb$ obtained from Strem. Studies on PLZT films by Khan [23] show a better result for samples assuming B site vacancies rather than A site vacancies since the B site vacancy concentration is only half that of the A site. Therefore, precursors of various compositions were made assuming that B site vacancies are created from the Nb doping. The dopant concentrations used were 2, 4 and 6 at.% for each dopant. All the compositions including pure PZT would be expressed by either of the two general formulae:

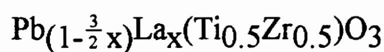

$$Pb_{(1-\frac{3}{2}x)}La_x(Ti_{0.5}Zr_{0.5})O_3$$

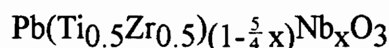

$$Pb(Ti_{0.5}Zr_{0.5})_{(1-\frac{5}{4}x)}Nb_xO_3$$

where x is the doping amount. The Zr/Ti ratio used here was 50/50 with 7 at.% excess lead, and the annealing temperature was 650°C for 30 min.

Precursors were made using the modified sol-gel method the details of which can be found elsewhere [21]. The solutions were deposited on both RuO_2 electrodes and Pt electrodes. Immediately before deposition, these solutions were filtered with a 0.45 μm syringe filter. The electrode films were deposited onto oxidized silicon wafer by sputtering. Films were deposited on these electrodes by spin-coating at a speed of 2000 rpm for 30 seconds, followed by baking at 150°C for 5 min on a hot plate to eliminate the organic solvents. The spin-bake cycle was repeated to prepare a thicker film. Typically, the films in this study consisted of three layers. The thickness of the films were determined using cross-sectional SEM. The deposited films were annealed at 650°C for 30 min to

obtain the perovskite phase. A shadow screen with 2.1×10^{-4} cm^2 area holes was used to deposit the top electrodes of RuO_x.

The standardized RT66A system was employed for the measurement of electrical properties, including hysteresis properties, fatigue, retention and TDDB. The leakage current was measured by a computer controlled electrometer. The bottom electrode was exposed by careful mechanical abrasion of the PZT films. XRD was performed for the examination of the perovskite phase transformation studies. The surface morphologies of the films were investigated by an ISI-SX-40 scanning electron microscope (SEM). Prior to loading the specimens into the SEM chamber, they were coated with a thin layer of gold (approximately 100 A thick) for the purpose of electric conduction. The SEM was operated at 20 kV.

3.3. Results and Discussion

A. Microstructure

The perovskite phase formation of the doped PZT films was consistent with the results reported by Chang [25]. The XRD analysis shows that a complete perovskite phase transformation has been achieved for all samples annealed at 650°C for 30 min. The lattice distortion of the doped PZT is not obvious from the x-ray diffraction patterns. A cross-sectional SEM micrograph for PZT films on a Pt electrode is shown in Fig.3.1. The PZT layer, Pt layer , and the silicon dioxide (SiO_2) layer can be distinguished very easily from the picture. The thickness of the PZT film is about 0.3 μm, while that of the Pt electrode and silicon dioxide substrate together is about 0.55 μm.

Fig.3.2 shows the SEM micrograph of PZT films on Pt and RuO_2 electrodes. No

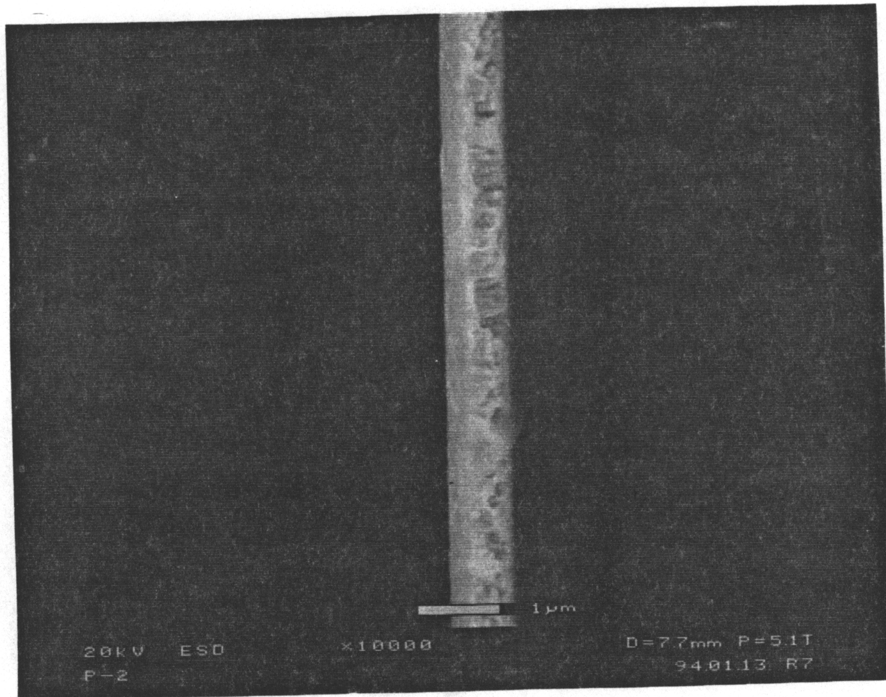

Fig. 3.1 Cross-sectional SEM of PZT on Pt Substrates

obvious substrate effect can be observed. Both films have very smooth surfaces and very fine grains. The grain boundaries are difficult to perceive. For the La doped PZT films, however, the substrate effect is obvious. Fig.3.3 shows micrograph of the 6 at.% La doped PZT on both Pt and RuO_2 electrodes. The grain size of the La doped PZT film on the Pt is larger than that of the film on the RuO_2.

The grain size is inversely proportional to the nucleation rate of the PZT perovskite phase on a substrate. The nucleation rate of the PZT films on both the Pt and RuO_2 are very high, small grains were formed and the electrode effect could hardly be observed. La doping decreases the nucleation rate of the PZT films on both the Pt and RuO_2 electrodes, and larger grains are formed. The PLZT nucleation rate on the RuO_2 electrode is higher than that on the Pt electrode due to a smaller lattice mismatch of the PLZT and the RuO_2, so the grain size on the Pt is much larger than that on the RuO_2 for the 6 at.% La doped PZT.

Fig.3.4 shows the effect of La doping on the morphology of the PZT films on Pt electrodes. Four micrographs with different La doping concentrations on Pt electrodes are shown. Larger grains and a well developed grain structure was observed for the PLZT films compared to the undoped PZT. The surface of the PLZT films becomes rough and a clear microstructure can be seen. As the La doping amount increases, the grain size tends to decrease slightly. This is consistent with the results of the studies conducted by Chang et al. [25]. The La doping will promote a uniform grain growth and homogeneous densification of the perovskite phase, but the grain growth rate may be slightly lower. The smaller grain size of the undoped PZT may be due to the fact that its nucleation rate is higher than that of the La doped PZT.

Nb doping was found to effect the PZT microstructure to a lesser degree than the La doping. Fig.3.5 and Fig.3.6 show the SEM micrographs of PNZT films of different

(a)

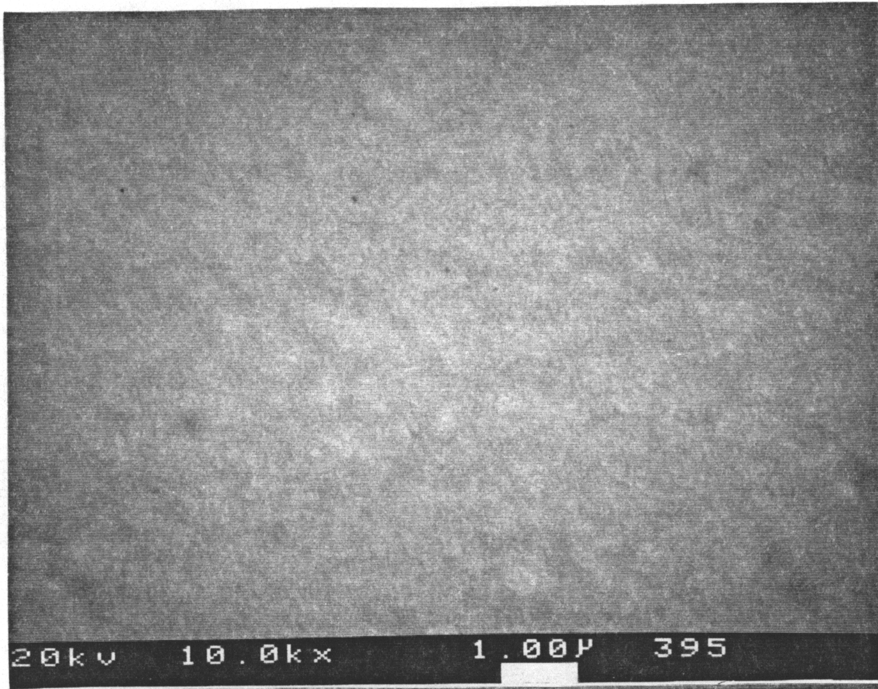

(b)

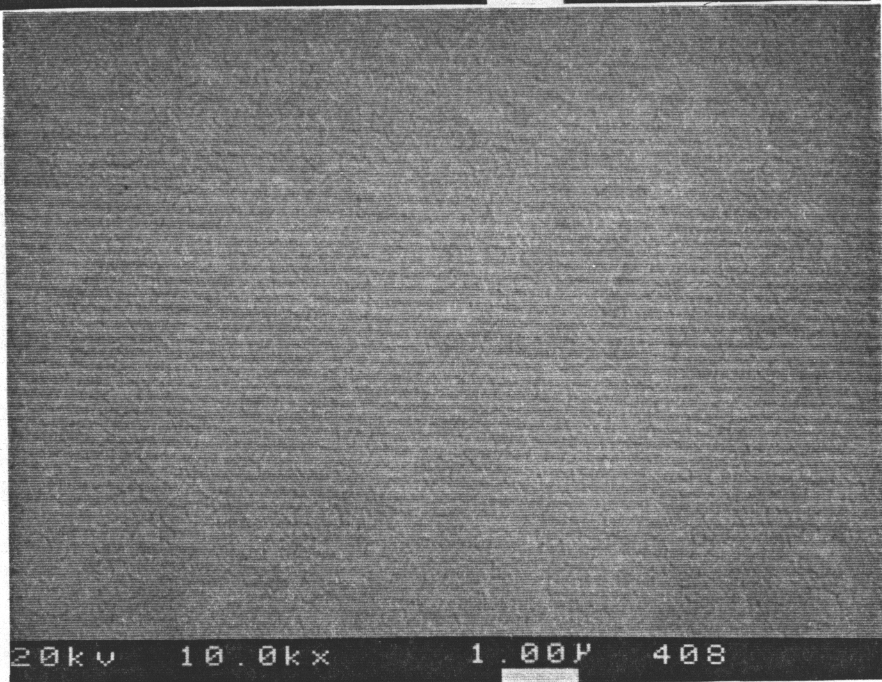

Fig. 3.2 Microstructure of PZT on (a)Pt and (b)RuO_2

(a)

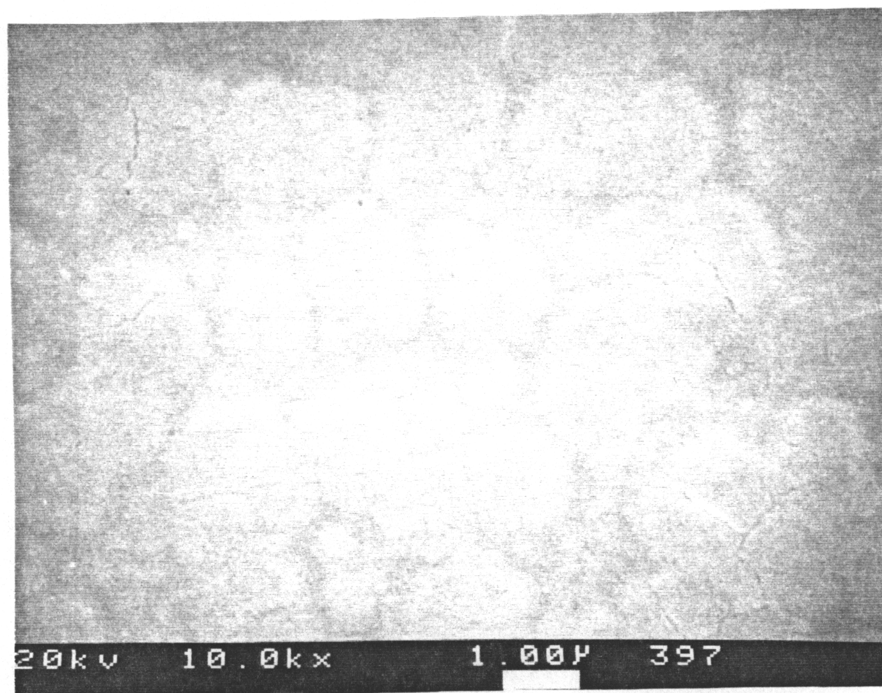

(b)

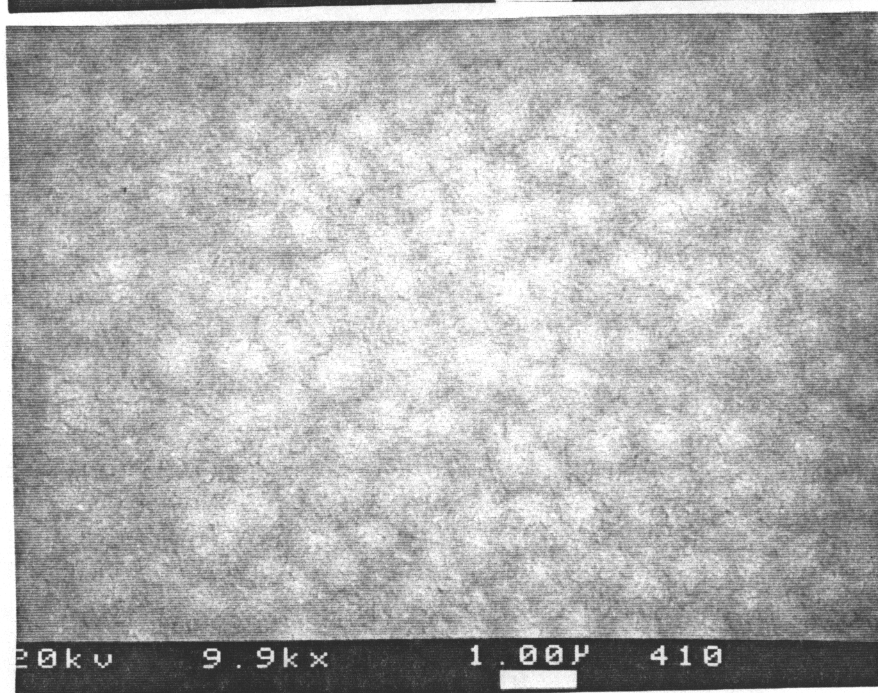

Fig. 3.3 Microstructure of PLZT (6%) on (a)Pt and (b)RuO_2

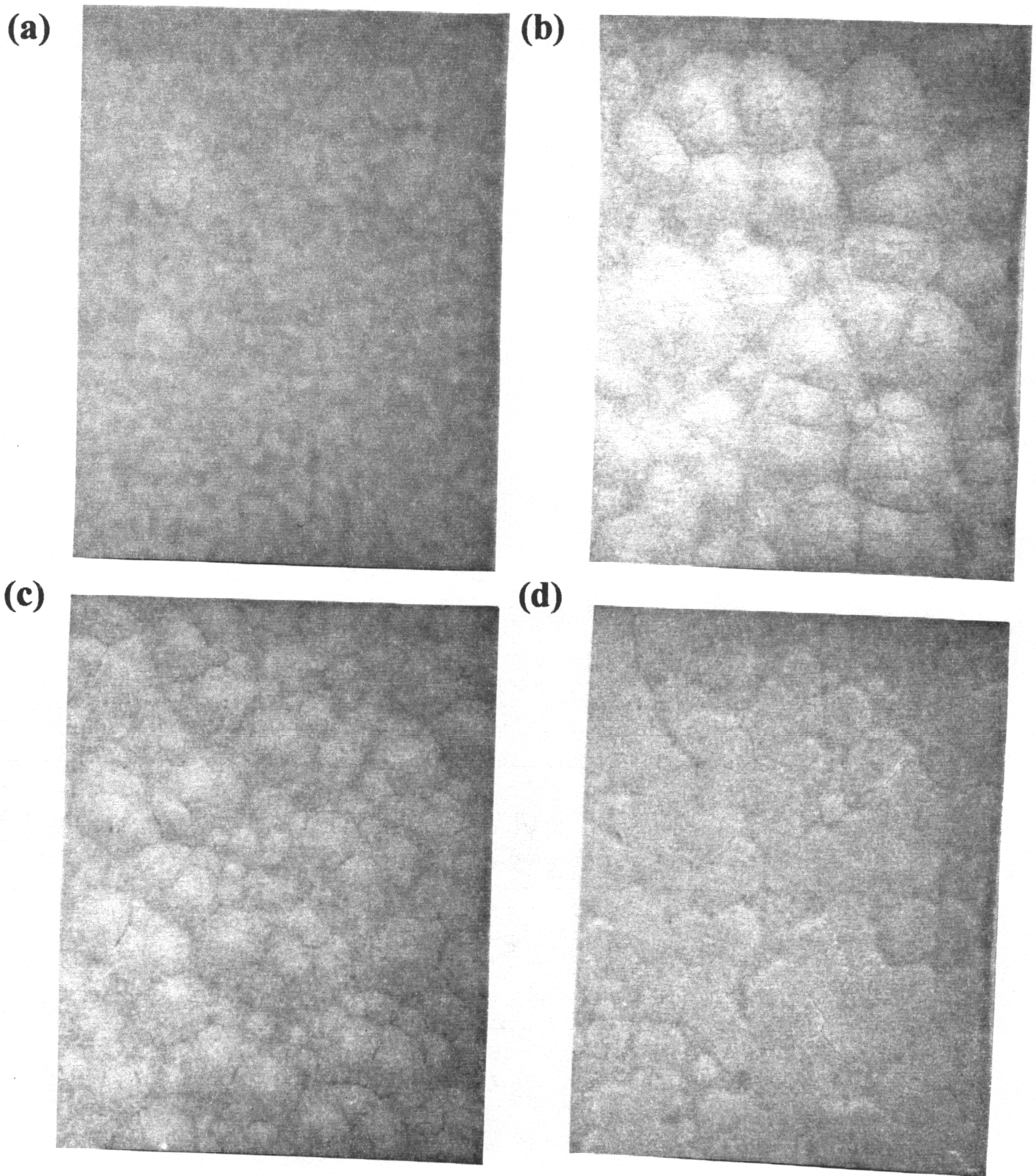

Fig. 3.4 Microstructure on Pt substrates. mag. ×10,000 PLZT (a)0%, (b)2%, (c)4% and (d)6%.

compositions on the Pt and RuO_2 electrodes, respectively. A clearer microstructure and rougher surface relative to the undoped PZT are only observed for the 2 at.% doped PZT, while the 4 at.% and 6 at.% doped PZT films have almost the same smooth surface and fine grain structure. No electrode effect has been observed for the PNZT samples.

In summary, the doped and undoped PZT films are very homogeneous and smooth. La doping shows a large effect on the grain structure development. Larger grain size and clear grain boundaries can be observed for the PLZT films. The Nb doping, however, does not show any appreciable effect on the microstructures except for the 2 at.% doped PNZT. The electrode effect on the microstructure is almost negligible for the undoped PZT, and becomes significant only when the amount of La doping increases.

B. Electrical Properties

The hysteresis properties, fatigue, leakage current, retention and TDDB have all been measured to study the doping effect. In generally, doping is known to detract from the hysteresis properties but improve the electrical reliability. The objective of this experiment is to study the doping effect on the electrical properties and the optimal doping amount for the PZT 50/50 composition with good reliability properties and acceptable hysteresis properties.

Hysteresis Properties. Fig.3.7 shows two polarization values for each Nb dopant concentration on the RuO_2 bottom electrodes. The saturated polarization does not change considerably with the dopant concentration, but the $2P_r$ value decreases steadily as the Nb dopant concentration increases. Fig.3.8 shows the variation of $2P_r$ with the La and Nb dopant concentration on both Pt and RuO_2 bottom electrodes. All remanent polarization

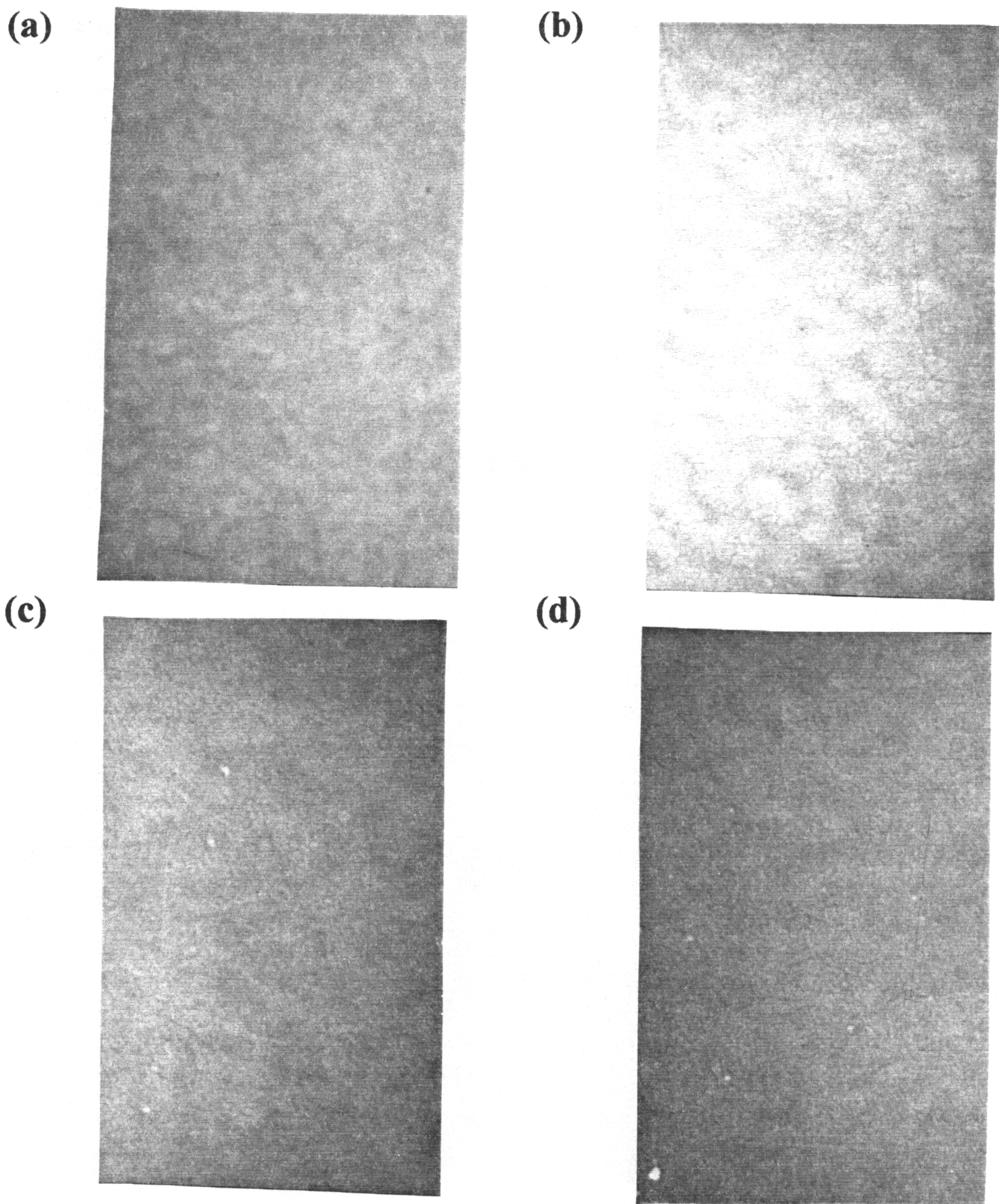

Fig. 3.5 Microstructure on Pt substrates, mag. ×10,000 PNZT (a)0%, (b)2%, (c)4% and (d) 6%

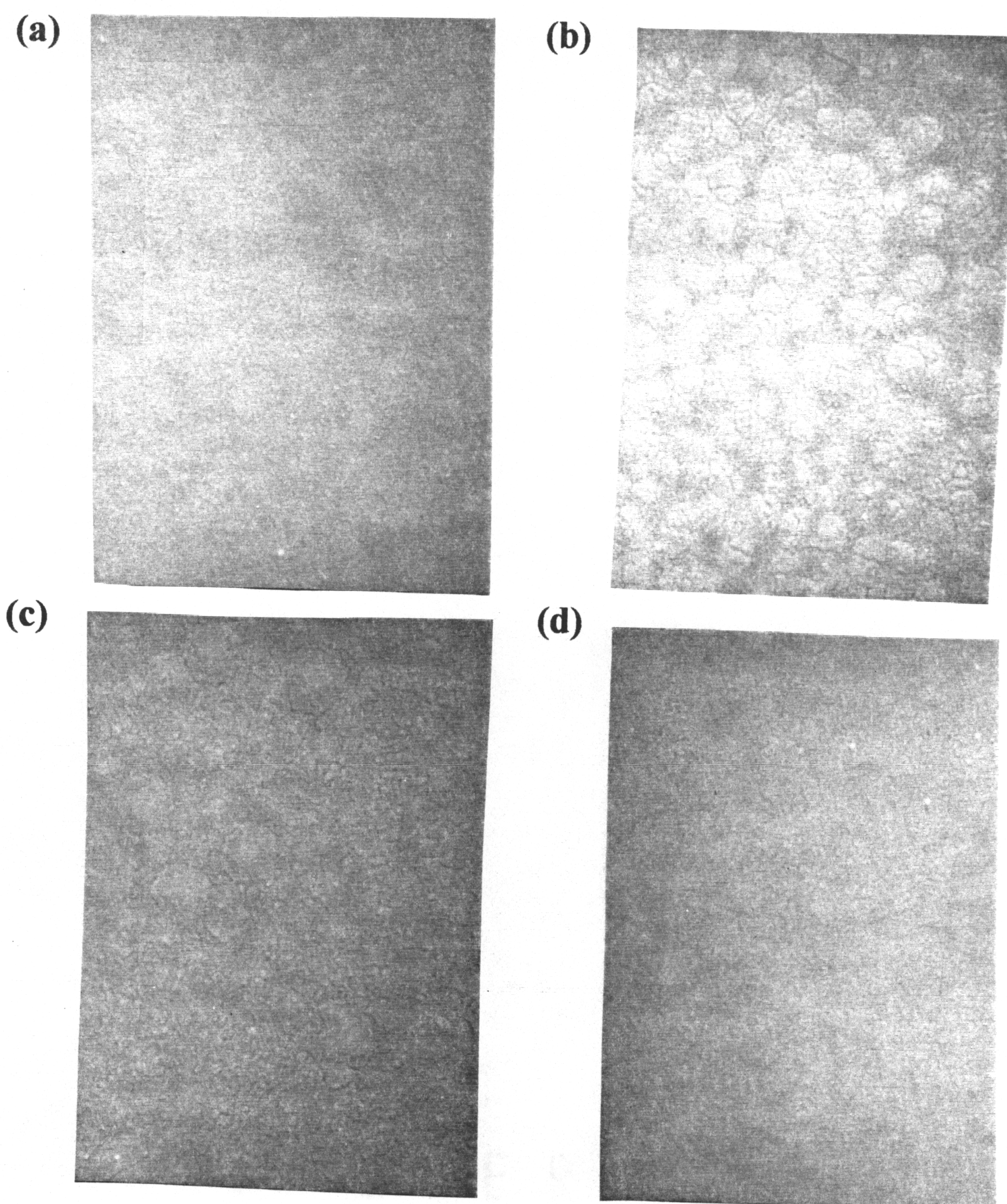

Fig. 3.6 Microstructure on RuO_2 substrates
mag. ×10,000
PNZT (a)0%, (b)2%, (c)4% and (d)6%

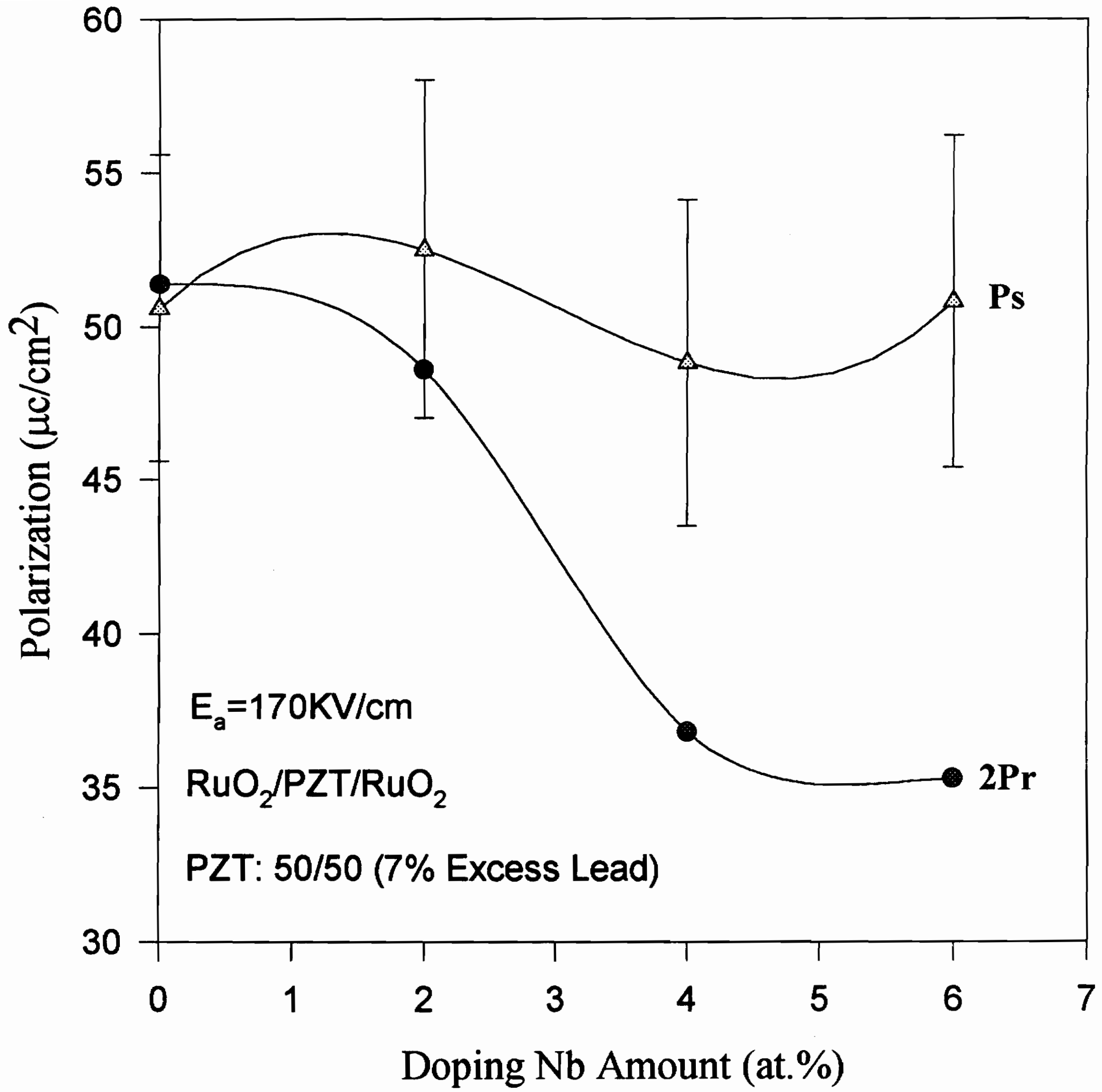

Fig. 3.7 Polarization as a Function of Nb Doping Amount

values decrease as the dopant concentration increases. For films on the RuO_2 bottom electrode, the remanent polarization decreases very slowly above 4 at.% doping. For films on the Pt electrodes, however, it decreases almost linearly. The remanent polarization of films on Pt is higher than that of the films on RuO_2 for the undoped PZT or 2 at.% doped films. On both RuO_2 and Pt bottom electrodes Nb doped films show a higher remanent polarization.

Fig.3.9 shows the variation of coercive field with the dopant concentration. The coercive field of PNZT films on both RuO_2 and Pt electrodes decreases with increasing Nb dopant concentration. For the PLZT films, the coercive field decreases when the doping amount increases up to 4 at.% and then increases at 6 at.% doping. The coercive field for the PNZT and PLZT samples ranged from 23 kV/cm to 43 kV/cm, regardless of the electrode material. This result is consistent with the Nb doped PZT study conducted by Ryder et al. [7].

The hysteresis properties of the doped PZT show that donor doping has an adverse effect on the ferroelectric properties. Typically, donor dopants such as La reduce Curie Point in a linear manner at a rate of approximately 37°C per at.% La. The remanent polarization is in direct proportion to the difference of the Curie temperature and the room temperature. This relationship can be shown below:

$$P_r \propto (T_c - T_r) \qquad (3.8)$$

where T_c is the Curie temperature, and T_r is the room temperature. The higher polarization of the Nb doped PZT compared to the La doped PZT may be indicative of improved properties for PZT films with B site vacancies rather than A site vacancies. This is consistent with the study conducted by Khan [23].

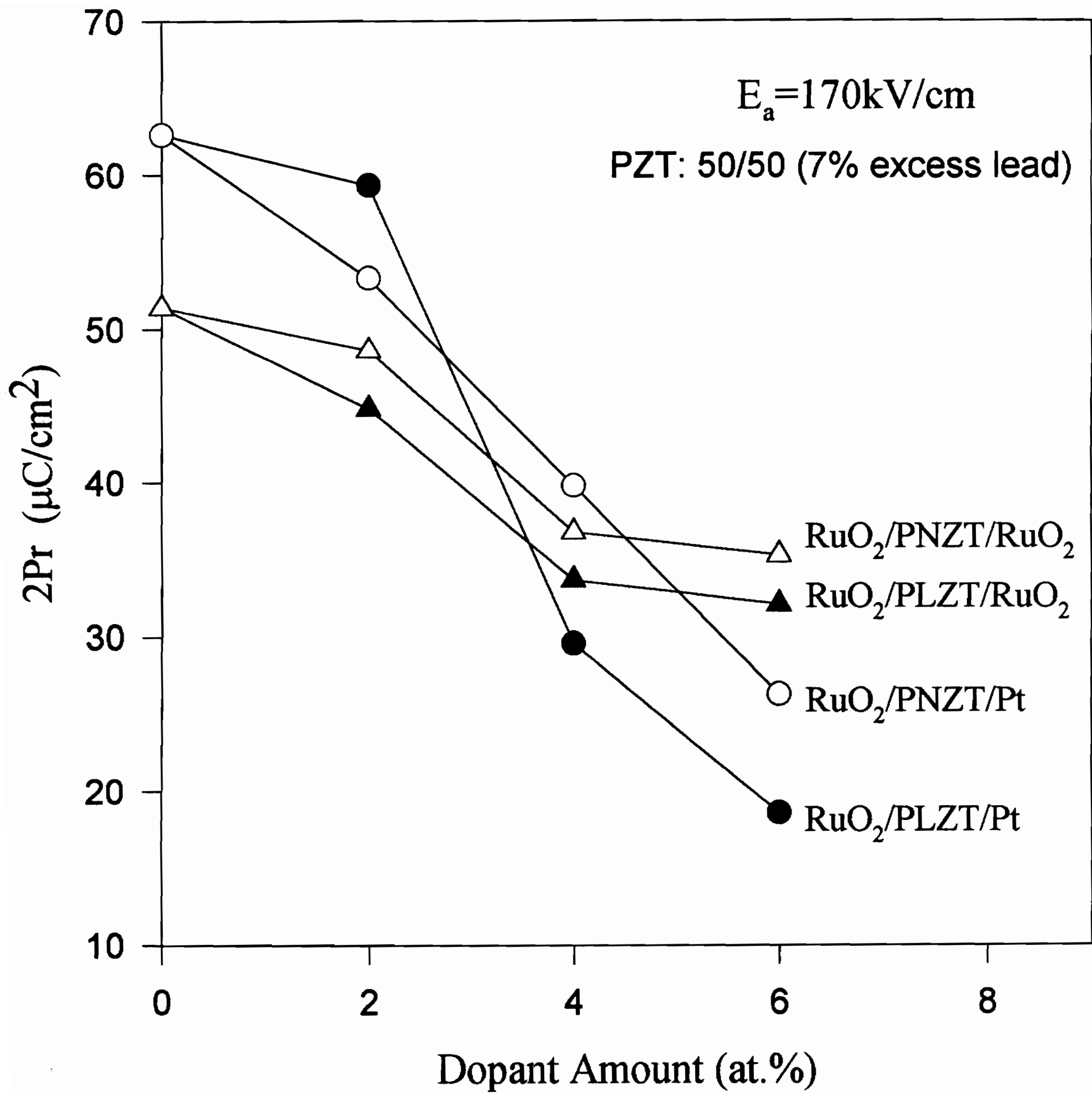

Fig. 3.8 Remanent Polarization as a Function of Doping Amount

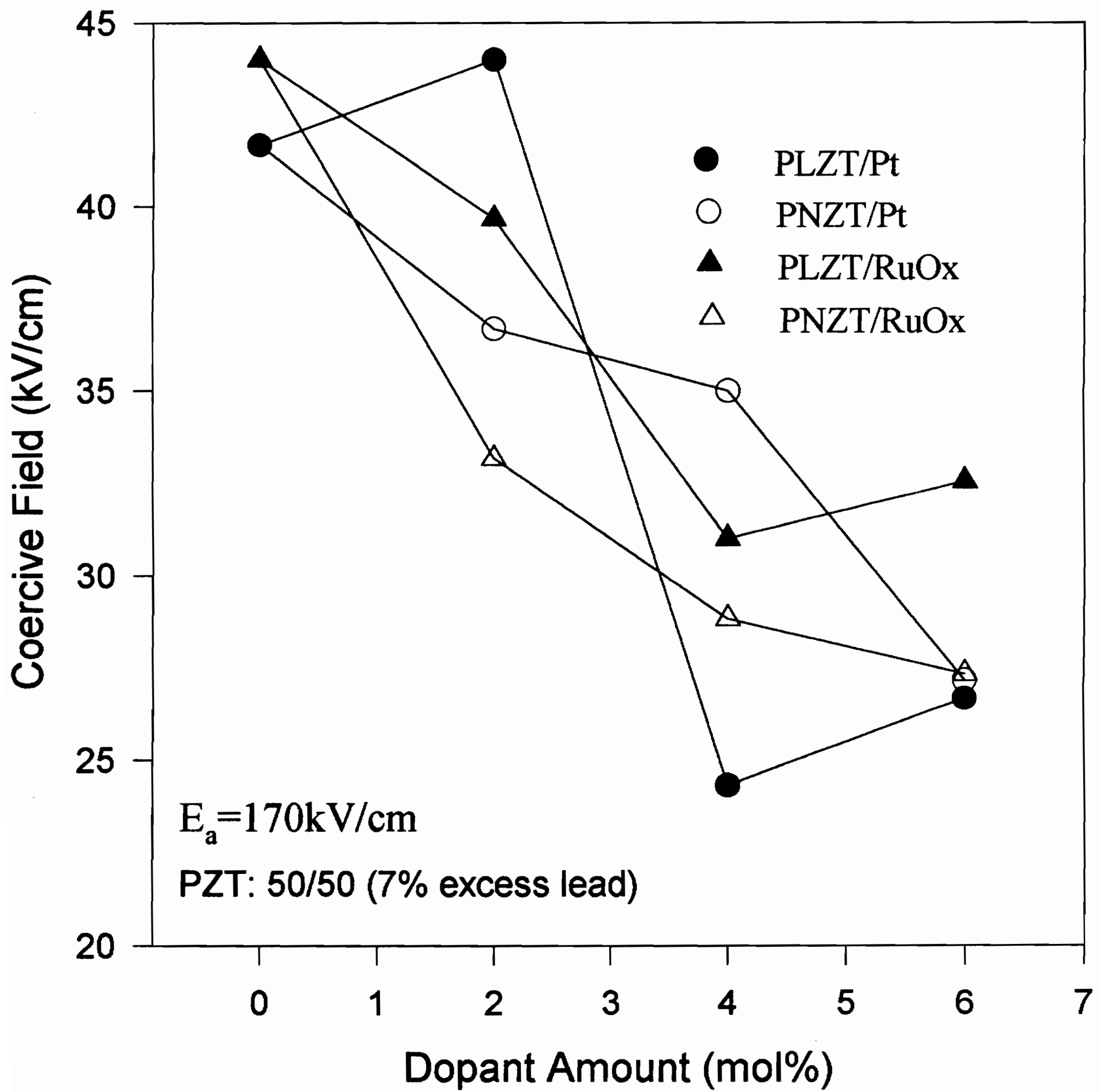

Fig. 3.9 Coercive Field as a Function of Doping Amount

The decrease in the coercive field may be due to a higher amount of the rhombohedral phase in the doped PZT. Nb and La favor the formation of the rhombohedral phase which has a lower coercive field compared to the tetragonal phase, and therefore the overall coercive field will decrease [7].

In summary, the nature of bottom electrodes does not seem to have an appreciable effect on the ferroelectric properties of the deposited films, while the dopant concentration effect on the hysteresis properties is obvious. Both the remanent polarization and coercive field decrease when the dopant concentration increases. The remanent polarization of the PNZT is slightly higher than that of the PLZT both on RuO_2 and Pt bottom electrodes, but the remanent polarization of both PNZT and PLZT on the Pt bottom electrodes decreases faster than that on the RuO_2 electrodes.

Fatigue & TDDB. The fatigue measurement was performed at room temperature using a 5 V square wave with a frequency of 10^6 Hz. It has been reported that RuO_2 electrodes can improve the PZT fatigue endurance up to 10^{11} cycles [17]. Fig.3.10 shows the normalized fatigue behavior of the PLZT on RuO_2 electrodes. No obvious fatigue was observed for different amount of doped PZT films. Since all samples on RuO_2 electrodes showed very good fatigue endurance, the fatigue data on the Pt bottom electrodes were used to study the doping effect.

Fig.3.11 shows the normalized fatigue behavior of PNZT on Pt bottom electrode. After more than 10^9 cycles, the switchable polarization retained for the 0, 2, 4, 6 at.% Nb doping films were 35%, 48%, 55% and 70%, respectively. The fatigue properties improved as the dopant concentration was increased. The same improvement was observed for the PLZT films on Pt electrodes which is shown in Fig.3.12. The switchable polarization retained for the pure PZT after more than 10^9 cycles is about 35% while with 2 at.% La addition, this value increases to about 61%. No obvious differences were

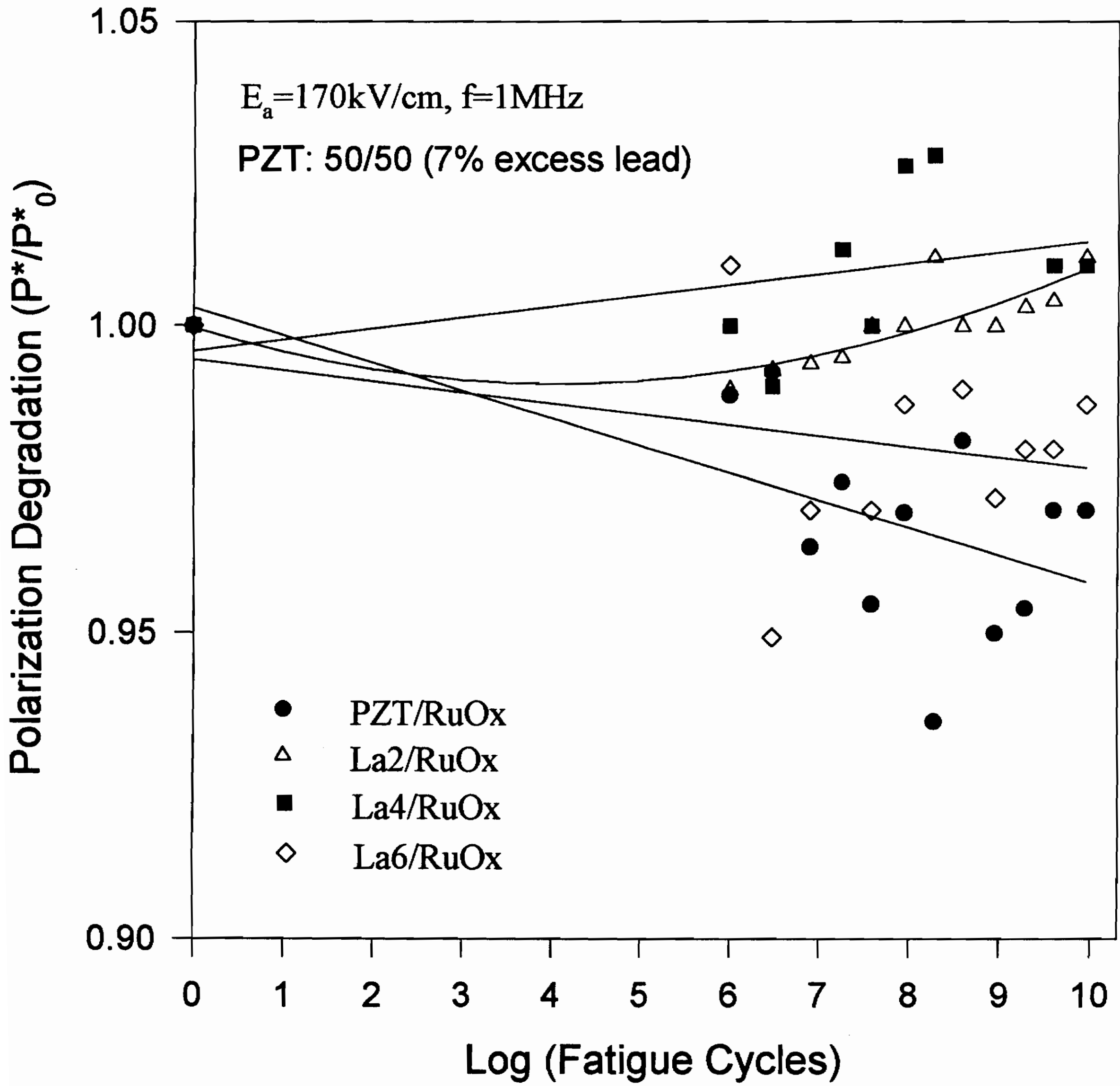

Fig. 3.10 Fatigue Endurance of PLZT on RuO_2

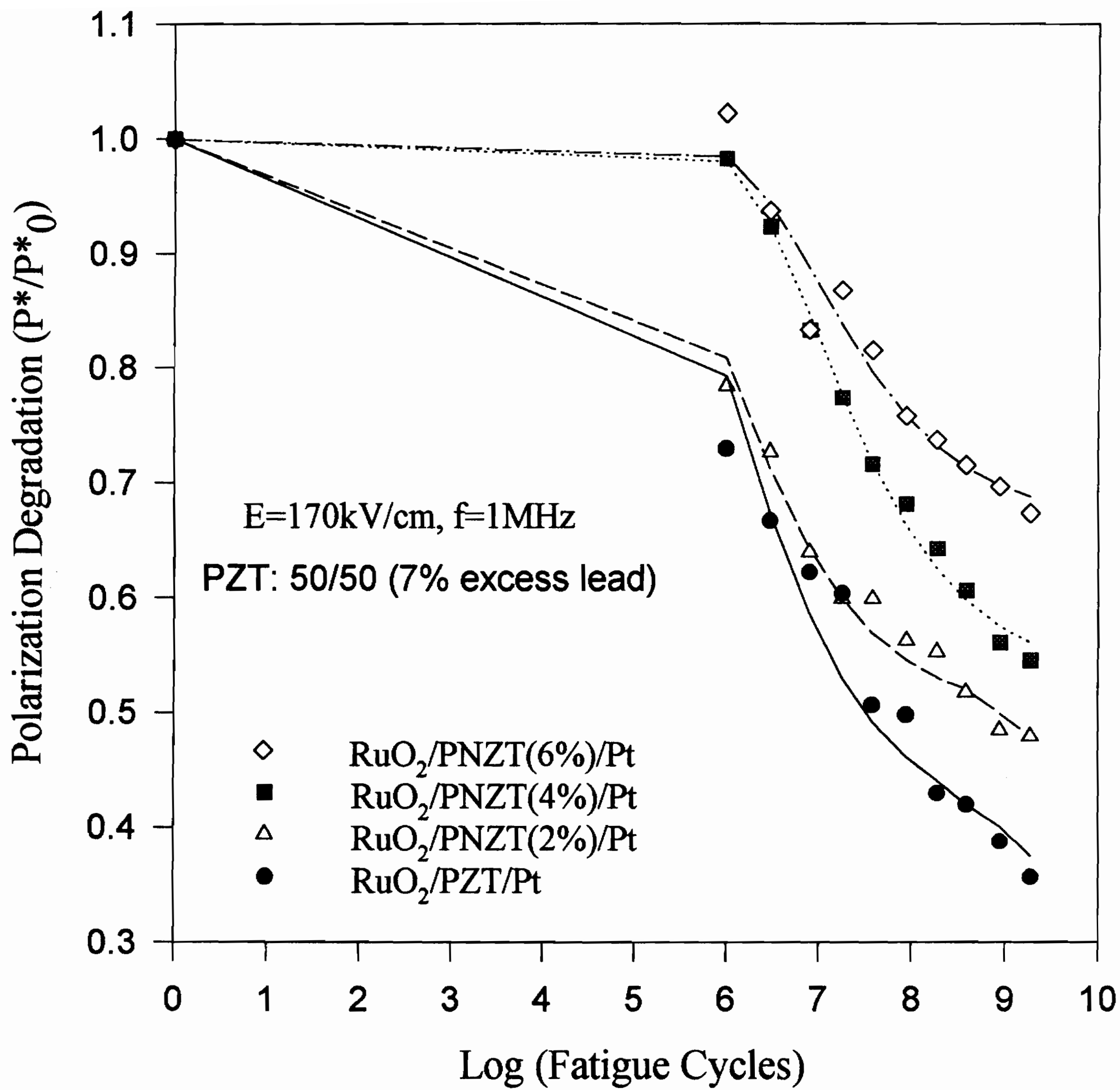

Fig. 3.11 Fatigue Endurance of PNZT on Pt

observed for the fatigue behavior of the 4 at.% and the 6 at.% La doped PZT films, both of which retain about 72% of their original switchable polarization after 10^9 switching cycles.

A fatigue model proposed by Yoo and Desu [28] assumes that the fatigue in PZT is caused by the movement and entrapment of oxygen vacancies. Equations (3.1) through (3.7) show that the La and Nb doping can lower the oxygen vacancy concentration and thus decrease the fatigue rate. However, fatigue still occurs since donor doping can not eliminate all the oxygen vacancies in the PZT.

There exists an optimal amount of donor doping above which the decrease in oxygen vacancy concentration is not obvious. For the Nb doping, the fatigue endurance continuously improve for doping amounts up to 6 at.%; while for the La doping, no additional improvement was observed for doping amounts above 4 at.%. Compared to the fatigue improvement of PZT using RuO_2 electrode material, the improvement for doped PZT is limited. The highest switchable polarization retained for the doped PZT thin films on the Pt electrodes is about 70% after 10^9 switching cycles.

The time dependent dielectric breakdown (TDDB) is also an important electrical degradation property for the dynamic RAM application. The TDDB of all films had been measured up to 10^4 seconds. The comparison of the TDDB behavior of PZT on RuO_2 and Pt is shown in Fig.3.13. No obvious degradation was observed for any of the films deposited on RuO_2 electrodes, so the films on Pt electrodes were used to study the effect of doping on the TDDB properties.

Fig.3.14 shows the degradation in the resistivity of PNZT films on Pt electrodes. A 5 V dc was applied to each sample for 10^4 seconds. For undoped PZT films, the resistivity decreased by about 4 orders of magnitude. For the 2 at.% Nb doped PZT, the degradation was less than one order of magnitude. For the 4 and 6 at.% Nb doped samples, no

resistivity degradation was observed. Fig.3.15 shows the TDDB of the PLZT films on the Pt bottom electrodes, which shows a similar trend as that of the PNZT.

No resistivity degradation was observed for the samples on the RuO_2 electrodes. For samples on the Pt electrodes, however, 4 at.% or more donor doping prevents the films from degrading up to 10^4 seconds. The donor doped PZT films have a much better degradation resistance than the undoped PZT films on the Pt electrodes.

Several models have been proposed to explain the electrical degradation of the PZT films, such as the reduction model [29], grain boundary potential barrier height model [30], de-mixing reactions of oxygen vacancies model [31] etc.. Most of these models are based on the idea of the accumulation of mobile oxygen vacancies at the interfaces or grain boundaries. When the oxygen vacancy concentration decreases from donor doping, the electrical degradation will slow down accordingly.

In summary, based on the fatigue and electrical degradation results, it can be concluded that the fatigue and TDDB behavior are determined by the oxygen vacancy concentration. Donor doped PZT films show improved fatigue endurance and better TDDB properties as a result of the lower oxygen vacancy concentration.

Although the donor doping can decrease the oxygen vacancy concentration, the percentage reduction becomes very small as the oxygen vacancy concentration reaches a very small value. For the PLZT films, the improvement in the degradation properties from 4 at.% doping to 6 at.% doping is very small; therefore 4 at.% is a sufficient amount of La doping. In the case of the PNZT films, the improvement continues up to 6 at.% and therefore 6 at.% Nb doping is considered to be optimal for the prevention of the electrical degradation.

No fatigue and TDDB degradation was observed for films on the RuO_2 electrodes. The application of the RuO_2 electrodes results in a much greater improvement in the

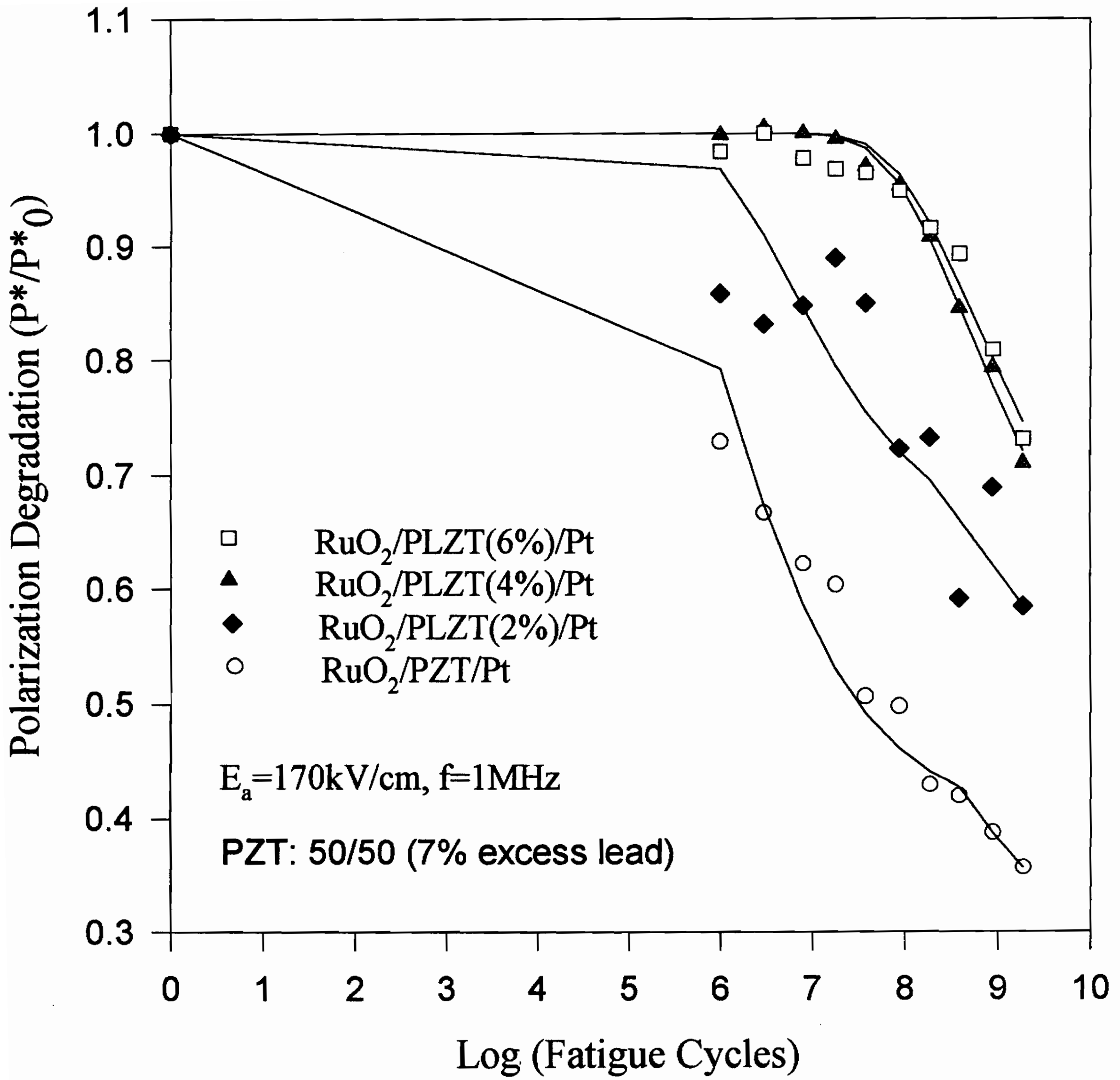

Fig. 3.12 Fatigue Endurance of PLZT on Pt

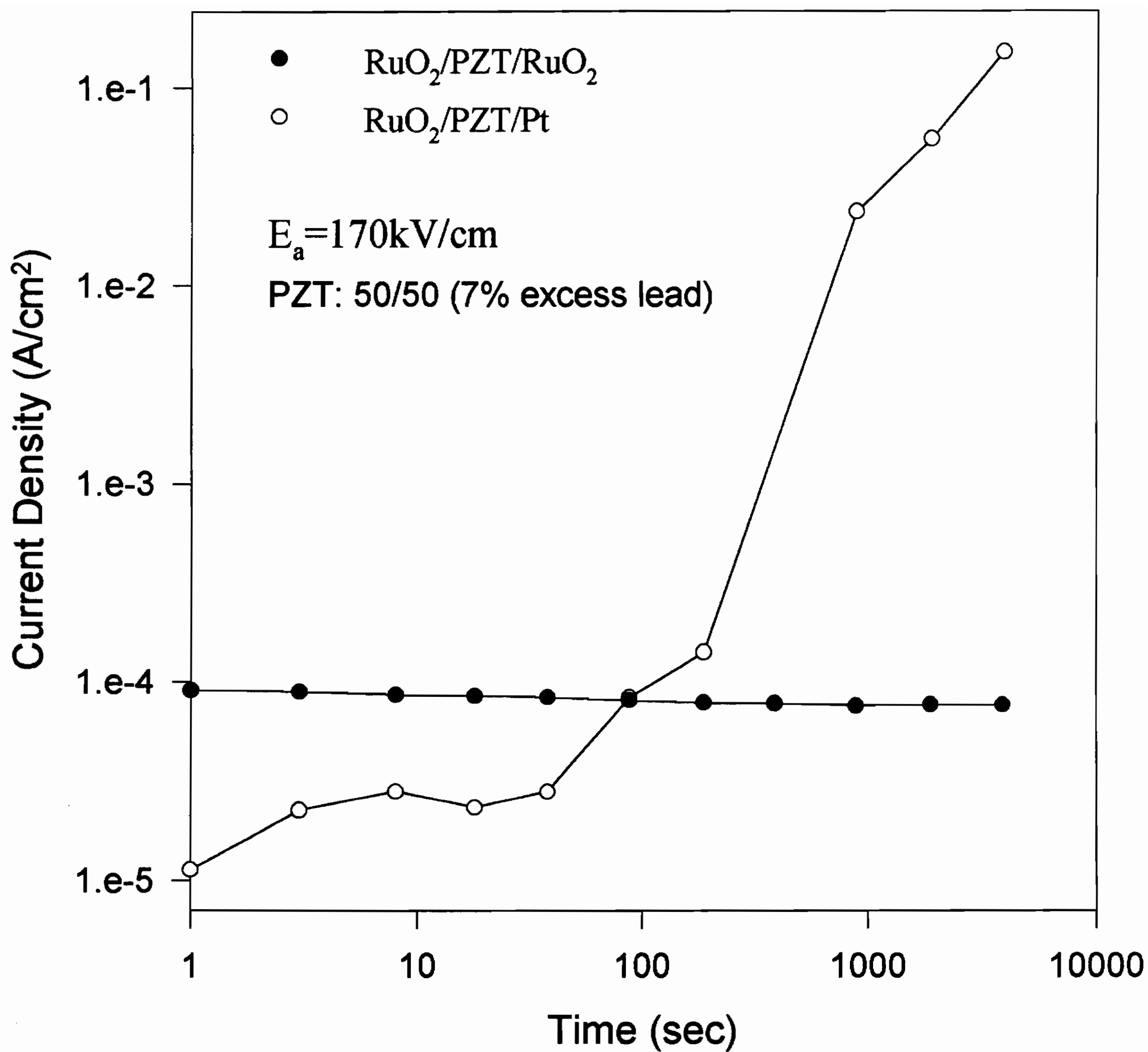

Fig. 3.13 TDDB of PZT on Pt & RuO_2

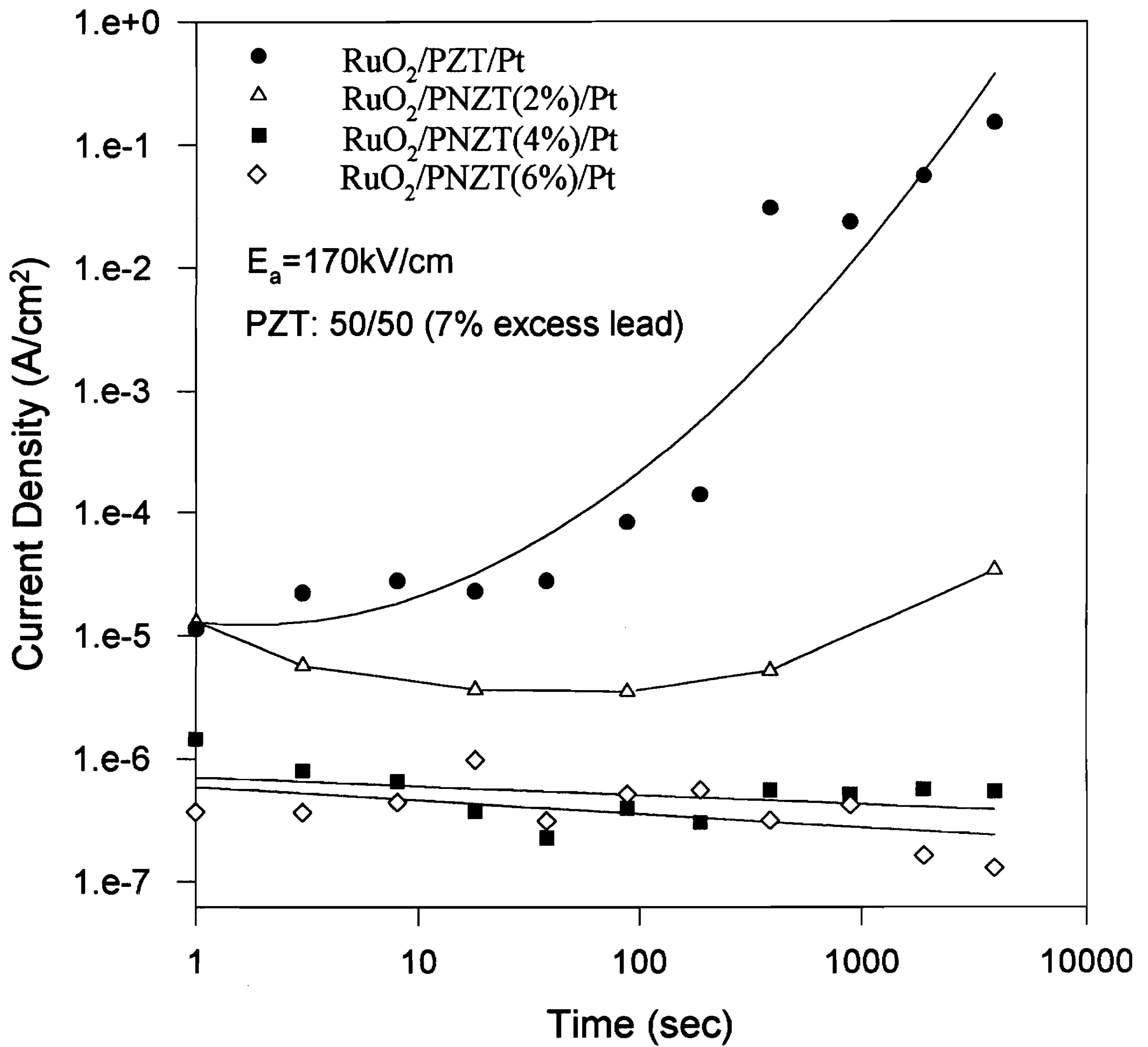

Fig. 3.14 TDDB of PNZT on Pt

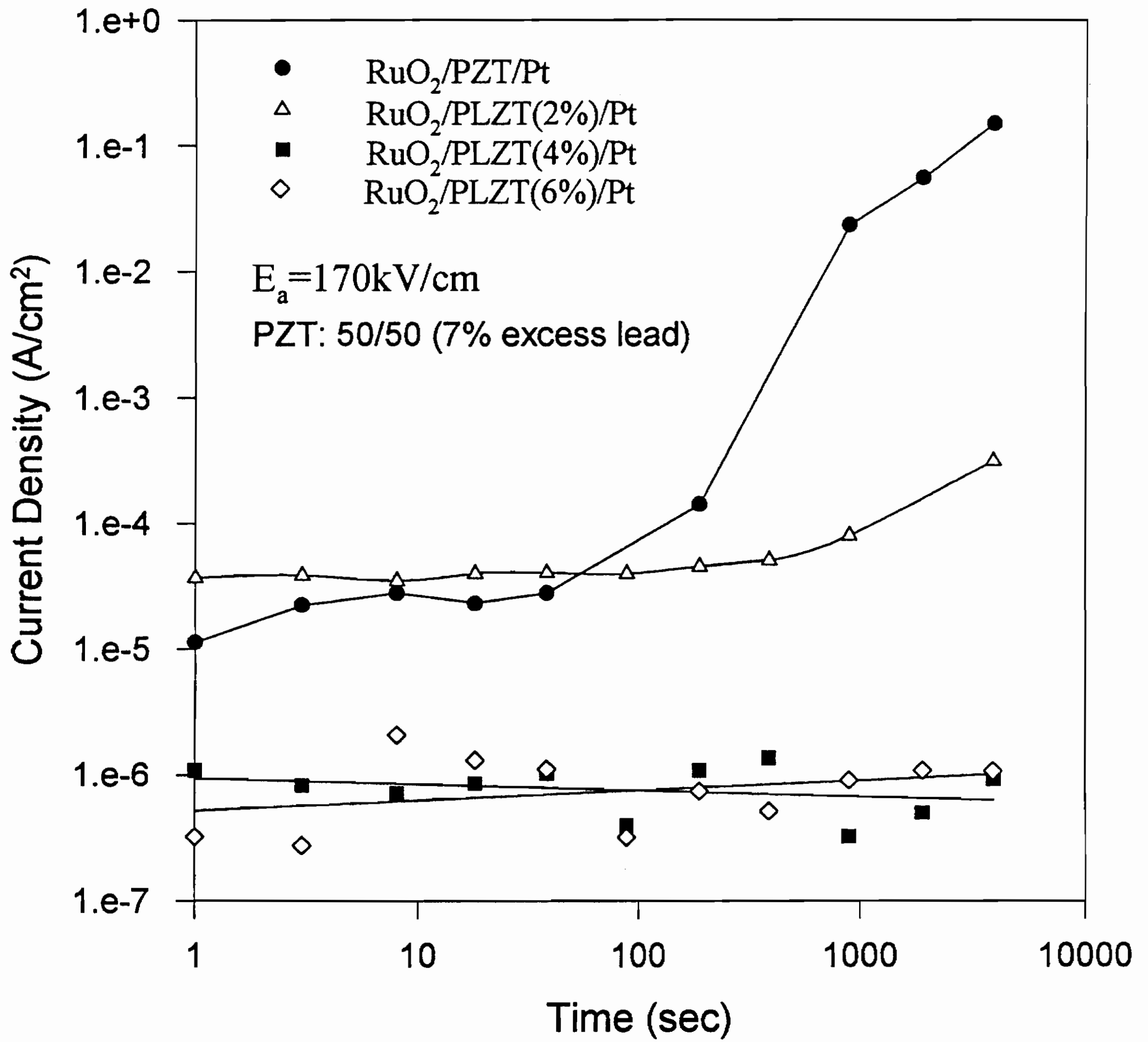

Fig. 3.15 TDDB of PLZT on Pt

electrical reliability properties of PZT films than the donor doping. It can be concluded that decreasing the rate of entrapment of defects by selecting a proper electrode material is a much more effective way to solve the electrical degradation problems than decreasing the oxygen vacancy concentration by donor doping.

Leakage Current. Fig.3.16 shows the leakage current values for La and Nb doped PZT films on Pt bottom electrodes. The La and Nb doping show the same trend on the Pt electrodes. The leakage current decreases when the doping amount increases up to 4 at.%, then increases slightly for 6 at.% doping. The I-V curves of 4 at.% Nb doped PZT and 4 at.% La doped PZT are compared to that of the undoped PZT in Fig.17(A) and (B), respectively. The doped PZT films have much lower leakage current values than those of the undoped PZT over the entire electric field range measured. The 4 at.% La doped PZT on Pt electrodes achieves the lowest leakage current value which is 11 nA/cm^2.

The I-V characteristics observed in PZT thin films is non-ohmic and is controlled by several types of conduction mechanisms, such as simple oxygen diffusion, space charge limiting, Poole-Frenkel emission and Schottky emission. It is reported that the Poole-Frenkel emission and Schottky emission are the dominant mechanisms in the conduction of PZT thin films [33]. Donor doped PZT films have lower leakage current than undoped PZT films due to two reasons: decrease in all oxygen vacancy related conduction in the films; decrease in hole concentration in PZT. thereby decrease the p-type conduction as well. The ionic conduction in PZT films is negligible below 150°C.

It is reported that the leakage current of PLZT achieved its lowest value for a dopant concentration of 10 at.% [36]. The increase in leakage current from 4 at.% doped PLZT to 6 at.% doped PLZT is still under investigation.

In summary, both the La and Nb doped PZT films on Pt electrodes have lower leakage current values compared to undoped PZT. The leakage current decreases as the

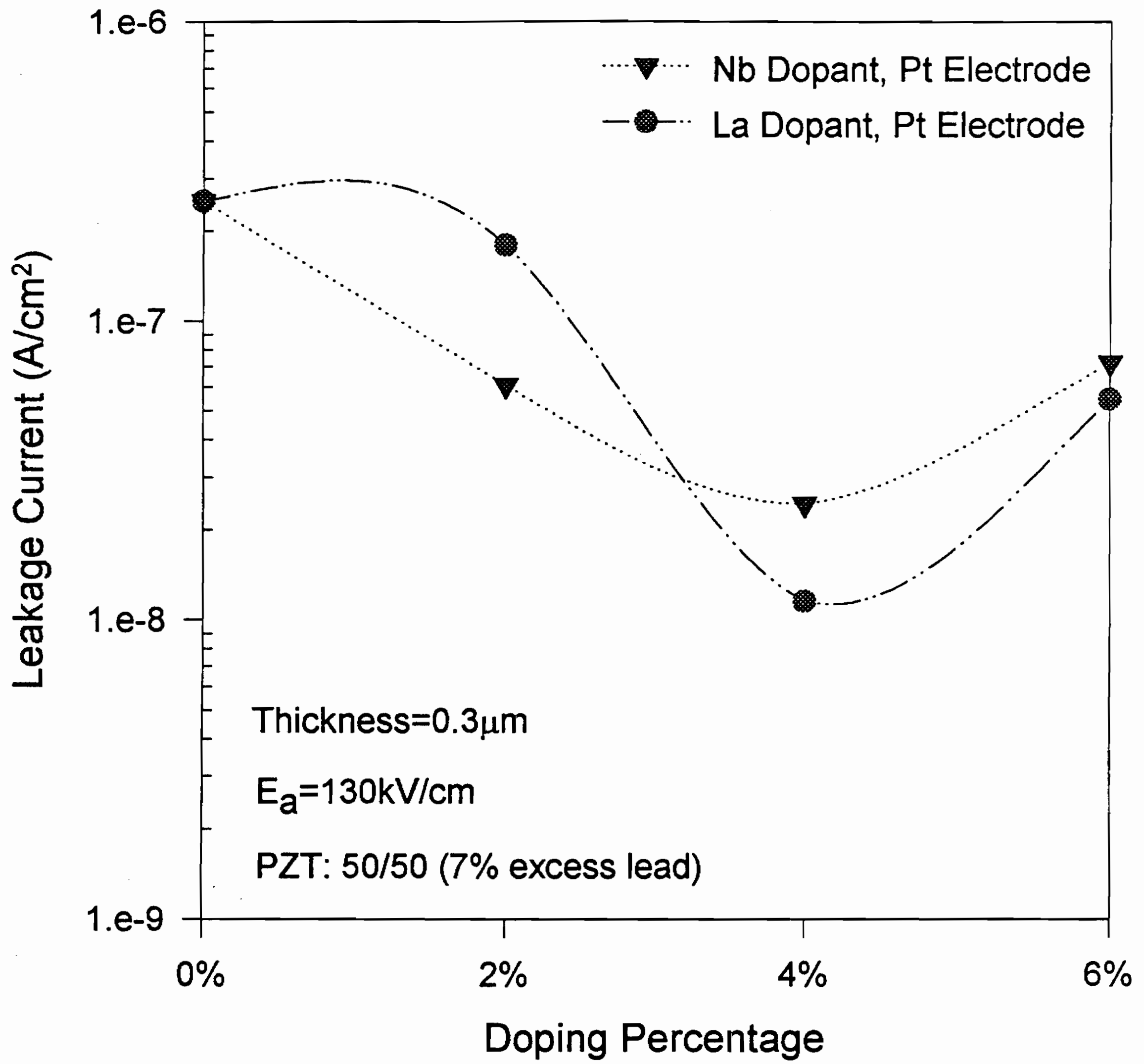

Fig. 3.16 Leakage Current as a Function of Doping Amount

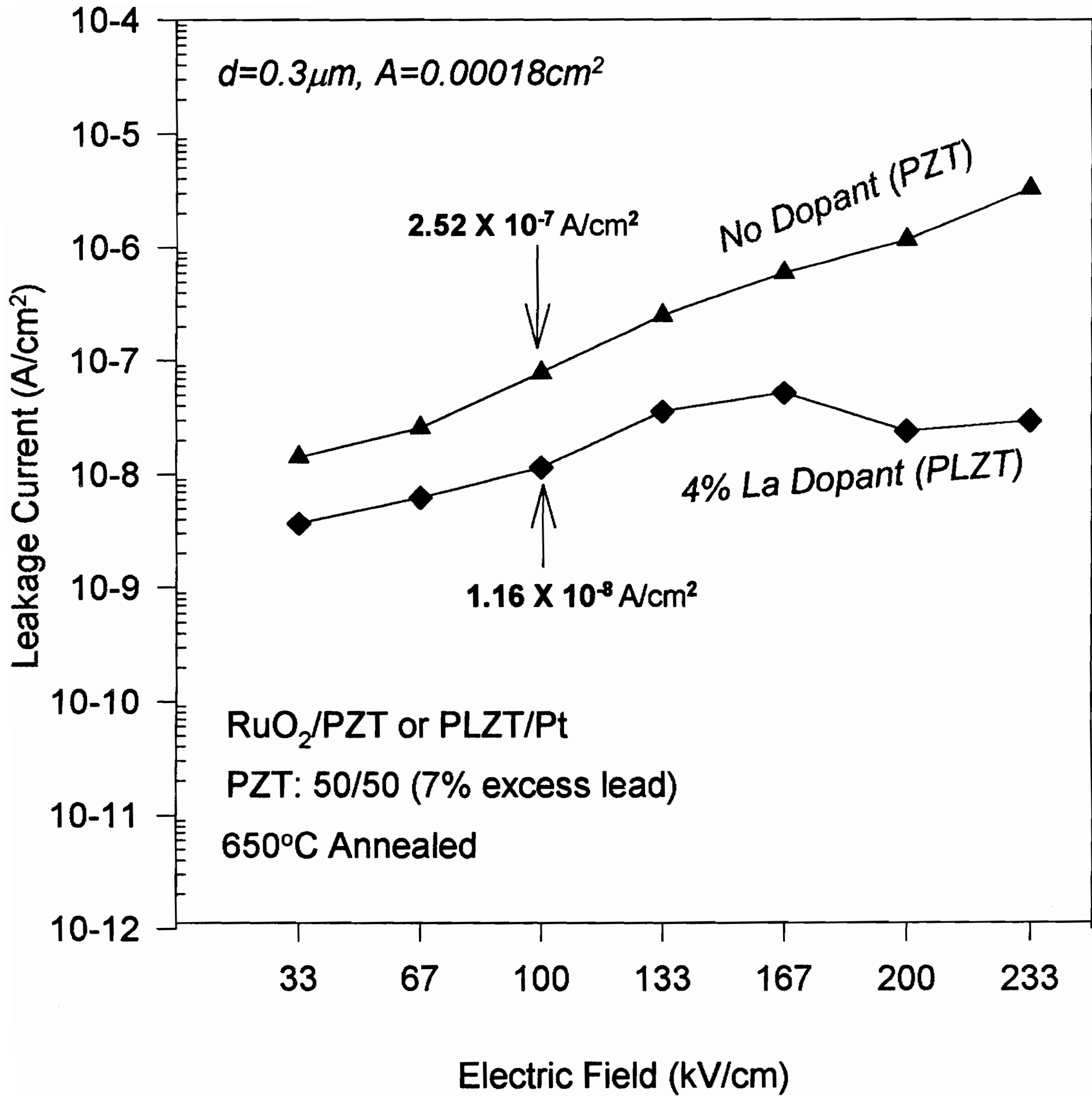

Fig. 3.17(A) I-V Curves of PZT & PLZT

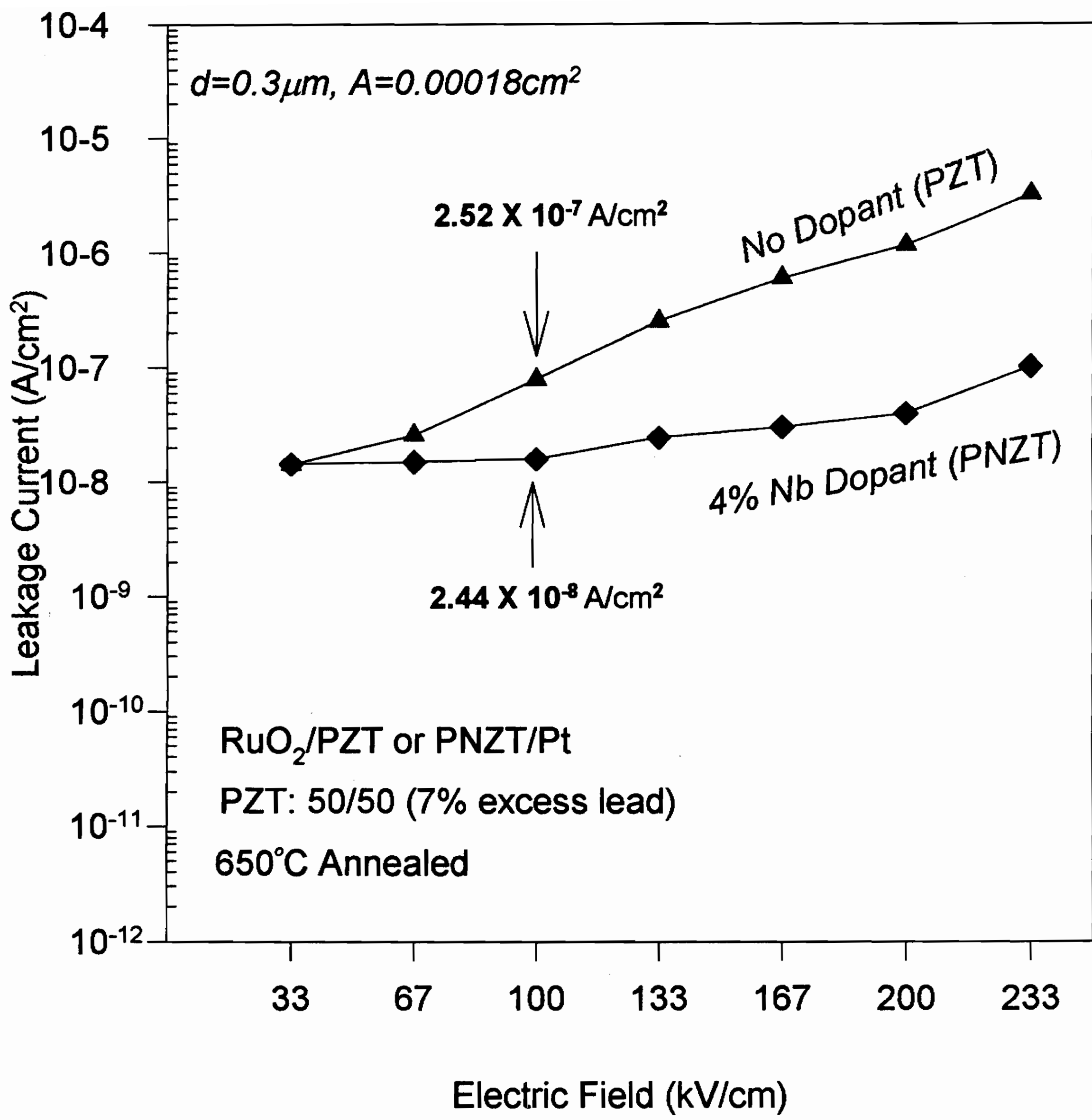

Fig. 3.17(B) I-V Curves of PZT & PNZT

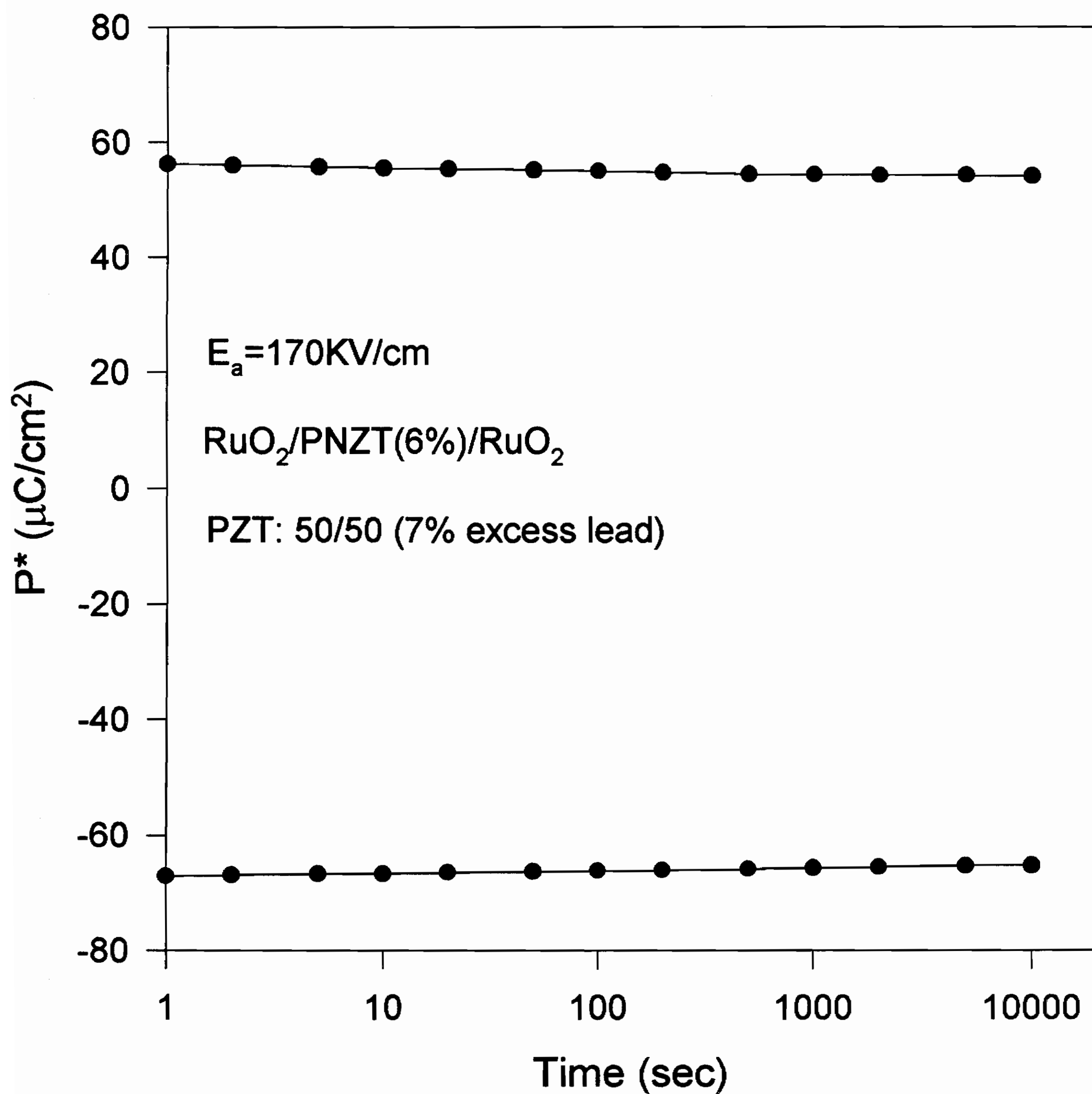

Fig. 3.18 Retention of PNZT (6%) on RuO_2

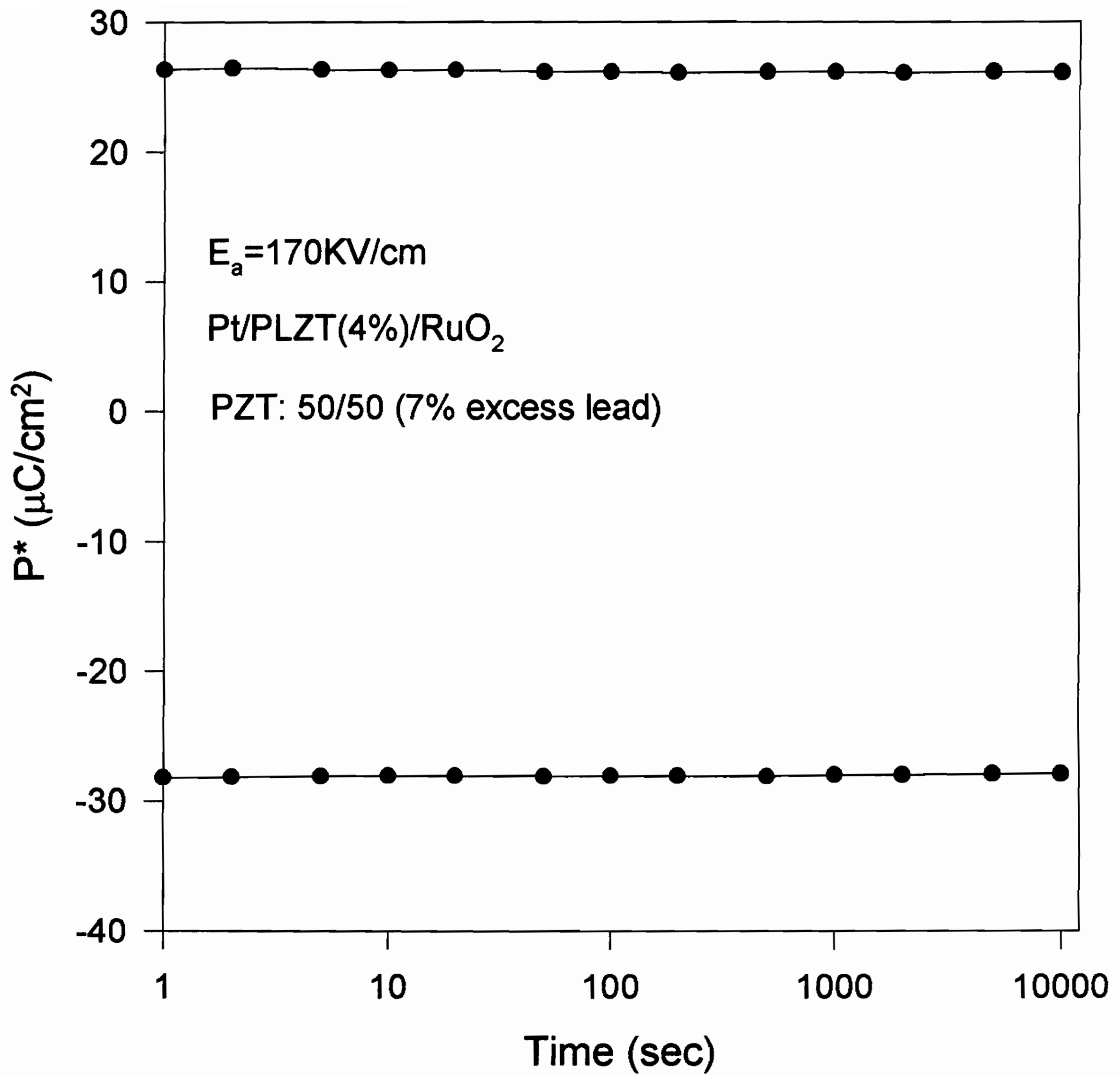

Fig. 3.19 Retention of PLZT (4%) on Pt

dopant concentration increases up to 4 at.%, and the lowest leakage current value obtained was 11 nA/cm^2 for 4 at.% La doped PZT.

Retention. Retention is the capability of the ferroelectric materials to retain their polarization under a certain set of circumstances. The polarization values have been measured up to 10^4 seconds for each sample, and no degradation has ever been observed for either the doped or the undoped films in this study. Fig.3.18 shows the retention of the 6 at.% Nb doped PZT films on RuO_2 electrodes, and Fig.3.19 shows the retention data of 4 at.% La doped PZT films on Pt electrodes. In both cases polarization was retained well up to 10^4 seconds.

The retention properties desired for ferroelectric memory applications is ten years, which is impossible to measure in the lab using the present experimental conditions. An accelerated experiment which can be performed at an elevated temperature or high electric field to simulate this long time period may be necessary.

3.4. Summary

The effect of La and Nb doping on the electrical properties and microstructure of PZT films was investigated emphasizing the improvement of their reliability properties. The oxygen vacancy mechanism was used as the theoretical basis of the PZT degradation in this study. A defect mechanism was also proposed to show the effect of donor doping on the oxygen vacancy concentration. The experimental results fit very well with the doping mechanism proposed. Donor doped PZT films on RuO_2 substrates achieve high fatigue endurance and low leakage current at the same time. The following conclusions can be drawn from the results:

(1) Up to 6 at.% La and Nb doping, PZT films can form complete perovskite structures at an annealing temperature of 650°C for 30 min.

(2) La doping can increase the nucleation and growth rate of the perovskite phase and thus achieve a larger grain size and a more well developed grain boundary structure.

(3) 2 at.% Nb doped PZT shows a rougher surface than the undoped PZT, while larger amounts of Nb doping results in a very smooth surface and a fine grain structure.

(4) Both La and Nb doping result in a higher fatigue and TDDB resistance compared to undoped PZT, indicating that the oxygen vacancies decrease as a result of donor doping.

(5) The improvement in the fatigue and TDDB properties on the PZT thin films by donor doping saturates as the dopant concentration reaches a certain amount. For La doping, the optimal amount is about 4 at.%, while for Nb doping it is around 6 at.%.

(6) The leakage current of La and Nb doped PZT thin films on Pt electrodes decreases when the doping amount increases up to 4 at.%, which can be related to a decrease in the p-type conduction and the oxygen vacancy conduction.

(7) Good retention properties have been observed for all samples up to 10^4 seconds. An accelerated test should be employed for the retention measurement.

Chapter 4 Summary

The major objectives of this study were to investigate the ferroelectric PZT materials for DRAM and FRAM applications. Emphasis was on the electrical reliability properties of the PZT materials, such as fatigue, leakage current, time dependent dielectric breakdown (TDDB) and retention. The movement and entrapment of oxygen vacancies were noted as the sources of all these degradation. In this research, RuO_2 electrode material was employed to decrease the entrapment of the oxygen vacancies at the PZT-electrode interfaces, and La and Nb donor doping were used to lower the oxygen vacancy concentration in PZT thin films. Both of them can improve the electrical reliability of PZT thin films as expected.

Based on the experimental results, it can be concluded that good fatigue endurance can be achieved without sacrificing the leakage current by employing both RuO_2 electrodes and donor doping at the same time. The electrical properties for 2 at.% La doped PZT annealed at 650°C for 30 min on RuO_2 electrode are compared with the properties required for nonvolatile memory applications:

1. $2P_r = 46\ \mu C/cm^2$ ($> 10\ \mu C/cm^2$)
2. $E_c = 40$ kV/cm (< 70 kV/cm)
3. Fatigue endurance $> 10^{11}$ cycles ($> 10^{12}$ cycles)
4. $I = 6.5\times10^{-7}\ A/cm^2$ ($< 10^{-8}\ A/cm^2$)
5. Retention $> 10^4$ seconds
6. TDDB $> 10^4$ seconds

The properties achieved are very close to those required for memory applications.

For continuous studying of the PZT materials, the following future works are proposed to achieve both high fatigue endurance and low leakage current:

1. Searching for new kind of electrode materials
2. Depositing multilayer films
3. Doping PZT up to 10 at.%

For the electrical property measurements, breakdown field, Cole-Cole plot before and after fatigue, and imprint should be measured to completely characterize the PZT and study the material structure change after the degradation.

Appendix A. Sol-Gel Method

The PZT solution or doped PZT solution can be made through the following procedures:

1. Add calculated amount of Zr-n-propoxide into a clean 50 ml beaker
2. Add calculated amount of Ti-iso-propoxide
3. React in ultrasonic sink for 5 min, covered with parafilm
4. Add calculated amount of Nb V Ethoxide, react in ultrasonic sink for another 5 min (for making PNZT solution only)
5. Add 5 ml acetic acid, react for a while in ultrasonic sink
6. Add approximate 10 ml of n-propanol, stir in the ultrasonic sink
7. Add calculated amount of Pb-acetate
8. Add calculated amount of La-acetate hydrate (for making PLZT solution using La-acetate hydrate precursors only)
9. Put the beaker in 90°C silicon oil, stir the solution a little until Pb and La-acetate dissolve completely
10. Add calculated amount of water ([water]/[Pb] = R = 10)
11. Add 5 ml acetic acid
12. Add 10 ml propanol, stir
13. Add 5 ml acetic acid, stir
14. Pour the solution in a 50 ml graduated cylinder, add propanol to make it 50 ml

Appendix B. Quantity of Chemicals for PZT Solutions

The quantity of chemicals required to make 50 ml of 0.4 M PZT solution is calculated below:

1. Excess lead

2 at.% excess lead:	PbAc.3H2O=7.739g	Water=2.5727g
5 at.% excess lead:	PbAc.3H2O=7.966g	Water=2.6480g
10 at.% excess lead:	PbAc.3H2O=8.345g	Water=2.7740g

2. Zr/Ti ratio

0/100:	$Zr(Pr^{n})$=0g	$Ti(Pr^{iso})$=5.685g
20/80:	$Zr(Pr^{n})$=1.872g	$Ti(Pr^{iso})$=4.548g
40/60:	$Zr(Pr^{n})$=3.744g	$Ti(Pr^{iso})$=3.411g
50/50:	$Zr(Pr^{n})$=4.680g	$Ti(Pr^{iso})$=2.843g
60/40:	$Zr(Pr^{n})$=5.616g	$Ti(Pr^{iso})$=2.274g
80/20:	$Zr(Pr^{n})$=7.487g	$Ti(Pr^{iso})$=1.137g
100/0:	$Zr(Pr^{n})$=9.359g	$Ti(Pr^{iso})$=0g

References

1. C. T. Lin, B. W. Scanlan, J. D. Mcneill, J. S. Webb, and L. Li, J. Mater. Res., 7, 2546 (1992).

2. S. S. Dana, K. F. Etzold, and J. Clabes, J. Appl. Phys., **69**, 4398 (1991).

3. N. Tohge, S. Takahashi, and T. Minami, J. Am. Ceram. Soc., **74**, 67 (1991).

4. W. A. Geideman, IEEE Transactions on Ultrasonics, Ferroelectrics, and Frequency Control, **38**, 704 (1991).

5. J. Carrano, C. Sudhama, V. Chikarmane, J. Lee, A. Tasch, W. Shepherd, and N. Abt, IEEE Transactions on Ultrasonics, Ferroelectrics, and Frequency Control, **38**, 690 (1991).

6. H. Hu and S. B. Krupanidhi, J. Appl. Phys., **74**, 3373 (1993).

7. D. F. Ryder, Jr, and N. K. Raman, Journals of Electronic Materials, **21**, 971 (1992).

8. M. Klee, R. Eusemann, R. Waser, and W. Brand, J. Appl. Phys., **72**, 1566 (1992).

9. S. D. Bernstein, T. Y. Wong, Y. Kisler, and R. W. Tustison, J. Mater. Res., **8**, 12 (1993).

10. D. Bondurant, and F. Gnadinger, IEEE Spectrum, 30 (1989).

11. R. Waser, T. Baiatu, and K. Härdtl, J. Am. Ceram. Soc., **73**, 1645 (1990).

12. T. Baiatu, T. Baiatu, and K. Härdtl, J. Am. Ceram. Soc., **73**, 1663 (1990).

13. J. F. Scott, and C. A. Paz De Araujo, Science, **246**, 1400 (1989).

14. J. F. Scott, C. A. Araujo, B. M. Melnick, L. D. McMillan, and R. Zuleeg, J. Appl. Phys., **70**, 382 (1991).

15. H. M. Duiker, P. D. Beale, and J. F. Scott, J. Appl. Phys., **68**, 5783 (1990).

16. B. A. Tuttle, D. H. Doughty, R. W. Schwartz, T. J. Garino, S. L. Martinez, D. Goodnow, and C. L. Hernandez, Microelectronic Systems, 179 (1988).

17. D. P. Vijay, and S. B. Desu, J. Electrochem. Soc., **140**, 2640 (1993).

18. G. Yi, Z. Wu, and M. Sayer, J. Appl. Phys., **64**, 2717 (1988).

19. R. W. Jones, The Institute of Metals, 1989.

20. C. K. Kwok, and S. B. Desu, J. Mater. Res., **8**, 339 (1993).

21. C. K. Kwok, "Processing-Structure-Property Interrelationships of Ferroelectric Thin Films with Emphasis on Formation Kinetics", PhD Dissertation, Materials Science Engineering Department, Virginia Tech, (1992).

22. G. Hearling, Am. Ceram. Soc. Bull., **43**, 875 (1964).

23. A. Khan, "Decomposition and Characterization of Lead Lanthanum Titanate Thin Film by MOD", Master Thesis, Materials Science Engineering Department, Virginia Tech, (1993)

24. J. F. Chang, "Preparation and Characterization of Doped Lead Zirconate Titanate $Pb(Zi_xTi_{1-x})O_3$ Films", Master Thesis, Materials Science and Engineering Department, Virginia Tech, (1992).

25. J. F. Chang, and S. B. Desu, J. Mater. Res., **9**, (1994).

26. I. K. Yoo, and S. B. Desu, Philos. Mag. B, **69**, 461, (1994)

27. S. E. Bernacki, Mat. Res. Soc. Sym. Proc., **243**, 135 (1992).

28. I. K. Yoo, and S. B. Desu, "Fatigue Modeling of Lead Zirconate Titanate Thin Films", Unpublished.

29. J. Rödel, and G. Tomandl, J. Mater. Sci., **19**, 3515 (1984).

30. Y. h. Yu, Ferroelectric Materials and Their Applications, North-Holland, (1991)

31. I. K. Yoo, F. W. Stephenson, and L. C. Burton, IEEE Trans. Components, Hybrids, Manuf. Technol. CHMT-10, **2**, 274 (1987).

32. R. Waser, Mater. Sci. Eng., **A**, 171 (1989).

33. I. K. Yoo, S. B. Desu, and J. Z. Xing, Mat. Res. Soc. Symp. Proc., **310**, 165 (1993)

34. V. G. Gavrilyachenko, R. I. Spinko, M. A. Martynenko, and E. G. Fesenko, Soviet Physics - Solid State, **12**, 1203 (1970).

35. C. Chen, and D. F. Ryder, Jr., J. Am. Ceram. Soc., **72**, 1495 (1989).

36. T. Okudaira, A. Hachisuka, and K. Horie, Extended Abstracts of the 1991 International Conference on Solid State Devices and Materials, Yokohama, 204 (1991).

37. L. Parker, and A. Tasch, IEEE Circuit and Devices, 17 (1990).

Vita

Jimmy Zhiqi Xing was born in Guangzhou, China on November 14, 1967. He entered Tsinghua University in Beijing in 1986 and obtained his Bachelor degree in Materials Science Engineering in 1991. He came to Virginia Tech in January 1992 persuing a Master degree in Materials Science Engineering, and joined the thin film group in May 1992, under the guidance of Dr. S. B. Desu.